SMART NANOGEL ARCHITECTURES FOR ANTICANCER THERAPY AND THEIR INTERACTIONS WITH BLOOD PROTEINS

Inaugural-Dissertation
to obtain the academic degree
Doctor rerum naturalium (Dr. rer. nat.)

submitted to the Department of Biology, Chemistry and Pharmacy
of Freie Universität Berlin

by

Enrico Miceli

from Udine, Italia

2017

This doctoral thesis was carried out from January 2014 to November 2017 in the research group of Prof. Dr. Marcelo Calderón at the Institute for Chemistry and Biochemistry, Faculty of Chemistry, Biology, and Pharmacy of the Freie Universität Berlin.

I hereby declare that this PhD thesis was prepared autonomously and that no illegal help was used. Contributions of others, e.g., content, quotes, or figures are indicated by referring to the original work.

Berlin, November 2017 _____ (Enrico Miceli)

1. Referee: Prof. Dr. Marcelo Calderón

2. Referee: Prof. Dr. Joachim Dzubiella

Date of Disputation: 17.01.2018

Acknowledgements

I gratefully acknowledge Prof. Marcelo Calderón for being my mentor for these four years. And for being the coolest boss one could ever have. I also thank Prof. Joachim Dzubiella for being my second supervisor, and the Helmholtz Virtual Institute “Biofunctional Materials for Medicine” for the funding.

I wish to thank the whole AG Calderón research group for being the funniest group ever to be involved with. Ernesto for all the brotherhood, Michael and Gregor for being the nicest guys, Laura for being the coolest, Stefanie, Julian, Emanuel, Loryn, the Latinos Exchange Squad (Cata, Lydia, Marcelo, Ana, Guido, Matias), the veterans Joy, Maria, Mazdak, Ana and Harald, all of you helped me not only to survive, but thrive and have fun every single day. I wish also to further thank all members of the AG Haag for the countless help and inspiration during these years in research, and my collaborators at AG Freund, AG Hedtrich and MPI Mainz for the strong contributions to the results throughout this thesis.

I have to thank my family, for supporting me as a poor PhD student and allowing me always to do what I want. My grandpa Rudi for being my role model.

I have friends all over the world, that I miss every day. I hope one day we could all be together in one physical place. And I hope that place is Puglia.

My Berlin family, I thank you very much for being my chosen family. Diego, Luca and Silvana for helping me most when I needed it. You are the best!

Dedicated to Giulio Regeni.

1. Introduction 6

1.1. Nanomedicine 6

1.1.1 Nanogel Architectures 9

1.1.2 Dendritic Architectures in Nanomedicine 14

1.1.3 Biosafety Issues in Nanomedicine 17

1.2. Blood Compatibility of Nanoparticles 19

1.2.1. Biological Implications of the Protein Corona 20

1.2.2. Physics of Competitive Protein Binding to Nanoparticles 22

1.2.3. Protein Corona Around Polymeric Nanoparticles 25

2. Motivation and Objectives 28

3. Publications and Manuscripts 30

3.1 Temperature Dependency of Elusive Protein Corona Around Thermoresponsive Nanogels: Key Interactions Above the Lower Critical Solution Temperature 30

3.2 Protein Corona Formation on Colloidal Polymeric Nanoparticles and Polymeric Nanogels: Impact on Cellular Uptake, Toxicity, Immunogenicity, and Drug Release Properties 62

3.3 Semi-interpenetrated, Dendritic, Dual-responsive Nanogels with Cytochrome *c* Corona Induce Controlled Apoptosis in HeLa Cells 84

3.4 Rational Design of Dendritic Thermoresponsive Nanogels that Undergo Phase Transition under Endolysosomal Conditions 102

3.5 Overcoming Drug Resistance with On-demand Charged Thermoresponsive Dendritic Nanogels 115

4. Summary and Conclusion 132

5. Outlook 135

6. Kurzzusammenfassung und Ausblick 137

7. References 142

8. Curriculum Vitae 149

9. Publications and Conference Contributions 150

1. Introduction

1.1 Nanomedicine

The use of nanotechnology in medical science, in short nanomedicine, is currently a bursting field of research. The involvement of nanomaterials in medicine allows the development of new, potent therapeutic agents that empower the conventional therapies by acting as drug carriers, imaging agents, biomarker recognition agents for early diagnostics,[1] scaffolds for regenerative medicine,[2, 3] or possess intrinsic therapeutic properties and have potential as stand-alone drugs.[4-6] The use of nanomaterials for this scope allows the optimization and tailoring of preexisting therapies, as well as reducing their side effects, provide combined therapeutic and diagnostic properties (theranostics),[7-9] as well as brand new therapeutic strategies. Their incorporation into nanodevices allows the screening and shielding of living tissues with unprecedented accuracy and programming.[10] Thus, the concept of nanomedicine is evolving and includes in its definition any use of nanosized materials, for the improved treatment of cancer,[11] auto-immune [12] or degenerative diseases.[13]

Several different classes of nanomaterials are encountered in nanomedicine, as they vary between polymeric,[14] lipidic,[15] inorganic (silicon- [16] or metal-based),[17] or carbonaceous.[18] A combination of these materials is also encountered, to combine the advantages provided by the single precursor materials together in one nanoparticle.[19] Depending on the desired application, researchers developed nanomaterials with tailored physicochemical characteristics and bioreactivities, to function as next generation therapeutics. Nanomaterials structures span over many dimensionalities, starting from zero-dimensional nanoparticles, to one-dimensional nanotubes or nanowires,[20, 21] to two dimensional nanosheets or nanomembranes,[22] all to be integrated into complex three-dimensional devices.[23] An overview of the various nanosystems is shown in **Fig. 1.1**. The hierarchies in multidimensionality allow the creation of precision materials that are needed to overcome the limitations of conventional therapies.

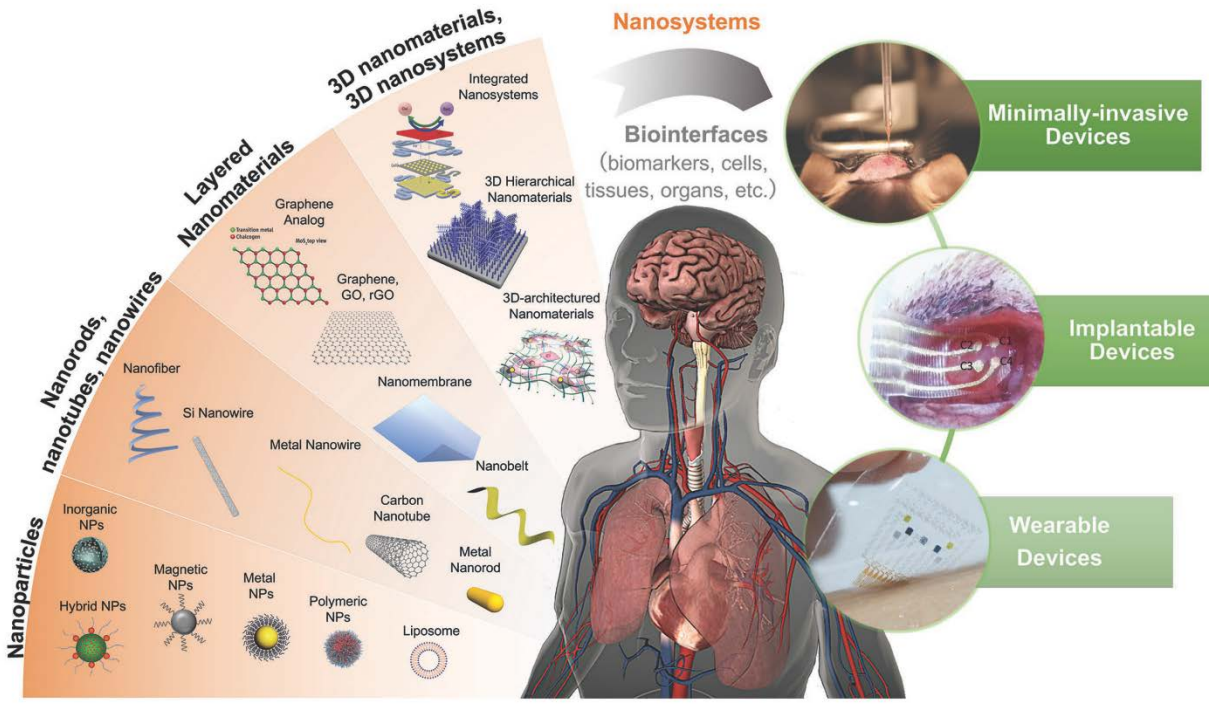

Fig. 1.1 Overview of nanoparticles employed in different classes of applications in nanomedicine. Reproduced with permission from Cai *et al.*[10] Copyright 2017 Wiley-VCH.

The use of macromolecules as drug carriers help vectoring the drug inside the target tissues, thereby improving its biodistribution profile, acting as a (sometimes self-immolating) skeleton, leading to an *in situ* sustained delivery of the encapsulated drug. In this way, nanocarriers inhibit the drug free diffusion by physical entrapment, allowing the single drug dose to stay longer inside the therapeutic window, as shown in **Fig. 1.2**.[24] Analogously, nanoparticle-drug conjugates allow the accumulation in selected tissues and the *in situ* release of the drug from the conjugate, by selective cleavage of self-immolating bonds.[25] Therefore, nanocarriers are responsible for extending the drug circulation and its blood retention, reduce immunogenic reactions, decrease systemic toxicities, and improve drug stability, thus effectively reducing the drug's side effects and effective dosages.[26]

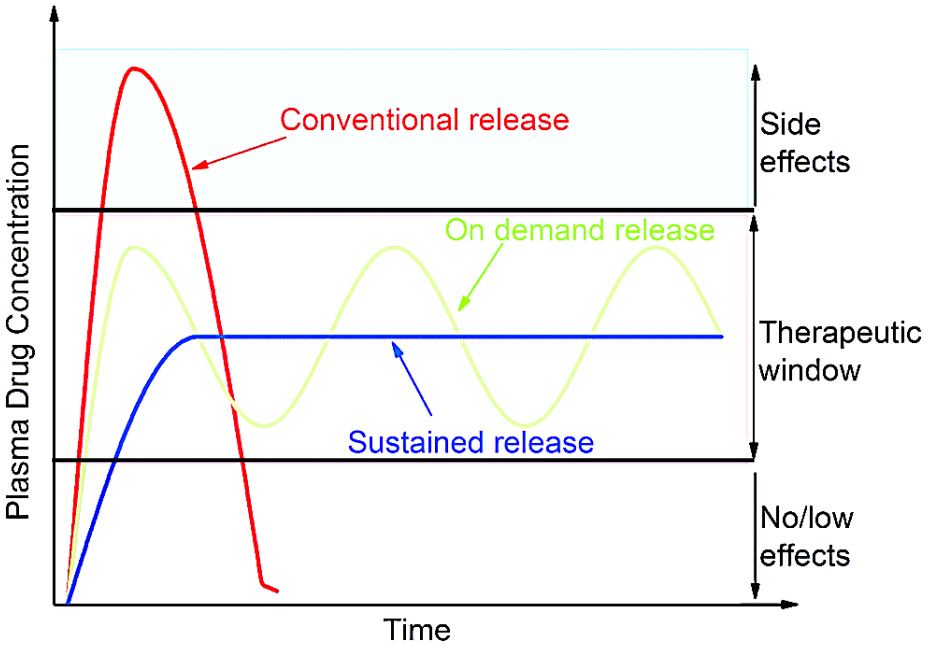

Fig. 1.2 Release kinetics by nanomedicine compared to conventional drug administration and their behavior in blood as shown from the therapeutic window. Modified with permission from Yi *et al.*, copyright 2015 Royal Society of Chemistry.[27]

These beneficial properties of drug nanocarriers were found not only to improve the efficacy of small drugs, but also for biomacromolecules: therapeutic proteins and nucleic acids (DNA, siRNA) are provided with sustained, site-specific release, and they showed improved stability towards enzymatic degradation and thermal denaturation, when encapsulated into nanoparticles.[28]

The imaging of biological tissues may also be accomplished with the use of nanomaterials, provided that high contrast materials are involved, from optical contrast, high electron density (plasmonic Au or Ag nanoparticles),[29] high fluorescence quantum yields (quantum dots,[30] organic dyes[31]), to magnetic contrast using magnetic nanoparticles,[32, 33] positron-emitting radioactive materials,[34, 35] or ultrasound.[36] Macromolecular imaging agents were developed for their improved performances *in vivo*, to improve the biocompatibility of high contrast agents by embedding them onto tailored nanoparticles, as well as increase focusing and resolution of the imaging technique.[37] Multimodal imaging techniques further increases precision and image resolution, by combining multiple contrast agents onto one single macromolecular scaffold.[6] In theranostic agents, the diagnostic moieties and therapeutic activities are colocalized inside a single nanoparticle, allowing an unprecedented precision of therapy and diagnostics.[7]

Both imaging agents and drug carrier nanoparticles can be directed towards the site of action by either active or passive targeting strategies.[38] Both are used in an attempt to address the nanoparticle towards its site of action and accumulate in the diseased tissues, thereby further reducing the therapy's side effects. Active targeting may exploit specific protein or cell

interactions with the macromolecule's tunable surface chemistry, using common bioconjugation pathways (avidin – biotin, transferrin – TfR1, antibody – antigen, sialic acid – carbohydrate, folic acid – RFC, RGD peptide – $\alpha_2\beta_3$ integrin) with receptors that are overexpressed on cancer cells.[39] Passive targeting exploits the physical properties of nanoparticles to specifically deliver the drug into tissues that are able to behold nanosized materials, due to the enhanced permeation and retention (EPR) effect. This effect is responsible for nanoparticle efficacy in tumor tissues, as they exhibit hyperpermeability, due to irregular tissue growth, arising from leaky vasculature and missing lymphatic drainage. A nanosized particle would selectively penetrate such tissues, and avoid the compact healthy tissues, that have too small pores.[40]

1.1.1 Nanogel Architectures

The use of polymers in nanomedicine comprises many different polymeric architectures, leading to new stand-alone drugs, drug-polymer conjugates, polyplexes, polymeric micelles, nanoparticles, and nanogels. Nanogels are a class of polymeric nanoparticles, formed by crosslinking of hydrophilic polymeric precursors.[41] Their marked propension to swell in water solutions facilitate the encapsulation of hydrophilic molecules, thus favoring their use as drug delivery agents. Due to their usually soft nature, they are well accommodated by soft biological tissues and have a distinct tendency to be uptaken by cells, another advantageous feature for drug delivery.[42] The ease of the nanogel's surface functionalization make them especially good candidates for exploiting active targeting strategies by bioconjugation,[43] and theranostic agents, by combining organic dyes or inorganic contrast agents.[19] Multiple drugs may be codelivered by nanogels specifically *in situ*, in a synergistic approach to overcome multidrug resistance and reduce the effective dosages. The combination of nanogels with other nanomaterials (both polymeric and inorganic) allows the formation of so-called hybrid nanogels, which retain the advantageous properties of all single components, in the form of nanogels, polymers or inorganic constituents, with fine control on the resulting hybrid nanogel morphology. The incorporation of magnetic, plasmonic, or carbonaceous nanomaterials led to hybrid nanogels as agents for imaging, photodynamic therapy, photothermal therapy, drug delivery, or a combination of these.[44, 45]

Polymer-nanogel composites can be subdivided into two different morphologies, being core-shell, or (semi-)interpenetrated nanogels. While both architectures show multicompartimental structures, (semi-)interpenetrated nanogels exhibit heterogeneous, isotropic structures, while core-shell nanogels have distinct radially distributed homogeneous layers. These next generation nanogels show multifunctional structures and may in general improve the performance of standard nanogels.

In core-shell nanogels, the reactivity as well as the physicochemical characteristics are dictated concertedly by all coexisting layers of the nanogel. The most common core-shell strategy is the grafting of poly(ethylene glycol) on the surface of nanoparticles, in a process known as PEGylation, which is regarded as the golden standard for improving biocompatibility of nanoparticles.[46]

Interpenetrated nanogels are provided by the colocalization of more than one independent polymer network, to give nanogels with multiple components that are not chemically bound to each other, although they cannot be separated by shear stress, rather only by chemical reactions.[47] As a result, interpenetrated nanogels retain all properties of the single precursor polymeric networks, which is an advantage over core-shell structures, while the relative amounts of the single networks may be adjusted according to the designed application. Semi-interpenetrated nanogel structures exhibit analogous properties, while they differ from interpenetrated nanogels, due to their non-crosslinked network within the nanogel.[48] Both categories of polymer-nanogel composites have specific advantages in nanomedicine, while core-shell may result in particles exhibiting improved targeting abilities, interpenetrated nanogels are developed as high affinity drug delivery agents.[49]

The rational design of multifunctional nanogels having different architectures has a noteworthy effect on the optimization of their performance as nanopharmaceutics. The employment of combined nanomaterials widens the applications of the resulting hybrid nanogel, as shown in **Fig. 1.3**. By incorporation of anisotropic Au or Ag nanoparticles, the nanogels become near-infrared (NIR) absorbing. This peculiar property arises from the plasmonic character of Au and Ag nanoparticles, that can be exploited for obtaining plasmonic nanogels for photothermal therapy and / or imaging agents. The NIR window in the electromagnetic spectrum (λ = 700 – 1300 nm) is useful in medicine, since either water or other components of biological tissues do not absorb in this region.[50] The irradiation of plasmonic nanogels *via* NIR laser may generate hyperthermia in localized tissues at a depth of 10 cm.[51] Other advanced nanomaterials may be employed, to combine their striking properties with those of nanogels. Magnetic Fe nanoparticles may be embedded in the nanogel architecture, to give magnetic nanogels, as cell sorting agents, magnetic resonance imaging (MRI) agents, or hyperthermia agents by application of an alternating magnetic field.[52] Analogously, carbonaceous nanomaterials were used to confer enhanced stiffness, conductivity and NIR activity to nanogels.[49]

The choice of polymer chemistry is also fundamental for achieving functional nanogels, not only regarding their biocompatibility, but also to obtain “smart”, reactive nanogels that can tune their properties according to the desired physicochemical stimuli. The design of advanced nanomaterials for medicine led to the development of “smart” nanogels, that are reactive towards the surrounding environmental conditions, by showing a phase transition regulated by

changes in temperature, pH, ionic strength, reducing conditions, glucose concentration, light, magnetic field, or ultrasound.[49] Many of these stimuli may conform to relevant biological interactions and can therefore interact with target tissues to benefit the therapy's efficacy, through careful tuning of the characteristics of the employed "smart" materials. Other stimuli like light and magnetic field can be applied externally, towards the target tissue to let the nanogel react *in situ*, after successful delivery of the bioactive from the nanogel. A sequential approach may be applied, for the delivery of multiple drugs in separated time instances, by using nanogels that react to multiple stimuli.

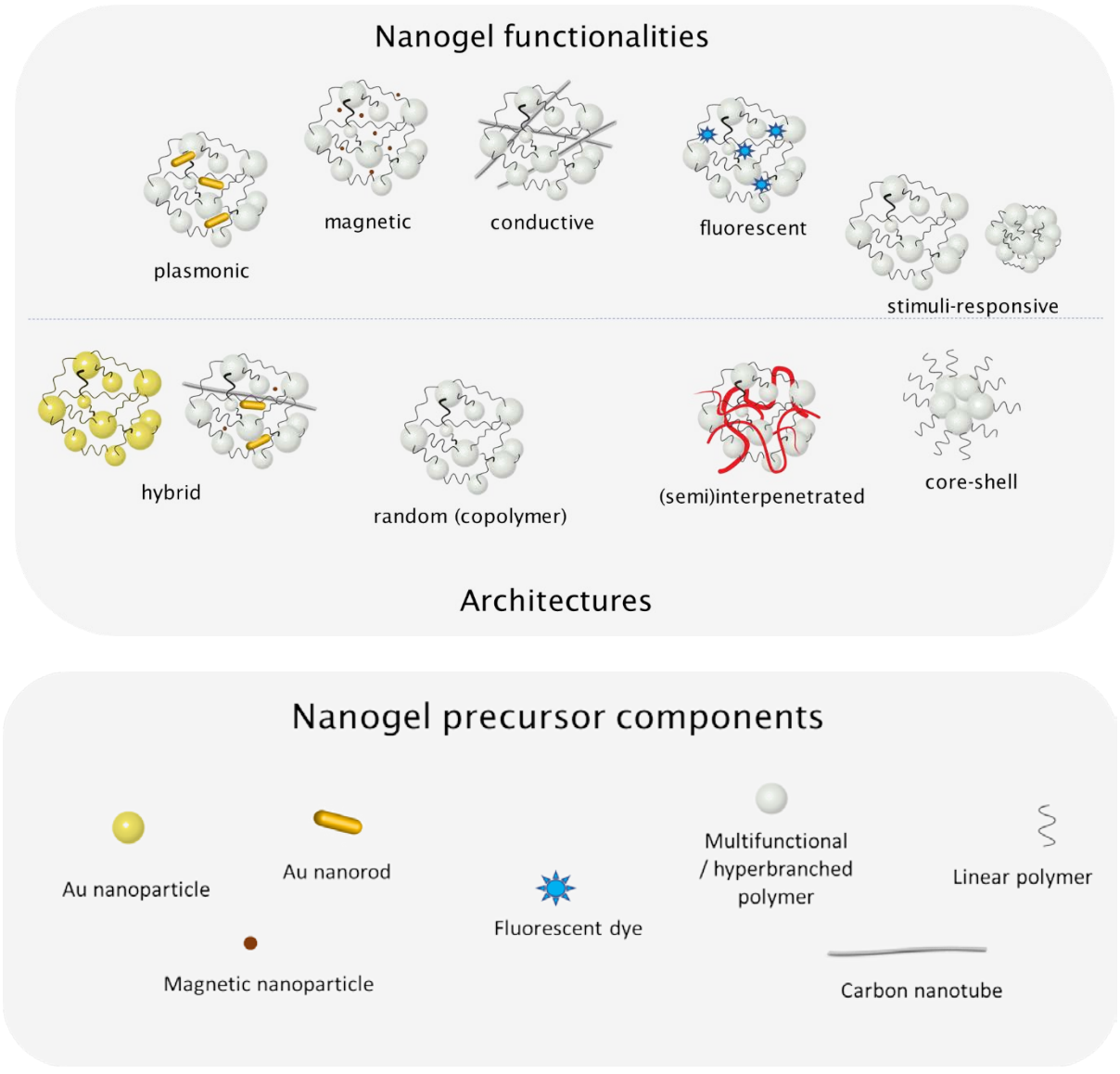

Fig. 1.3 Overview of nanogel architectures and their advanced functionalities

Thermoresponsive nanogels are the most researched for their applicability in various therapeutic instances, due to the readily available thermoresponsive polymers, as the ones shown in **Fig. 1.4**.[19]

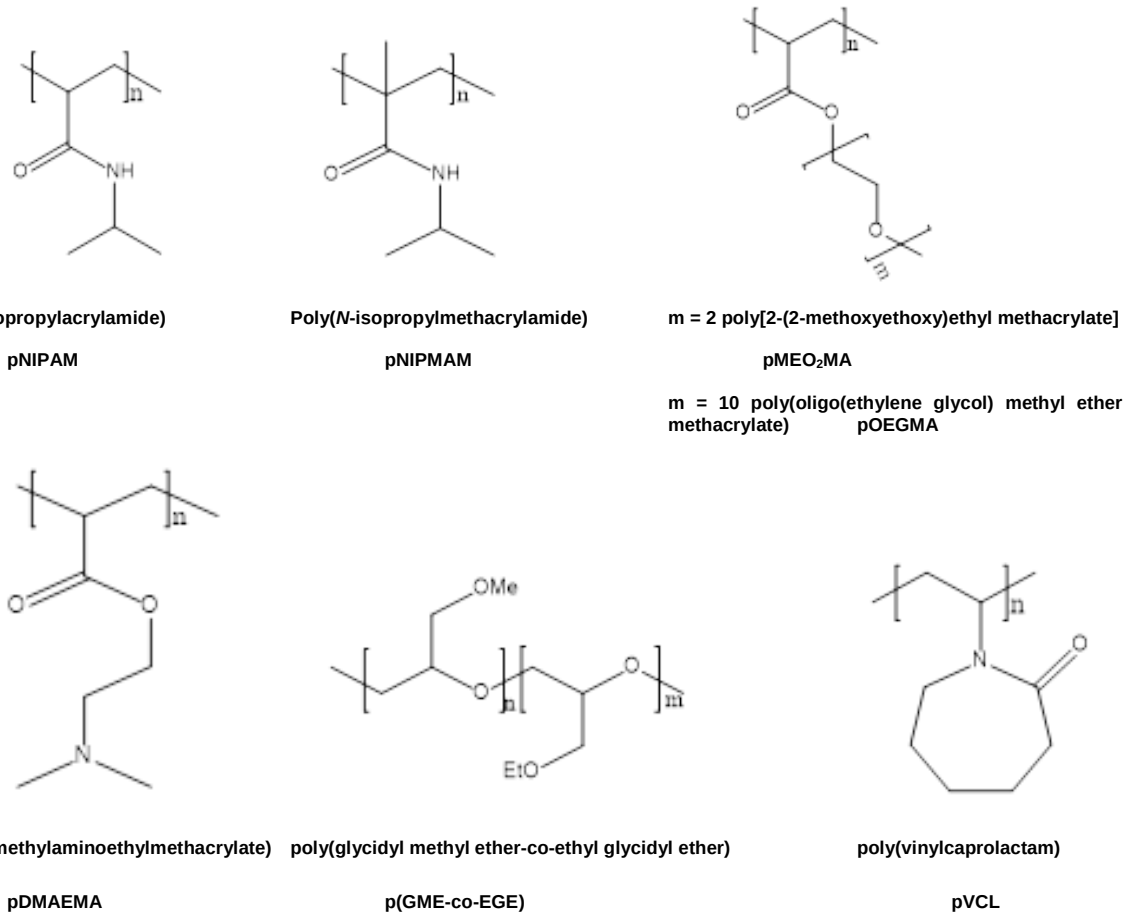

Fig. 1.4 Common LCST-type thermoresponsive polymeric precursors for the synthesis of thermoresponsive nanogels.

Thermoresponsive polymers exhibit a sharp phase transition in water, regulated by the loss of solubility upon reaching of a critical temperature. Polymers with a lower critical solution temperature (LCST) are the most common, and they show solubility in water only below this temperature, with a negative solvation entropy, leading to coil-to-globule transition of the polymer chain above the LCST. Thermoresponsive behavior may be subdivided in three different modes: a type-I thermoresponsive polymer follows a typical Flory-Huggins behavior, leading to concentration and molecular weight-dependent LCST values.[53] Type-II polymers do not show vast LCST variations according to polymer concentration or molecular weight, while type-III polymers show a bimodal thermoresponsive behavior in water.[54] In other less common instances, polymers exhibit an upper critical solution temperature (UCST), with a positive solvation entropy, leading to soluble polymers above this value.[55] Polymers with a CST close to the physiological 37 °C are those which show extended applications in nanomedicine. The CST values can be fine–tuned by changing the hydrophilic / hydrophobic ratio of the polymers in question. The most used thermoresponsive polymer is poly(N-isopropylacrylamide) (pNIPAM), which shows a LCST type-II behavior, with the transition at a constant 32 °C, independently from the polymer chain length / concentration. The LCST close to that of the

human body makes pNIPAM particularly interesting for biomedical purposes. The copolymerization with hydrophilic comonomers, such as acrylic acid or acrylamide would lead to increase of the LCST towards the body temperature. The copolymerization of pNIPAM with hydrophobic comonomers such as N-tert-butylacrylamide would decrease the resulting LCST.[56] Poly(N-isopropylmethacrylamide) (pNIPMAM) shows a LCST type-II behavior at a higher 46 °C. Both pNIPAM and pNIPMAM may be copolymerized, to obtain intermediate LCST values closer to the desired 37 °C. Other examples include 2-(2-methoxyethoxy) ethyl methacrylate (MEO_2MA), oligoethylene glycol methacrylate (OEGMA) and their copolymers, to obtain polymers with tunable LCST.[57] Poly(2-(dimethylamino)ethyl methacrylate) (pDMAEMA) shows dual pH- and thermoresponsiveness,[58] while poly(glycidyl methyl ether-co-ethyl glycidyl ether) (p(GME-c-EGE)) exhibits tunable LCST according to the EGE / GME ratio, also named thermoresponsive polyglycerol (tPG).[59] In turn, poly(N-vinylcaprolactam) (pVCL) is another example of biocompatible polymer, showing a type-I behavior, its LCST value depending on polymer length / concentration in aqueous solution.[53]

By crosslinking such thermoresponsive polymers, one can form nanogels with reversible phase change around their CST. The CST proper of polymers contributes to the overall nanogel phase transition temperature (VPTT). The associated reversible coil-to-globule phase transition may promote the release of the encapsulated cargo from the nanogels in a controlled fashion. Thermoresponsive nanogels may be subjected to phase change upon entering cancerous tissues, that exhibit a temperature gradient with the surroundings, due to increased metabolic rates. A rational tuning of the critical solution temperature of the nanogels may allow the temperature gradient to be used as trigger for drug release. By incorporation of NIR - active nanoparticles inside thermoresponsive nanogels, a similar hyperthermia effect may be activated remotely, *via* NIR laser irradiation. This may be combined with the thermoresponsive polymer network, to get remotely controlled nanogel shrinkage for improved *in situ* drug delivery.

pH-responsive polymers are as well used as nanogel precursors, as they may also act as selective delivery agents towards cancerous tissues, that are slightly more acidic than healthy tissues, or towards specific intracellular compartments that are naturally more acidic, such as endosomes and lysosomes. Other stimuli, such as reducing conditions or concentration of proteolytic enzymes reflect the need of nanoparticles that degrade specifically after their uptake into the cytosol. Glucose concentration was as well investigated as stimulus for diabetes therapy, through the use of phenylboronic acid derivatives as nanogel components, that are specifically swelling after binding with glucose.[49]

1.1.2 Dendritic Architectures in Nanomedicine

Another class of functional materials that were implemented for biomedical applications are dendrons / dendrimers. These macromolecules possess a repetitive branched tree-like structure, that exhibit exponential increase in end points, according to the generation used (number of repetitive branchings). The presence of an array of repetitive end groups favor the multivalent binding of (macro)molecules to dendrimers. By increasing the generation number and end-group chemistry, one could tune the dendron's self-assembly features, to give rise to specific, unique three-dimensional arrangements of macromolecules, ranging from micelles to vesicles, cylindrical micelles to helical ribbons, as well as nanotubes.[60] This property of dendrons make them suitable as nanocarriers, as well as for the development of sensing agents, catalysts, vaccines, agents for MRI contrast, neutron capture, gene therapy, or photodynamic therapy.[61-63] Moreover, the rigidity imposed by the structure of dendrimers opens wide hollow gaps in the dendrimer core, a useful feature for the efficient loading of guest molecules, both hydrophobic or hydrophilic, according to the core chemistry. Their incorporation onto other nanomaterials facilitates their solubilities, inhibiting interchain aggregation of linear polymers.[64] Dendritic structures often exhibit improved characteristics as drug delivery agents as compared to their linear counterparts. The industrial handling of dendritic materials is also facilitated, due to their decreased solution viscosities. Dendrimers and dendrons are monodisperse architectures, they differ from polydisperse architectures (hyperbranched, dendrigrafts, linear – dendritic) for their synthetic methodologies and overall physicochemical characteristics. Dendrimers are globular nanoparticles which bonds stem from a single focal point (core), radially expanding with regular branched units. Dendrons are similarly originating as radial expansion of branched units, however they exhibit anisotropic expansion of the branching units in one favored direction. The intrinsically regular dendritic structures yield monodisperse nanoparticles (PDI = 1.0), a useful feature for high-end technologies. The downside relies in the complexity of the synthesis of a perfect dendron / dendrimer, according to the repetitive chemistry needed to increase the generation number, leading to elevated costs and high amounts of waste products. Hyperbranched polymers exhibit irregular dendritic structures and polydispersity, as they are obtained by non-controlled polymerization techniques. This leads to polymers maintaining many of the dendritic properties, however providing at the same time much lower production costs. **Fig. 1.5** provides an overview of the most used dendritic structures for applications in medicine.

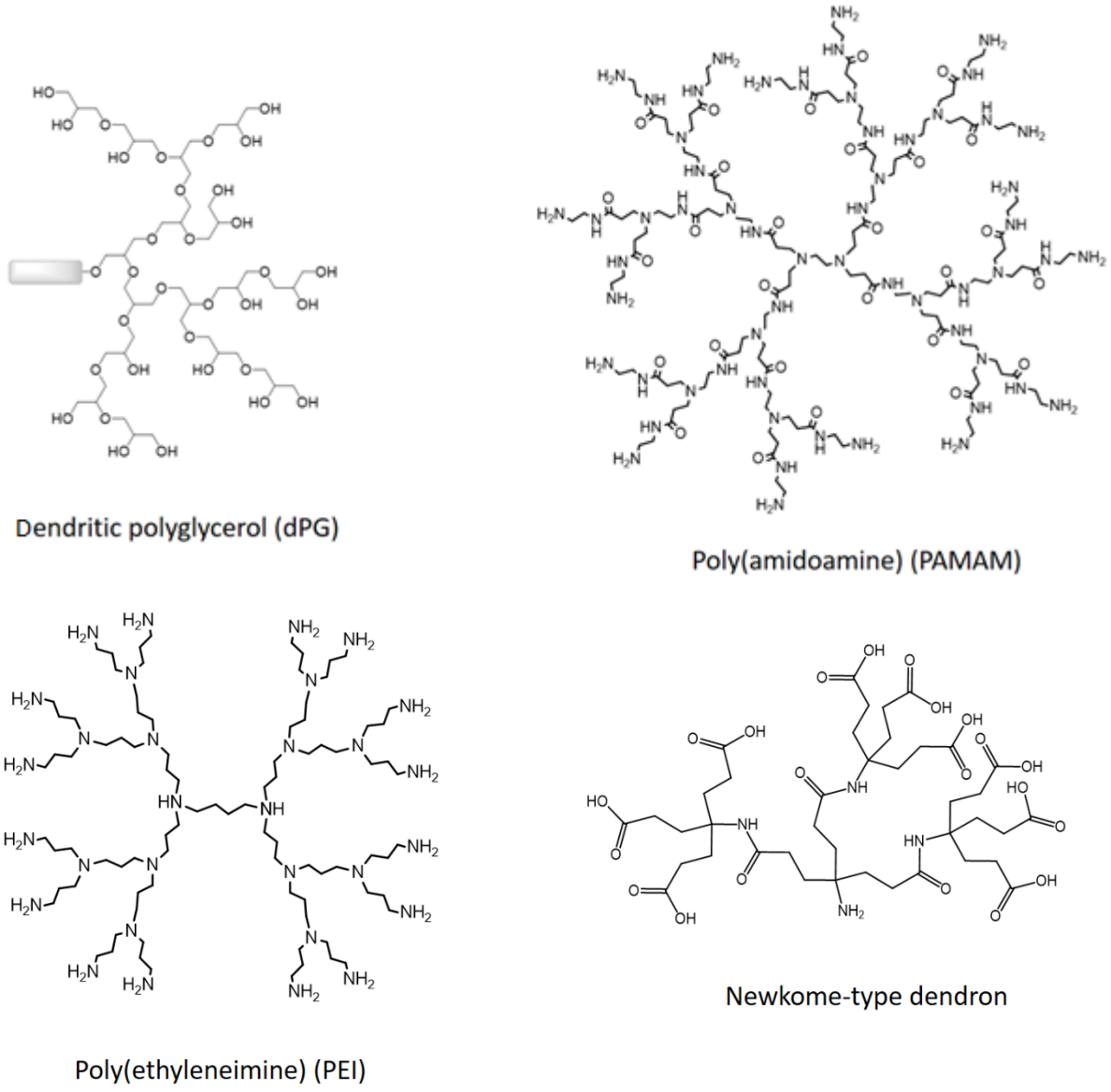

Fig. 1.5 Overview of common dendritic structures with versatile applications in nanomedicine.

Hyperbranched polyglycerol is an example of a dendritic structure, that showed versatility for the generation of biocompatible macromolecules and nanogels for therapeutic purposes.[65] The synthesis of dendritic polyglycerol (dPG) affords *via* controlled, anionic ring-opening polymerization of glycidol. The hyperbranched structure allows the packed polyhydroxyl surface to mimic that of water, is therefore highly soluble and biocompatible. Its tunable size allows for a controlled formation of nanoparticles in the order of 3-10 nm, which size allows a fast renal excretion upon systemic administration of dPG. Its ease of functionalization was exploited for its incorporation inside stimuli-responsive nanogel structures, in order to improve their bioavailability and colloidal stability, even above the LCST of thermoresponsive polymers. They show a broad versatility for their application in anticancer therapy, as well as for topical agents for the treatment of skin diseases [57, 66-69] or as smart components embedded in porous surfaces for the controlled release of proteins.[70] Thermoresponsive dPG-pNIPAM nanogels

developed by the Calderón group show tunable LCST values between 32.5 °C to 34.6 °C, according to the adopted feed ratio of dPG. The nanogels were successfully internalized by human U-937 cells, and show low cytotoxicity.[71] Dual-responsive nanogels were obtained by copolymerization with pH-sensitive 2-(dimethylamino)ethyl methacrylate (DMAEMA), to provide tunable LCST ranging between 37 - 41 °C, and enhanced loading of doxorubicin and methotrexate.[58] In another report by the Calderón group, NIR-active poly(aniline) was semi-interpenetrated into dPG-pNIPAM nanogels, to provide light sensitivity to the nanogels, useful for promoting PTT *in vivo* upon NIR laser irradiation of tumor cells.[72] **Sections 3.1 - 3.3 and 3.5** in this thesis regard the use of dPG-based thermoresponsive nanogels for anticancer therapy and their interactions with blood proteins.

Newkome-type dendrons are a class of polyamidic, dendritic structures that allow easy surface functionalization.[63] They show a 1 -> 3 C-branching pattern (**Fig. 1.5**, bottom right) which impairs high density of functional groups, together with dimethylene spacers that allow high flexibility and avoid steric overcrowding. These materials showed a broad applicability in many technological fields, ranging from catalysis,[73, 74] to biosensing,[75] surface self-assembly [76] and nanomedicine. Newkome-type dendrimers showed interesting features as host-guest interactions promoters, for the solubilization of antichagasic compound (2'-(benzo[1,2-c] 1,2,5-oxadiazol-5(6)-yl (N-1-oxide) methylidene]-1-methoxy methane hydrazide)[77] or the antitumoral benzimidazole carbamate,[78] while the grafting of both polar and apolar versions of Newkome dendrons was successful for the synthesis of hybrid Au nanoparticles [79] as well as dendronized chitosan films for wound repair and antibacterial activity.[80] In another case study, Newkome dendrons were incorporated onto latex beads and functionalized with mannose to obtain glycodendrimers, that were able to modulate $CD3^+$ T-cell proliferation to mimic *Leishmania* activity.[81] Acid-functionalized Newkome dendrons allow the generation of pH-responsive, dendritic linear polymers that are biocompatible and are used as components of thermoresponsive nanogels, both by semi-interpenetration and copolymerization, as shown in **Sections 3.3 and 3.4** of this thesis.

1.1.3 Biosafety Issues in Nanomedicine

The increasingly growing field of nanotechnology reaches over several different fields of applications, from cosmetic to medicine, to high-end consumer electronics, sensing, among others. Many commercially available nanoparticle formulations provide however no long-term solution to the issue of sustainable life-cycles and toxicities after prolonged exposures. It is already well known that the inhalation of microparticles found in the atmosphere as byproducts of combustion constitutes an important health threat to humans, due to the interaction with the alveolar tissues in the lungs.[82] While some information is provided regarding health issues of industrial micro- / nanoparticles and their undesired uptake in biological systems, less is currently disclosed about nanoparticle safety in medicinal applications.

Like any other pharmaceutic agent, a Food and Drug Administration Agency (FDA) approval is required for nanoparticle applications in humans. As of November 2017, 57 drug nanoformulations were approved by the FDA, with other 81 candidates involved in different stages of clinical trials. This framework is in rapid expansion, showing a 3-fold increase in clinical trials between 2013 and 2016.[83] Most of the approved formulations are composed by simple nanoparticle systems, or small drug-polymer conjugates, mostly obtained by PEGylation, for achieving a prolonged circulation in the bloodstream.[84] These formulations differ greatly for their chemical nature, ranging from polymeric or metallic nanoparticles, liposomes, to recently approved micelles or protein-based nanoparticles. Most approved formulations are administered intravenously or orally, while rare cases of topical applications are present as well. A noteworthy increase in clinical trials of nanotherapeutics / imaging agents today signifies a likely expansion of the actual list of approved formulations in the next few years, as depicted in **Fig. 1.6**.

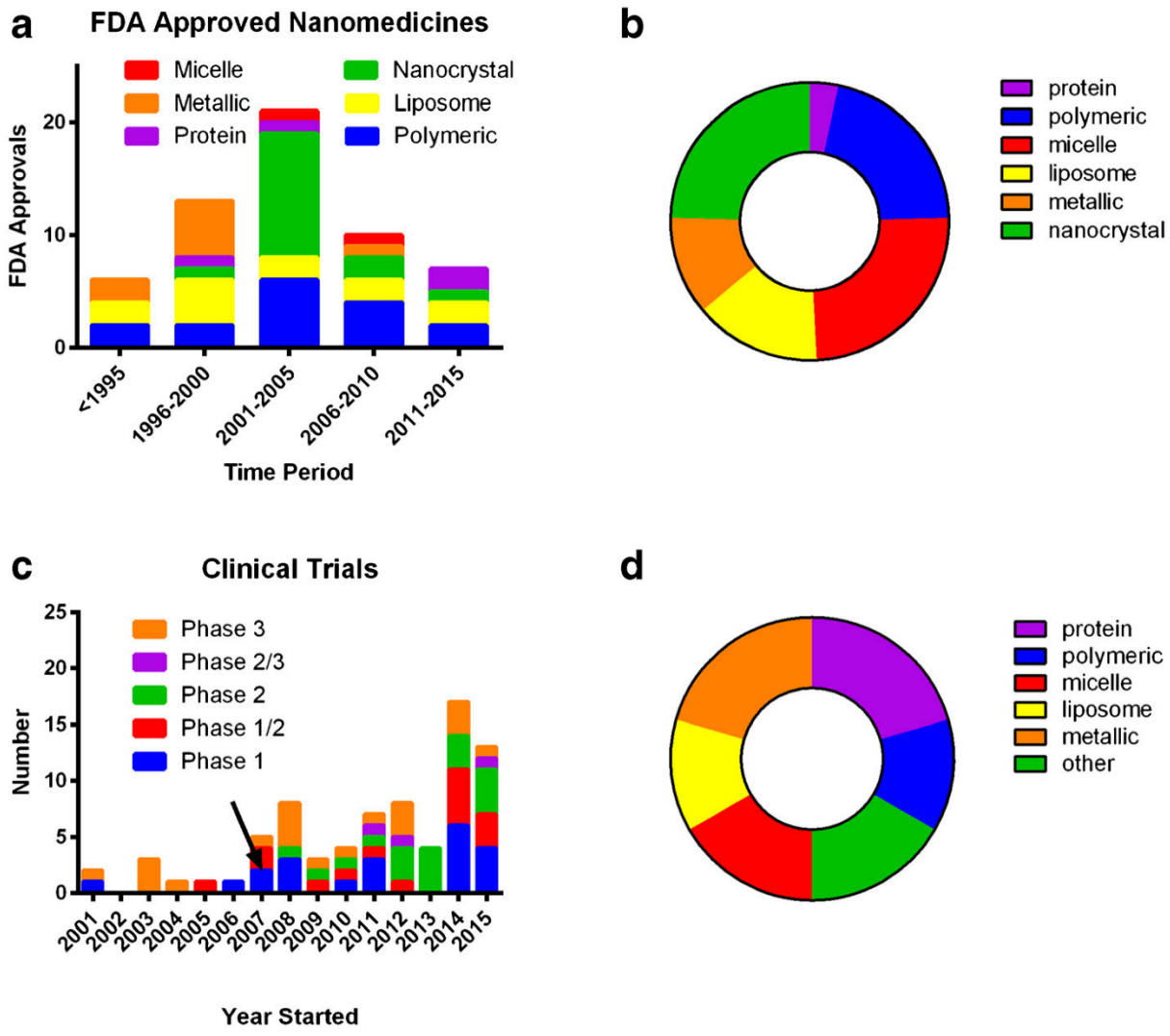

Fig. 1.6 a) FDA approved nanomedicines listed by category and year of approval until 2015; b) classification of approved nanomedicines by category; c) clinical trials ongoing for nanomedicines according to their starting date; d) classification of nanomedicines currently involved in clinical trials for FDA approval, by category. Reproduced with permission from Bobo *et al.*, copyright 2016 Springer. [83]

In average, an FDA approval procedure requires 11 years of clinical investigations, to cover four stages of clinical trials, which overall account for $1 billion expenses for every candidate. During the four stages of clinical trials however, nanoparticle-based treatments often fail, due to issues posed by unexpected biodistributions and / or nanoparticle accumulation in healthy organs, mostly those belonging to the mononuclear phagocyte system (MPS), namely liver, kidneys and spleen.

A new approach in nanosafety is thus needed to understand the issues of wrongful *in vivo* biodistribution, at a molecular level. The strong surface interactions of nanoparticles with the

surroundings is what ultimately has to be investigated *in vitro*, to understand the so-called bio-nano interface, before having to recur to actual *in vivo* tests.

1.2. Blood Compatibility of Nanoparticles

A successful nanoparticle design for *in vivo* applications should comply to a few biophysical principles, regarding their compatibility at the bio-nano interface. Nanoparticle size, surface chemistry, hydrophobicity, roughness and shape are the primary aspects to take into consideration for investigating their surface interactions, as demonstrated in the diagram in **Fig. 1.7**.[26]

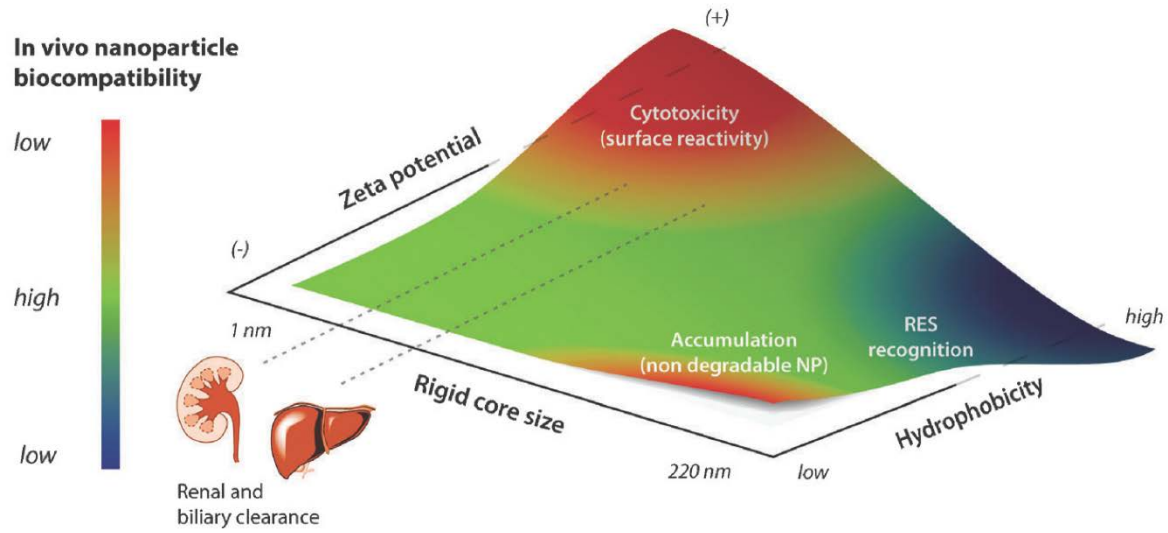

Fig. 1.7 Biophysical assessments of nanoparticle safety and blood availability. Reproduced with modifications from Nel *et al.*, copyright 2009 MacMillan Publishers Limited. [85]

Positively charged nanoparticles are regarded as cytotoxic, due to strong interactions with the negatively charged cell membrane, as a consequence they are as well more likely to induce hemolysis and platelet aggregation.[86] A common example for this behavior was shown by poly(amidoamine) (PAMAM) dendrimers, that are used as stand-alone drugs, as they intrinsically exhibit high cytotoxicity.[87] By reducing cationic densities through coating with hydrophilic polymers (PEGylation), or by using negatively charged or neutral / zwitterionic end-groups, dendrimers and nanoparticles in general show improved biocompatibility and lower toxicities.[88]

Nanoparticle size is another crucial factor that influences *in vivo* bioavailability. Particles smaller than 10 nm will be efficiently cleared by the kidneys, and will not be circulating in the bloodstream after some hours following administration. Particles bigger than 200 nm will be likely be uptaken by the MPS, to be conveyed towards liver and spleen and accumulate in

healthy tissues, as they are not able to escape through the biliar ducts that are only 30 nm wide. Similarly, hydrophobic nanoparticles show van der Waals interactions at a protein level, leading to recognition by the reticuloendothelial system (RES) and cleared from blood circulation.[85] Therefore, an ideal nanoparticle to show prolonged circulation and accumulate into tumor tissues should rely in a size range between 30 – 200 nm and have hydrophilic character by some degree.

All the aforementioned physical characteristics define the nanoparticle's way of interacting with tissues. Since nanoparticles exhibit extremely high surface densities, when compared to their bulk counterparts, they promote the unspecific binding of (macro)molecules onto the nanoparticles' surface. As a result, unpredictable short- and long-term effects on the health of the individual are observed and documented.[89] In order to investigate those effects, studies about blood compatibility are needed, where nanoparticles should be tested for their ability to bind blood components, especially proteins and lipids. While also the cellular component of blood may interact with nanoparticles, especially positively charged nanoparticles that generate hemolysis, major health issues are arising from the unspecific binding of blood proteins, to form a so-called "protein corona".

1.2.1. Biological Implications of the Protein Corona

The human blood is the medium responsible for the circulation of nutrients, oxygen, signaling agents and molecular precursors of tissues in the body, it constitutes roughly 35% of the overall extracellular fluids. Its complex composition shows a 45% amount of cellular components, which are subdivided in erythrocytes, leukocytes and platelets. The cell-free component accounts for the remaining 55% of the blood volume, is also known as plasma. In human plasma, approximately 3700 different proteins are present, in a broad range of concentrations (10^{-8} to 10^{2} g/L) and molecular weights (5 to 700 kDa). Due to the very high protein concentration (60 – 80 g/L according to patient characteristics / water intake) and the extremely high surface density of colloidal nanoparticles, the binding of proteins is a spontaneous and fast phenomenon, when in contact with blood. The kinetics of binding are also very fast, ranging from 10^{-4} s to 10^{3} s for the binding of single proteins onto nanoparticles.[90] The supramolecular protein corona obtained on the surface of nanoparticles has a strong impact on the biodistribution and overall on the biological identity of nanoparticles.

New surface interactions arise with signaling / immune / cell membrane proteins, thus changing the reactivity of nanoparticles unpredictably. For example, the binding of immune proteins, immunoglobulins and complement proteins, may trigger an immune response, which leads to sequestration of nanoparticles from the bloodstream and delivery into the MPS.[91, 92] The process is also called opsonization, and the proteins involved in the process are called

opsonins.[93] Opsonization is not recommended for a nanoparticle-based therapy, unless the purpose is the effective targeting of the organs belonging to the MPS. Another detrimental effect may arise from the binding of prothrombin, that signals initial blood coagulation.[94] On the other hand, carrier proteins in the blood enhance the bioavailability of small drugs, as well as bind to hydrophilic nanoparticles, thereby enhancing their circulation time in blood and preventing their sequestration to the MPS. These proteins are called dysopsonins.[93]

Human serum albumin (HSA) is the main protein of the dysopsonin family, accounting for more than 50% of the overall protein mass in blood. HSA is a natural carrier of cations (Ca^{2+}, K^{+}, Na^{+}), hormones, bilirubin, fatty acids and small hydrophobic drugs. Due to its very high concentration in both serum and plasma, an initial binding of HSA is expected on any nanoparticle, which may be subsequently replaced by proteins exhibiting higher affinities, according to the Vroman effect.[95] Alongside HSA, other dysopsonins such as α-1-acid glycoprotein, afamin, α-2-macroglobulin all belong to the albumin family, they contribute to binding of nanoparticles and improve their retention times, thus favoring the blood availability of the bound nanoparticles. HSA-drug conjugates favor the drug bioavailability, in the same way as nanoparticle-drug conjugates. HSA functions as autonomous nanocarrier in commercially available formulations, for example in Abraxane®, an HSA-paclitaxel conjugate for the handling of metastatic breast and lung cancers.[96]

The presence of certain proteins in the corona of nanoparticles has shown interesting effects on the nanoparticle properties / stability / therapeutic efficacy. The prolonged residence of HSA, as well as ApoA-IV, ApoC-III, or clusterin in the corona of nanoparticles, showed to inhibit nanoparticle cell uptake.[97-99] On the other hand, the presence of vitronectin, ApoA-I, ApoA-II, ApoB-100, ApoC-II, on the protein corona was correlated to an enhanced uptake of nanoparticles through receptor-mediated endocytosis.[97, 100-103]

The presence of one or several layers of coated proteins may shield the active targeting moieties on the nanoparticle's surface by steric crowding,[104-108] except for monoclonal antibodies, that retain their specificity and binding affinities towards their antigen, even in physiological high concentrations of protein.[109] Coincidentally, new protein-cell interactions may generate corona-directed targeting. The presence of apolipoproteins (ApoA-I, ApoB-100) or retinol-binding protein improved targeting of liver Kupffer cells, for the treatment of hyperlipidemia or other cholesterol-related diseases.[110-112] The presence of ApoE was in turn correlated with the ability of nanoparticles to cross the blood-brain barrier (BBB), for improved brain targeting,[113, 114] while vitronectin was promoting association with $\alpha_2\beta_3$ integrin found on cell surfaces, due to the interaction with the tripeptide arginine – glycine – aspartic acid (RGD) motif, found enriched in the protein.[115]

The formation of a protein corona may mitigate the cytotoxicity of nanoparticles, by preventing generation of reactive oxygen species (ROS),[116, 117] or by neutralizing positively charged surfaces of nanoparticles.[118, 119] However, other reports show new cytotoxic effects arising from the loss of the protein's native structure after binding to the nanoparticle's surface.[120-123]

The presence of a layer of coating proteins has a curbing effect on the release kinetics of molecular cargo by nanocarriers, due to sterics that limit free diffusion through the protein layers.[124] This effect may counteract boost release in some instances, to give a more desired sustained kinetics and improve the nanocarrier's efficacy.[125]

The colloidal stability and nanoparticle conformation may also be affected by its protein corona. The most striking example being that of lipoplexes, that are liposomal nanocarriers complexed to nucleic acids for gene transfection. When in contact with proteins, lipoplexes are able to intercalate proteins inside a multilamellar structure, thereby increasing their size and consequently altering the transfection efficiency,[126] while in specific cases the altered lipoplex conformation improved the DNA loading capacity.[127] In other reports, the bridging of nanoparticles due to protein intercalation after incubation in plasma or serum caused nanoparticle aggregation and loss of the colloidal stability of nanoparticles.[128-131]

1.2.2. Physics of Competitive Protein Binding to Nanoparticles

Due to the heterogeneity of blood protein samples, the outcomes of a systematic study about thermodynamics and kinetics of protein corona formation are affected by a wide number of parameters, such as incubation time, protein concentration, temperature, pH and ionic strength. A combination of hydrophobic interactions (van der Waals) with apolar segments of proteins and coulombic interactions with charged residues on the polypeptide chains is the driving force that regulates the thermodynamics of protein binding onto nanoparticles, in a spontaneous attempt to reduce the nanoparticle's surface energy.[132-138] Many physicochemical characteristics of nanoparticles show a direct influence on the protein corona composition, surface charge and hydrophobicity being the two main factors. Nanoparticle size, roughness, and density are also concurring in defining the protein affinity towards nanoparticles, as seen in **Fig. 1.8**.

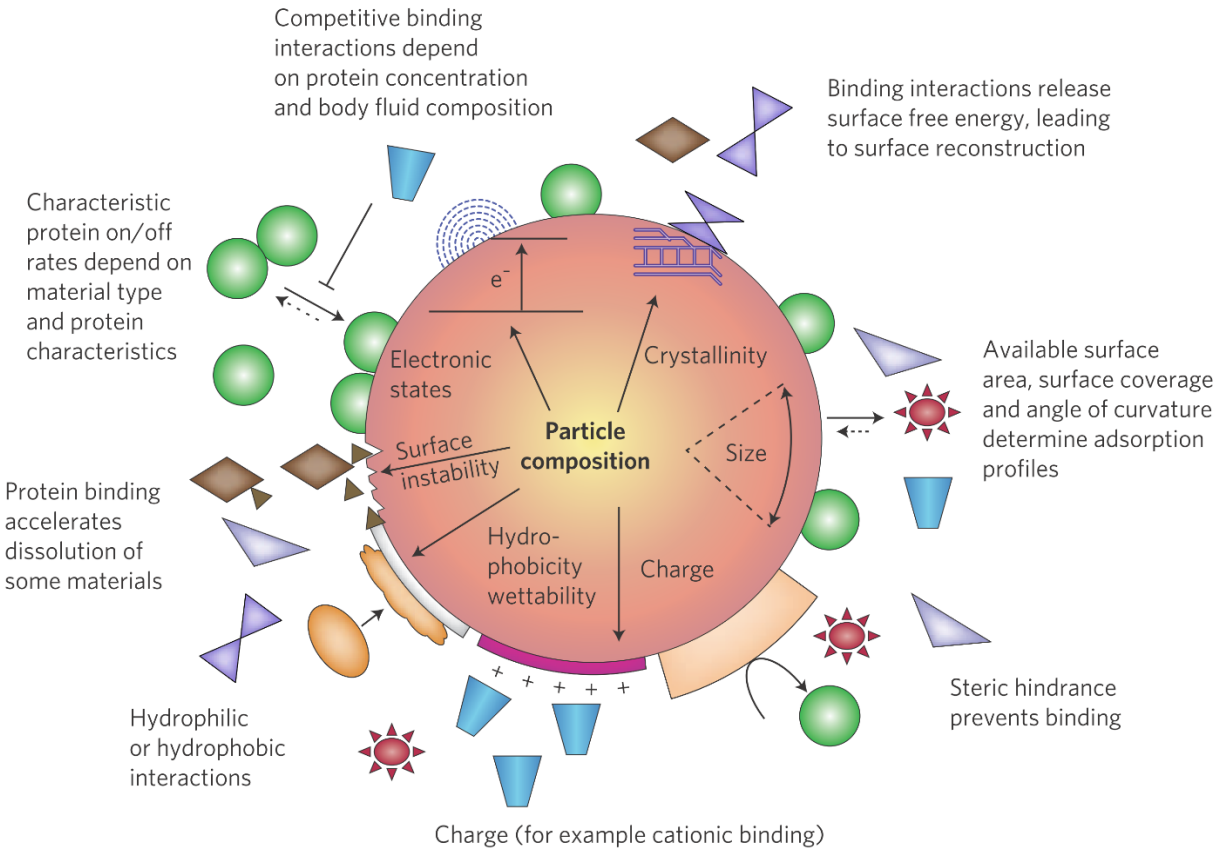

Fig. 1.8 Main physicochemical properties of nanoparticles that influence the protein binding. Reproduced with permission from Nel *et al.*, copyright 2009 MacMillan Publishers Limited. [85]

The size of a nanoparticle is defining its curvature angle. It was shown that the bigger the nanoparticle, the smaller the curvature angle, and the docking of a protein onto a flat surface is a more favored process.[139] In this case, the binding of the first layer of proteins, especially onto big, hydrophobic nanoparticles, may result in protein unfolding, generally by flattening of the protein and loss of native structure.[140] The roughness of a nanoparticle is also associated with an increase in protein binding, due to localized pitfalls in surface energy that promote protein nucleation.[141]

All of the aforementioned trends in protein binding are useful during the initial stage of nanoparticle design for blood compatibility. However, these trends are not able to fully predict the protein corona composition, due to the broad spectrum of variables involved in the process. A few reports approached the issue of modelling thermodynamics of competitive protein absorption processes,[142-146] to predict the protein corona. In presence of multiple different proteins, the process can be formalized into a multicomponent Langmuir absorption isotherm, provided that the protein association is a reversible process. Starting from a single component isotherm, for the modeling of a reversible single protein binding, we get $\Theta = \frac{K_b[P]}{1+K_b[P]}$, where Θ is the fraction of bound sites on a nanoparticle occupied by protein P, with a concentration [P]

and a binding constant K_b. A two-component Langmuir isotherm may be expressed as $\theta_i([P_i],[P_j]) = \frac{K_{b,i}[P_i]}{1+K_{b,i}[P_i]+K_{b,j}[P_j]}$, provided that no protein-protein interactions are involved in the binding process.[147] Knowing the K_b values, measured by isothermal titration calorimetry (ITC) from single protein absorption studies, the two-component isotherm is still solved analytically by a quadratic equation. In more complex environments such as human plasma or serum, due to the great heterogeneity of the protein samples, such an equation may not be solved analytically.

The Langmuir isotherm may also be correlated with the kinetic constants of protein binding, which show $K_b = k_{on} / k_{off}$, where k_{on} is the association constant for the single protein and k_{off} the dissociation constant. The two kinetic parameters usually differ, they range from 10^{-3} s^{-1} to 10^4 s^{-1} for the binding onto nanoparticles.[90] These values relate to a competitive binding setting, where many proteins attach and detach on a single surface. As shown by Vroman in 1986, the association of proteins onto surfaces is a dynamic process, in which a preliminary assembly may arise from the binding of the most abundant proteins in solution, to be gradually replaced by proteins with higher affinities and lower concentrations in the medium (Vroman effect).[95]

Due to multi-component competitive binding, a prediction for the composition of the protein coronae in serum or plasma cannot be assessed *via* modeling of the nanoparticle binding. Thus, for a full quantitative profiling of the protein coronae, *in vitro* protein binding studies are necessary. After incubation in protein - rich media (human plasma or serum, cell culture medium, fetal bovine serum, mouse plasma or serum), the isolation of the protein corona requires several consecutive washing steps to eliminate residual unbound proteins. The separation of the unbound proteins affords usually via centrifugation, size exclusion chromatography,[148] or asymmetrical flow-field flow fractionation.[149] The characterization of the isolated protein corona samples usually involves the use of proteomics (SDS-PAGE, LC-MS) for the quantitative profiling of proteins.[102] Structural information about the nanoparticle-protein corona complex may be obtained by dynamic light scattering (DLS) measurements even without the need of isolating the samples from the incubation medium.[150, 151] For a thermodynamic assessment of the protein binding process, ITC is regarded as the standard methodology.[56, 150, 152] Other methodologies include hyperspectral imaging,[153] fluorescence correlation spectroscopy,[154] or UV-VIS spectroscopy. A combination of these methodologies helps to disclose full information about protein corona of nanoparticles incubated in complex biological media.[155-157]

1.2.3. Protein Corona Around Polymeric Nanoparticles

The research involved in the understanding of nanoparticle interactions with proteins were first implemented for the assessment of the nanotoxicity of hard, inorganic nanoparticles arising from industrial applications and their unwanted interaction with biological tissues.[158-163] The involvement of researchers for the understanding of protein interactions with nanoparticles that were specifically designed for their use in medicine was the next step. In the last ten years, an increasing number of studies were performed to understand the interactions of polymeric or lipid-based nanocarriers with proteins in physiological conditions. In these studies, nanoparticles were incubated in different biological media, mostly human plasma or serum. The two media differ for their protein composition, as serum is thermally inactivated plasma, which leads to fibrinogen polymerization to depleted insoluble fibrin by spontaneous clotting. Human plasma is the full proteinaceous component of blood, and it has added bivalent cations such as Ca^{2+} to stabilize fibrinogen in solution, which in turn inactivates at the same time the complement system. Therefore, depending on the main focus of the studies, a careful choice of the used biological medium is required, especially for the investigation of fibrinogen binding (plasma) or complement activation (serum). This said, for a full protein corona profiling, both media should be investigated in parallel experiments, when applicable.[164] The predictions for protein associations based on the nanoparticle's polymer chemistry shows distinct tendencies. While hydrophilic nanoparticles will bind dysopsonins belonging to the albumin family, in turn hydrophobic nanoparticles will be involved in apolipoprotein binding. A definite number of proteins were found associated to polymeric nanoparticles, especially complement C3, IgG, and fibrinogen, as shown in **Table 1.1**.

Nanoparticle*	Size (nm)	Main components of protein corona*	Ref.
PLA	161	IgG, ApoE, HSA, antithrombin, complement C3, ApoJ	164, 165
PLA-PEG	164-270	IgG, ApoE, HSA, fibrinogen, ApoA-IV, ApoA-I, ApoC-II, Ig light chains	165, 166
PLA-PVP	226-248	Complement C3, C4, C5, C8, C9	166
PLGA	227	ApoE, histidine-rich glycoprotein, vitronectin, kininogen-1, β-2-glycoprotein 1, coagulation factor V, serum amyloid A-4 protein	167
PLGA-PEG	173	ApoE, IgG, fibrinogen, ApoA-IV, ApoA-I	165
PCL-PEG	164	IgG, ApoC-II, HSA, fibrinogen, ApoA-I, ApoC-III, Ig light chains	165
PCL-DEX	136-188	IgG, ApoE, HSA, fibrinogen, ApoA-IV, ApoA-I, complement C3	168
PS-PEG	118	Clusterin	98
PS-PEEP	120	Clusterin	98
PS-Glu	725-853	Complement C3, ApoA-I, ApoA-IV, HSA, ApoC-I, ApoC-III, ApoE	169
PS-Gal	747-852	Complement C3, ApoA-I, ApoA-IV, HSA, ApoC-I, ApoC-III, ApoE	169
PNIPAM-BAM	70-700	ApoA-II, ApoE, HSA, ApoA-IV, ApoA-I, ApoB-100	56, 135, 170
dPG-PNIPAM	127	HSA	171
dPG	115	HSA	171
dPG-NH_2	163	HSA	171
CMS	18	HSA	171
Mannan	170	ApoE, HSA, ApoA-I, ApoB-100	172
PIBCA-DEX	152-297	Fibrinogen, ApoA-I, complement C3	173
PIBCA-DEX-Hep	186	IgG, fibrinogen, complement C3	173
PIBCA-DEX-SO_3^-	274	IgG, fibrinogen, complement C3	173
PIBCA-Hep	93	IgG, fibrinogen	173
PHDCA, PEG-PHDCA	165-171	ApoA-II, IgG, ApoA-I, ApoA-IV, ApoJ, ApoC-II, ApoC-III, ApoE	174
HES capsules	200-275	ApoA-I	150
HES particles	165	ApoJ, fibulin-1	107
HES-PEG	166	ApoA-I, complement C1q, ApoJ	107
HES-PEG-Man	168-176	ApoJ, fibulin-1	107
Ethyl cellulose	175	HSA, complement C3, ApoA-I	175
PMA copolymer (Eudragit®)	62	Complement C4b, ApoB-100, fibronectin, vitronectin, clusterin, ApoA-IV, gelsolin, ApoE	175

Table 1.1 List of main components of protein corona around polymeric nanoparticles. Reproduced with modifications from Miceli *et al.*, copyright 2017 Royal Society of Chemistry.[176]

*PLA = poly(lactic acid); PLGA = poly(lactic-co-glycolic acid); PEG = poly(ethylene glycol); PVP = poly(vinylpyrrolidone); PCL = poly(e-caprolactone); DEX = dextran; PS = polystyrene; PEEP = poly(ethyl ethylene phosphate); Glu = glucose; Gal = galactose; PNIPAM-BAM = poly(N-isopropylacrylamide-co-tert-butylacrylamide); dPG = dendritic polyglycerol; CMS = core multi-shell nanocarrier; PIBCA = poly(isobutylcyanoacrylate); Hep = heparin; PHDCA = poly(hexadecylcyanoacrylate); HES = hydroxyethyl starch; Man = mannose, PMA = poly(methacrylic acid). Apo = apolipoprotein; Ig = immunoglobulin; HSA = human serum albumin.

By comparing the behavior with blood proteins of inorganic nanoparticles, polymeric nanoparticles seem to bind a less diverse group of proteins, supposedly due to their soft nature. The binding of IgG and complement C3 was found in many instances, while these proteins are opsonins, their impact on the clearance of the bound nanoparticles cannot be understood without analyzing the interactions with macrophages, as a follow up study. It is known that an immune reaction may be initiated only when a substantial amount of opsonins were depleted from human plasma and bound to the nanoparticles.[177]

Another common feature of protein corona of polymeric nanoparticles is the binding of apolipoproteins, such as ApoA-I, ApoB-100, ApoE, ApoA-IV, ApoC-II, ApoC-III, among others. The binding of apolipoproteins is ubiquitous in hydrophobic nanoparticles, and according to the ApoA-I / ApoB-100 ratio found in the corona, a switch from high density lipoprotein (HDL) to low density lipoprotein (LDL) can occur.[170] The values of lipoprotein concentration in blood are indicative of cholesterol-related diseases, and the presence of nanoparticles inside these lipoproteins may target the lipid metabolic processes and act as therapeutics. As previously discussed, ApoE in the corona may act as vector for the targeting of nanoparticles towards the brain,[113, 114] while other apolipoproteins interact with the nanoparticle's ability to target and / or penetrate cellular compartments.[97-103]

pNIPAM copolymer nanogels showed a protein corona that was dependent on the copolymerization degree with N-tert-butyl acrylamide (BAM). The presence of the hydrophobic BAM increased the apolipoprotein binding, towards full lipoprotein (HDL) formation for nanogels having a 1:1 pNIPAM / BAM ratio. By increasing the hydrophilicity of the nanogels towards a 65:35 pNIPAM / BAM ratio, no lipoproteins were residing anymore in the corona.[170] A further discussion on the protein corona of pNIPAM-based nanogels is provided in **Sections 3.1-3.2** of this thesis.

Overall, the binding of proteins onto nanoparticles is a complex interplay of multiple macromolecular actors, to generate heterogeneous supramolecular structures, that drastically alter the way in which the underlying nanoparticle is perceived, when interacting with biological tissues. The efficacy of therapeutic nanoparticles cannot be investigated without considering their interactions with proteins in a physiological environment, which may also help reducing harmful and failing *in vivo* tests. The protein corona itself may impair new improved characteristics to the nanoparticle, for a better bioavailability, reduced toxicity, improved release characteristics, or an improved targeting towards diseased tissues. The pre-coating with specific proteins before the intravenous administrations of nanoparticles may partially direct the structure of the protein corona *in vivo*, by delaying the Vroman effect, for an improved nanocarrier stability.[130, 178, 179]

2. Motivation and Objectives

This work addresses the need for an improved design and performance of stimuli-responsive nanogels as macromolecular drug carriers in the framework of cancer therapy. The clinical target applications of nanogels require the optimization of the features of next generation drug carriers, obtained from a narrow range of starting materials, for an improved target selectivity and *in situ* drug delivery. pNIPAM-based nanoparticles show a wide range of applications for the fabrication of thermoresponsive devices, their application in medicine is of strong interest, due to its LCST close to the human body temperature. However, conventional pNIPAM nanoparticles exhibit LCST-dependent interchain aggregation in the micrometer range. The incorporation of dPG as nanogel component gives colloidally stable nanogels even above the pNIPAM LCST.[71] Thermoresponsive, dendritic dPG-pNIPAM nanogels function as biocompatible drug delivery agents and the screening of different synthetic strategies for their optimization will be investigated in **Section 3**. The combination of innovative materials (dendritic or linear polymers), together with implementing different three-dimensional architectures into nanogels is the main paradigm of this thesis. In this way, new strategies will be used for the synthesis of stimuli-responsive nanogels, which allow an improved performance for drug loading and sustained release, and at the same time provide safe interaction with blood proteins, as shown in **Fig. 2**.

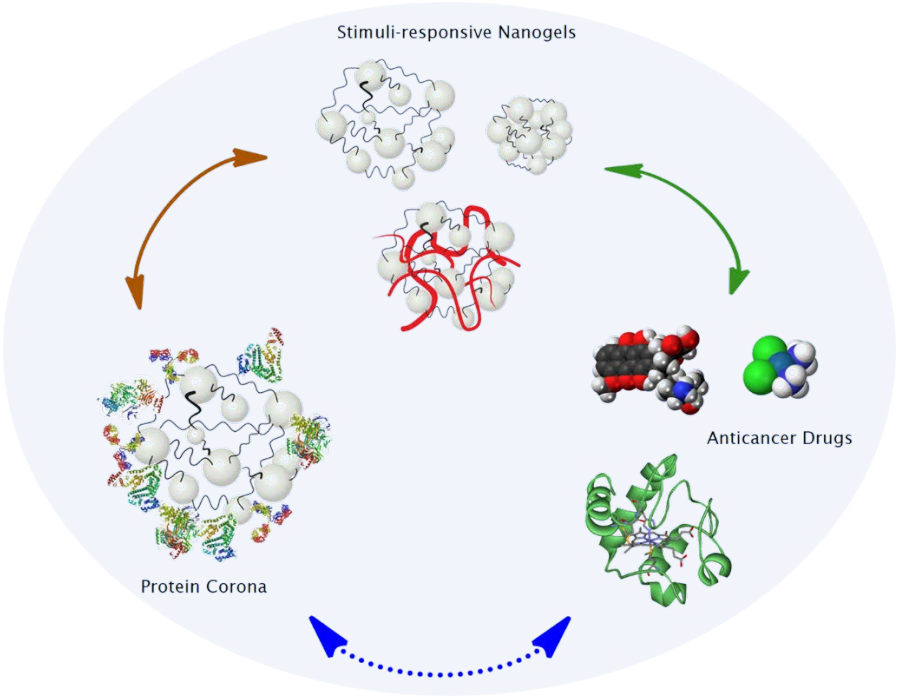

Fig. 2. Main research topics involved in this doctoral thesis work. The interactions between stimuli-responsive nanogels and chemotherapy drugs, together with their interplay with serum proteins are crucial factors involved in the design of successful new generation nanogels for anticancer therapy.

The ability of dPG to inhibit the unspecific binding of proteins in physiological conditions is a fundamental part of the studies conducted in this thesis, as shown in **Sections 3.1 – 3.2**. The resulting findings will disclose information regarding the interactions at the bio-nano interface, which can lead to a new biological identity of the nanogels by formation of a protein corona. As a consequence, the performances of nanogels as drug carriers will be affected. Thus, the studies in this thesis are needed to assess these implications, to give a better understanding on the strong impact of the protein corona on the nanogel's morphology and function.

Semi-interpenetration is a useful way to obtain multicompartimental, dual-responsive nanogels, without perturbing the ability of dPG-pNIPAM nanogels to respond to thermal stimuli. The synthesis of responsive nanogels and the investigation of release kinetics of encapsulated drugs poses the fundaments for the framework of the research in this thesis and the related published articles. The optimal tuning of binding affinities towards therapeutic molecules of interest, as well as the responsive modalities of the nanogels to respond to changes in the surrounding environment will be explored with a screening of synthetic conditions and different polymer ratios. In this way, semi-interpenetrated nanogels are obtained, to achieve pH-responsive networks within the thermoresponsive nanogel scaffolds, for the optimal binding and sustained release of therapeutic proteins (**Section 3.3**), as well as small drugs (**Section 3.5**).

The use of dendritic components is investigated in detail, as they can be implemented in combination with linear polymers, and function as multifunctional agents, in order to tune the reversible binding of therapeutic moieties. The effects of introducing a Newkome-type dendron as dendritic component in nanogels will be thoroughly discussed in **Sections 3.3 - 3.4**. In this way, this thesis attempts to fully assimilate all efforts reported for the screening of synthetic conditions for obtaining stimuli-responsive nanogels, and successfully translate them into clinical outcomes.

3. Publications and Manuscripts

3.1 Temperature dependency of elusive protein corona around thermoresponsive nanogels: key interactions above the lower critical solution temperature

E. Miceli, B. Kuropka, C. Rosenauer, E. R. Osorio Blanco, L. Fechner, M. Kar, C. Weise, S. Morsbach, C. Freund, M. Calderón, *manuscript submitted.*

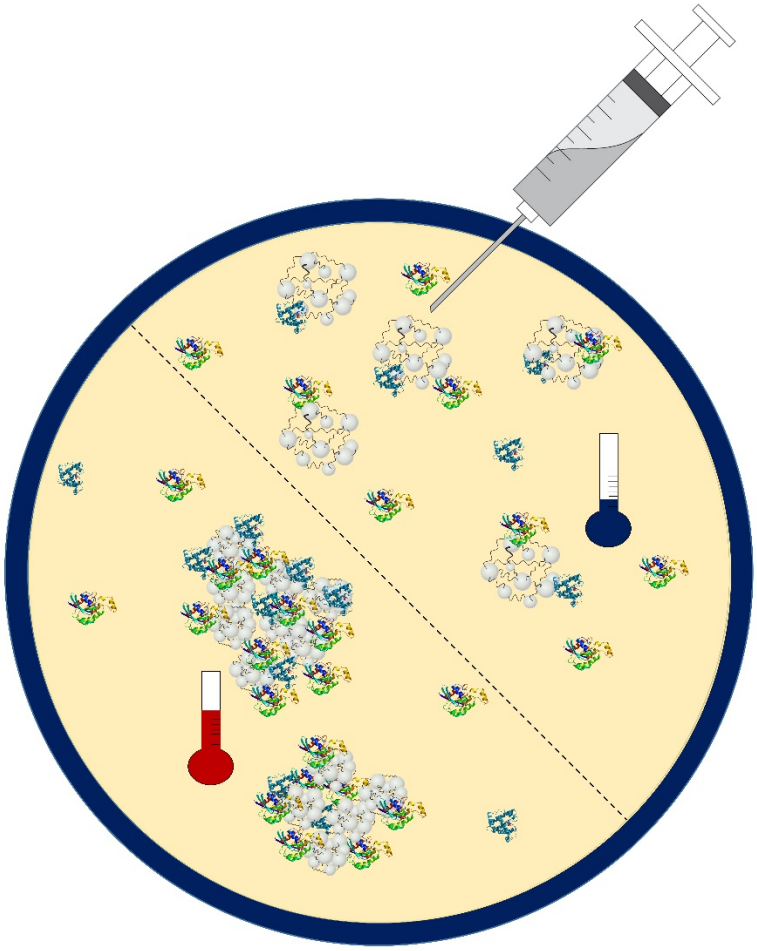

Fig. 3.1 Thermoresponsive dPG-pNIPAM nanogels show temperature-dependent aggregation in serum.

Author contribution: In this work, the author was responsible for the overall concept, the synthesis of thermoresponsive nanogels with screening of different dPG / thermoresponsive polymer ratios, as well as the generation of the protein corona samples and their isolation from human serum. The coordination with the research partners for the characterization of the protein corona was also done by the author, as well as the writing of the research report.

Abstract: In this work, a systematic study about protein corona characterization around thermoresponsive nanogels was carried out. Both dendritic polyglycerol (dPG) and poly(N-isopropylacrylamide) (pNIPAM) are regarded as protein-resistant, biocompatible materials, thus we analyzed the elusive protein corona of thermoresponsive, pNIPAM- or poly (N-isopropylmethacrylamide) (pNIPMAM)-based nanogels (NGs), crosslinked with dPG or N,N'-methylenebisacrylamide (BIS). At 37 °C, we compare protein coronae of shrunken dPG-pNIPAM NGs with swollen dPG-pNIPMAM NGs, to examine the influence of the NG solvation state on its protein binding. All dPG-containing NGs showed drastically lower protein absorption when compared with NGs without dPG. Apolipoprotein B-100 (ApoB) and serum albumin (HSA) were the main components of the protein coronae of NGs, alongside complement C3, C4, α-2-macroglobulin and transferrin. For dPG-pNIPAM NGs, a temperature-dependent protein corona profile was observed. At 37 °C, when pNIPAM is hydrophobic, a pronounced aggregation was detected in serum, as well as a specific increase in immunoglobulin absorption in the low abundance regime. Overall, we found that small changes in the composition of protein corona around thermoresponsive nanogels may affect the NG's colloidal stability and in vivo biocompatibility. Thus, similar studies are encouraged for other nanoparticle-based systems, to understand their propensity to bind proteins on their surface and preview their unspecific association with other components in tissues. The corona-dependent aggregation of dPG-pNIPAM NGs at 37 °C may be exploited for enhanced localized toxicity. dPG-PNIPMAM NGs are hydrophilic at 37 °C and show safe profiles in serum for their use as drug carriers, due to a dysopsonin-rich protein corona.

Temperature dependency of elusive protein corona around thermoresponsive nanogels: key interactions above the lower critical solution temperature

Enrico Miceli[ab], Benno Kuropka[a], Christine Rosenauer[c], Ernesto Rafael Osorio Blanco[a], Loryn Fechner[a], Mrityunjoy Kar[a], Christoph Weise[ab], Svenja Morsbach[c], Christian Freund[a], Marcelo Calderón[ab]*

a) Freie Universität Berlin, Institute of Chemistry and Biochemistry, Takustr. 3, 14195 Berlin, Germany.

b) Helmholtz Virtual Institute ‘‘Multifunctional Biomaterials for Medicine’’, Kantstr. 55, 14513 Teltow, Germany

c) Max Planck Institute for Polymer Research, Ackermannweg 10, 55128 Mainz, Germany

*E-mail: marcelo.calderon@fu-berlin.de

Abstract

An intravenous administration of nanoparticles used for drug delivery faces the hurdle of the unspecific binding of proteins, to form a so-called protein corona. Such a supramolecular structure may induce unpredictable protein-cell associations, that influence the nanoparticle’s biodistribution profile, leading to changes in therapeutic efficacy and overall to a new biological identity. The use of antifouling polymers in nanoparticle synthesis helps decreasing unspecific protein absorption, however not quantitatively. While both dendritic polyglycerol (dPG) and poly(*N*-isopropylacrylamide) (pNIPAM) are regarded as protein-resistant, biocompatible materials, we analyzed the elusive protein corona of thermoresponsive, pNIPAM- or poly (*N*-isopropylmethacrylamide) (pNIPMAM)-based nanogels (NGs), crosslinked with dPG or *N,N’*-methylenebisacrylamide (BIS). pNIPAM and pNIPMAM exhibit sharp, reversible phase transitions at 33 °C and 46 °C, respectively, due to entropy-driven interchain aggregation. At 37 °C, we compare protein coronae of shrunken dPG-pNIPAM NGs with swollen dPG-pNIPMAM NGs, to examine the influence of the NG solvation state on its protein binding. All dPG-containing NGs showed drastically lower protein absorption in comparison with BIS-crosslinked NGs. Traces of protein corona detected after 1 h incubation in human serum at either 25 °C or 37 °C were characterized by quantitative proteomics. Apolipoprotein B-100 (ApoB) and serum albumin (HSA) were the main components of the protein coronae of NGs, alongside complement C3, C4, α-2-macroglobulin and transferrin. For dPG-pNIPAM NGs, a temperature-dependent protein corona profile was observed. At 37 °C, when pNIPAM is

hydrophobic, a pronounced aggregation was detected in serum, as well as a specific increase in immunoglobulin absorption in the low abundance regime. Overall, we found that small changes in the composition of protein corona around thermoresponsive nanogels may affect the NG's colloidal stability and *in vivo* biocompatibility. A corona-dependent aggregation of NGs may be exploited for enhanced localized toxicity. The small changes in protein corona composition arose from the NG solvation state, regulated by the choice of thermoresponsive polymer as well as the system temperature. dPG-pNIPMAM NGs are hydrophilic at 37 °C and show safe profiles in serum and a dysopsonin-rich protein corona.

Introduction

Nanogels (NGs) are nanosized, crosslinked polymers that absorb large quantities of water. Stimuli-responsive NGs may be obtained by employing "smart" materials, whose properties can be regulated by applying changes in the environmental conditions. Physical stimuli such as changes in temperature, pH, light, enzyme or disulfide concentrations may be used to control the properties of NGs. [1] Poly(*N*-isopropylacrylamide) (pNIPAM) and poly(*N*-isopropylmethacrylamide) (pNIPMAM) polymers exhibit temperature-dependent solubilities, as they show a coil-to-globule transition around their lower critical solution temperature (LCST). Such polymers allow the synthesis of NGs that exhibit reversible shrinking/swelling around the LCST (33 °C and 46 °C, respectively for pNIPAM and pNIPMAM). [2, 3] The use of pNIPAM as a thermoresponsive polymer is widespread and has been thoroughly researched in the last 24 years as the gold standard for thermoresponsive NGs. [4] Its LCST of 33 °C, close to the temperature of the human body, together with low unspecific plasma protein absorption [5], no hemolytic activity, and antithrombotic behavior, [6] make pNIPAM a polymer of choice for biomedical applications. [1] In order to overcome pNIPAM aggregation above its LCST, our group reported the synthesis of thermoresponsive pNIPAM NGs, with the aid of dendritic polyglycerol (dPG) as macromolecular crosslinker. dPG-pNIPAM NGs are colloidally stable above the pNIPAM LCST since dPG increases the hydrophilicity of the NG to counterbalance pNIPAM interparticle aggregation. [7] The use of dPG has proven beneficial as antifouling polymer / nanoparticle (NP). It showed no complement activation as well as no induced cytotoxicity and very low affinity for protein binding. [8] dPG belongs to a class of antifouling materials, such as poly(ethylene glycol) (PEG), poly(ethyl ethylene phosphate) (PEEP), [9] or zwitterionic polymers, [10] that have been demonstrated to improve NP biocompatibility, however, many times they show traces of protein corona. The binding of proteins on the surface of NPs is an unavoidable phenomenon, when nanoparticles are immersed in bodily fluids, such as blood plasma or serum. [11] As a result, a supramolecular protein corona alters the therapeutic properties of NPs by introducing new protein - protein, or protein - cell

interactions. [12-14] Such new interactions may benefit the host NP in some instances, however, usually they reduce NP potency [12] as well as confer toxicity due to opsonization and accumulation in the mononuclear phagocyte system (MPS). [15] It is therefore of fundamental importance to characterize the protein corona around NPs, to gain an understanding of NP blood compatibility and *in vivo* therapeutic efficacy. [16]

The main driving forces regulating NP - protein binding are hydrophobic (van der Waals) and coulombic interactions. Other NP properties (size, roughness, density) are directly affecting the protein binding, as shown by several experimental and computational reports. [16-18] As a result, hydrophobic and charged NPs are more prone to protein binding, and by regulating these two factors one could steer the protein corona towards a more desired composition. While it is not possible to maintain a specific composition of the protein corona due to constant exchange of bound proteins (Vroman effect), [17] another strategy that was proven beneficial to partially control the corona composition is the pre-coating of NPs with the desired proteins, prior to their incubation in biological fluids. [18]

While there are no reports for the protein corona of pNIPMAM, previous reports for pNIPAM NGs show little to no absorption of proteins. [5, 12] By increasing the hydrophobicity of pNIPAM, through copolymerization with tert-butylacrylamide, an increase in apolipoproteins and full lipoproteins (mostly HDL) was reported in the corona below the LCST. [19, 20] Overall, these studies lack, however, the understanding of the role of pNIPAM thermoresponsiveness on its protein absorption behavior. In fact, for thermoresponsive poly(2-isopropyl-2-oxazoline) NPs, studies show a temperature dependency of the protein corona, and a reversible aggregation of NPs when incubated in human serum above their LCST. [21]

This study aims to distinguish between protein coronae of dPG-pNIPAM NGs in the two different solvation states of pNIPAM (swollen at 25 °C, shrunken at 37 °C), as well as understanding the influence of the antifouling dPG on the protein corona. Furthermore, we compare protein coronae of shrunken dPG-pNIPAM and swollen dPG-pNIPMAM NGs at 37 °C, to gain insight into the role of the NGs' solvation state. Structural data was provided by dynamic light scattering (DLS) in concentrated human serum, which could determine a size increase of the species *in situ*, without having to isolate the sample from the medium. Liquid chromatography-electrospray ionization-tandem mass spectrometry (LC-ESI-MS/MS) in conjunction with ^{18}O-labeling was performed to achieve a quantitative profile of the compositions of the elusive protein coronae.

Materials and Methods

dPG-pNIPAM NGs were synthesized by one-pot precipitation polymerization according to procedures already published by our group. [7] The same procedure was adapted for the synthesis of dPG-pNIPMAM NGs by using potassium persulfate as initiator and discarding tetramethylethylenediamine as accelerator. Different feed ratios of dPG were used to obtain NGs with increasingly high dPG amounts. The synthesis of pNIPAM/BIS and pNIPMAM/BIS NGs was performed by similar procedures previously reported in the literature. [4]

The incubation of NGs in human serum was performed by mixing a 20 mg/mL NG solution with an approximately 9-fold excess in volume of human serum, provided to keep the NG surface density constant at 8 m^2 / L serum. All samples were incubated for 1 h, either at 25 °C or 37 °C.

The isolation of the protein corona was performed by ultrafiltration (molecular weight cutoff MWCO = 1 MDa) by washing with excess PBS, which was previously kept at a constant 25 °C or 37 °C, according to the previous incubation temperature in serum. Short centrifugation steps of maximum 10 s were employed to prevent sample cooling from 37 °C.

In order to quantify protein amount, Bradford assay was used: 100 mg Coomassie Brilliant Blue G250 was dissolved in 50 mL of Ethanol, 100 mL of concentrated phosphoric acid was added, and the volume was adjusted to 200 mL with MilliQ water. The reagent was mixed in a 1:1 ratio to the protein sample, absorbance values were recorded at 595 nm.

The obtained NG-protein corona samples were filtered through a 450 nm syringe filter and proteins were eluted with SDS sample buffer at 95 °C for 10 min. Subsequently, the corresponding samples were separated by SDS-PAGE (Tris-glycine gradient gel, 10%, Bio-Rad). The run was stopped after 2 min so that all proteins were retained in a single gel band. Gel bands of corresponding samples were cut, reduced with 100 mM dithiothreitol (DTT) and alkylated with 55 mM iodoacetamide. In-gel protein digestion and $^{16}O/^{18}O$-labeling was performed as described. [22, 23] In brief, corresponding samples were incubated overnight at 37 °C with 50 ng trypsin (sequencing grade modified, Promega) in 25 µL of 50 mM ammonium bicarbonate in the presence of heavy water (Campro Scientific GmbH, 97% ^{18}O) and regular ^{16}O-water, respectively. To prevent oxygen back-exchange by residual trypsin activity, samples were heated at 95 °C for 20 min. After cooling down, 50 µL of 0.5% TFA in acetonitrile was added to decrease the pH of the sample from ~8 to ~2. Afterwards, corresponding heavy- and light-isotope samples were combined and peptides were dried under vacuum. Peptides were reconstituted in 15 µL of 0.1% (v/v) TFA, 5% (v/v) acetonitrile and 6.5 µL were analyzed by a reversed-phase capillary nano liquid chromatography system (Ultimate 3000, Thermo Scientific) connected to an Orbitrap Velos mass spectrometer (Thermo Scientific). The LC

system was coupled to the mass spectrometer via a nanospray flex ion source equipped with a stainless-steel emitter (Thermo Scientific). Samples were injected and concentrated on a trap column (PepMap100 C18, 3 µm, 100 Å, 75 µm i.d. × 2 cm, Thermo Scientific) equilibrated with 0.05% TFA, 2% acetonitrile in water. After switching the trap column inline, LC separations were performed on a capillary column (Acclaim PepMap100 C18, 2 µm, 100 Å, 75 µm i.d. × 25 cm, Thermo Scientific) at an eluent flow rate of 300 nL/min using a linear gradient of 3–50% B in 50 min. Mobile phase A contained 0.1% formic acid in water, and mobile phase B contained 0.1% formic acid in acetonitrile. Mass spectra were acquired in a data-dependent mode utilizing a single MS survey scan with a resolution of 60,000 in the Orbitrap, and MS/MS scans of the 20 most intense precursor ions in the linear trap quadrupole. The MS survey range was m/z 350-1500. The dynamic exclusion time (for precursor ions) was set to 60 s and automatic gain control was set to 1×10^6 and 5.000 for Orbitrap-MS and LTQ-MS/MS scans, respectively.

Identification and quantification of $^{16}O/^{18}O$-labeled samples was performed using the Mascot Distiller Quantitation Toolbox (version 2.6.1.0, Matrix Science). Data were searched against the SwissProt human protein database (May 2017). A maximum of two missed cleavages was allowed and the mass tolerance of precursor and sequence ions was set to 10 ppm and 0.35 Da, respectively. Cysteine carbamidomethylation was set as a fixed modification. Methionine oxidation, acetylation (protein N-terminus), and C-terminal $^{18}O_1$- and $^{18}O_2$-isotope labeling were used as variable modifications. A significance threshold of 0.05 was used based on decoy database searches. For quantification at protein level, a minimum of two quantified peptides was set as a threshold. Relative protein ratios were calculated from the intensity-weighted average of all peptide ratios. Known contaminants (e.g. keratins) were removed from the protein output tables. Normalization of protein ratios was performed using the median ratio of all proteins. Only proteins that were identified and quantified in all three replicates were considered.

All light scattering experiments were performed on a commercially available instrument from ALV GmbH (Langen, Germany) consisting of an electronically controlled goniometer and an ALV-5000 multiple tau full-digital correlator with 320 channels (resolution of $10^{-7}\ s \leq t \leq 10^3\ s$). A HeNe laser with a wavelength of 632.8 nm and an output power of 25 mW (JDS Uniphase, Milpitas, USA, Type 1145P) was utilized as the light source. For each sample containing a mixture of serum and NPs 1 mL of concentrated serum was filtered through Millex GS filters with a pore size of 220 nm (Merck Millipore, Billerica, USA) into dust-free quartz light scattering cuvettes (inner diameter 18 mm, Hellma, Müllheim), which were cleaned before with acetone in a Thurmont-apparatus. Afterwards, 25 µL of the corresponding NP suspension with a concentration of 1 w/w% were added. For reference measurements either pure serum (1 mL,

filtered with Millex GS 220 nm) or NPs in MilliQ water (25 µL NP suspension in 1 mL water, Millex GS 220 nm filtered) were used. All samples were incubated at either 25 °C or 37 °C for 1 hour prior to the measurement.

Data analysis was performed according to the procedure described by Rausch et al.[24] using exponential fits of pure serum and pure NP suspensions as a reference. The mixture of both was then fitted by the sum of the pure components and additionally formed species were described by an additional exponential term, giving the intensity contribution and decay rate of the found diffusing species.

Results and discussion

We synthesized NGs by one-pot precipitation polymerization of NIPAM or NIPMAM, by crosslinking with dPG-acrylate or *N,N'*-methylenebisacrylamide (BIS), according to procedures already published by our group and others. [4, 7] We obtained NGs with increasing dPG content, in the range 0 – 38 w/w%, by repeated polymerizations with increasing dPG amounts. A dPG content higher than 40 w/w% in the NGs led to the loss of thermoresponsiveness and was therefore not used in this study. The control NG samples without dPG were crosslinked with 4 mol% BIS. The resulting NGs were characterized *via* DLS and nuclear magnetic resonance (^{1}H-NMR) spectroscopy, the resulting data is shown in Table S1, please refer to the Supporting Information.

pNIPAM samples with up to 5% dPG show aggregation at 37 °C. A higher amount of dPG in the NGs led to colloidally stable particles, that shrunk at 37 °C, without undergoing interparticle aggregation. pNIPMAM samples in turn do not shrink below 46 °C, as shown from the characterization data in Table 1, and they are swollen at a physiological temperature of 37 °C. To form a protein corona, the NGs were incubated in human serum, for 1 h @ 37 °C, at a constant surface density of 8 m^2 NG / L serum. The isolation of the protein corona - NG complex was performed *via* ultrafiltration (molecular weight cutoff MWCO = 1 MDa), and extensive washing with sodium phosphate buffer saline (PBS). All corona isolation steps were done at constant 37 °C or 25 °C, in case the samples were not colloidally stable at 37 °C. The protein amount was then determined by a Bradford assay, the results are shown in **Fig. 1**.

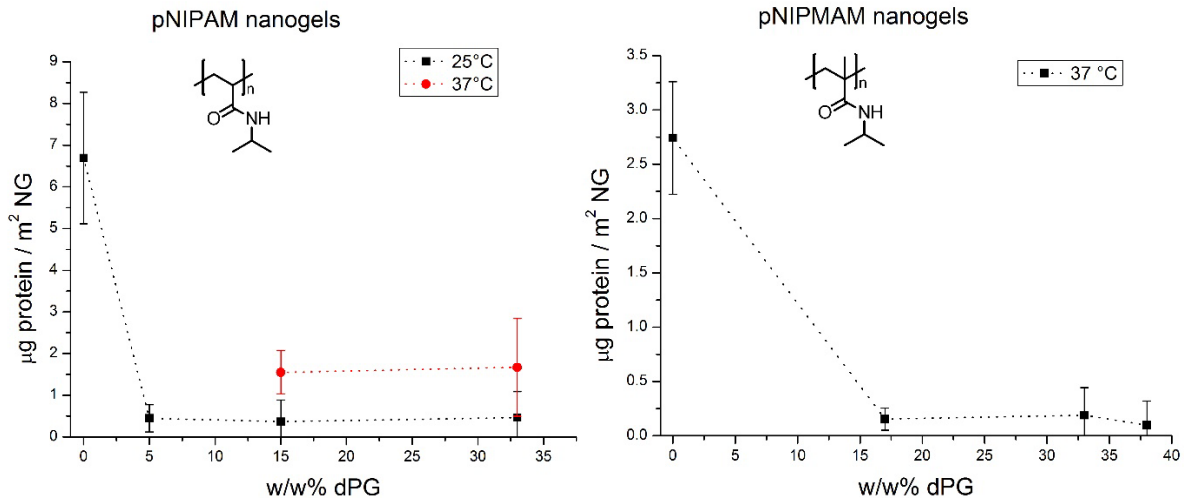

Fig. 1 Protein corona quantification for pNIPAM- (left) and pNIPMAM-based (right) nanogels, measured *via* Bradford assay.

The results showed that the protein absorption of control pNIPAM/BIS and pNIPMAM/BIS NGs was already low, as previously reported, with concentrations of 3 – 7 µg protein / m^2 NG. For comparison, for the protein corona around hydroxyethylstarch (HES) nanocapsules a higher content of 320 – 470 µg / m^2 was found. [25] Nevertheless, by introducing dPG as crosslinker, the amount of absorbed protein was further reduced 13-fold for pNIPAM and 10-fold for pNIPMAM, leaving only traces of protein absorbed by NGs.

By comparing the two data sets in Fig. 1, we observe a moderately higher protein absorption of pNIPAM samples in comparison with pNIPMAM NGs. By increasing the concentration of the hydrophilic antifouling reagent dPG, the amount of protein in the corona was drastically reduced in compliance with the literature. [8] dPG-pNIPAM NGs showed a thermal dependency of the overall amount of absorbed protein, being higher at 37 °C, as expected for the increased hydrophobicity of pNIPAM, as previously reported. [6] pNIPAM/BIS and 5% dPG-pNIPAM NGs were not stable in water above the LCST (Table S1), thus they were only investigated in serum at 25 °C.

While we expect a safe profile for the NG's hemocompatibility with such low protein amounts, we proceeded by analyzing their behavior in human serum *via* DLS. In this way, no sample isolation was needed, to prevent the loss of structural information and include the elusive layers of protein corona (the so-called "soft" protein corona, that may not be isolated from the protein medium, as it may be too loosely bound to the NP). [25] The DLS analysis was performed according to the method described by Rausch et al., [24] by the differential analysis of the autocorrelation functions (ACFs) obtained by the single scattering components. First, the ACFs of the individual components (pure concentrated serum and pure NG solutions) were determined. After that the mixtures can be evaluated with the so-called "force fit": a sum of the individual ACFs with variable intensity contributions. Should the force fit not be sufficient to

describe the data, a third “aggregate” term is added to fit the additionally formed species, which is larger than the individual components. This results in the expression $g_{1,S}(t) = a_{1,Serum} \exp\left(-\frac{t}{\tau_{1,Serum}}\right) + a_{2,NG} \exp\left(-\frac{t}{\tau_{2,NG}}\right) + a_{3,Agg} \exp\left(-\frac{t}{\tau_{3,Agg}}\right)$ with the amplitudes a_i and the decay times $\tau_i = \frac{1}{q^2 D_i}$, where $q = \frac{4\pi n}{\lambda_0} sin\left(\frac{\theta}{2}\right)$ is the scattering vector and D_i the single component’s Brownian diffusion coefficient. Following this method, the size increase of a nanomaterial due to protein absorption (if the increase is significant) or aggregation phenomena can be monitored. The ACFs of the evaluated NGs together with the corresponding fits are shown in **Fig. 2** and the resulting aggregate sizes and intensity contributions are summarized in **Table 1**.

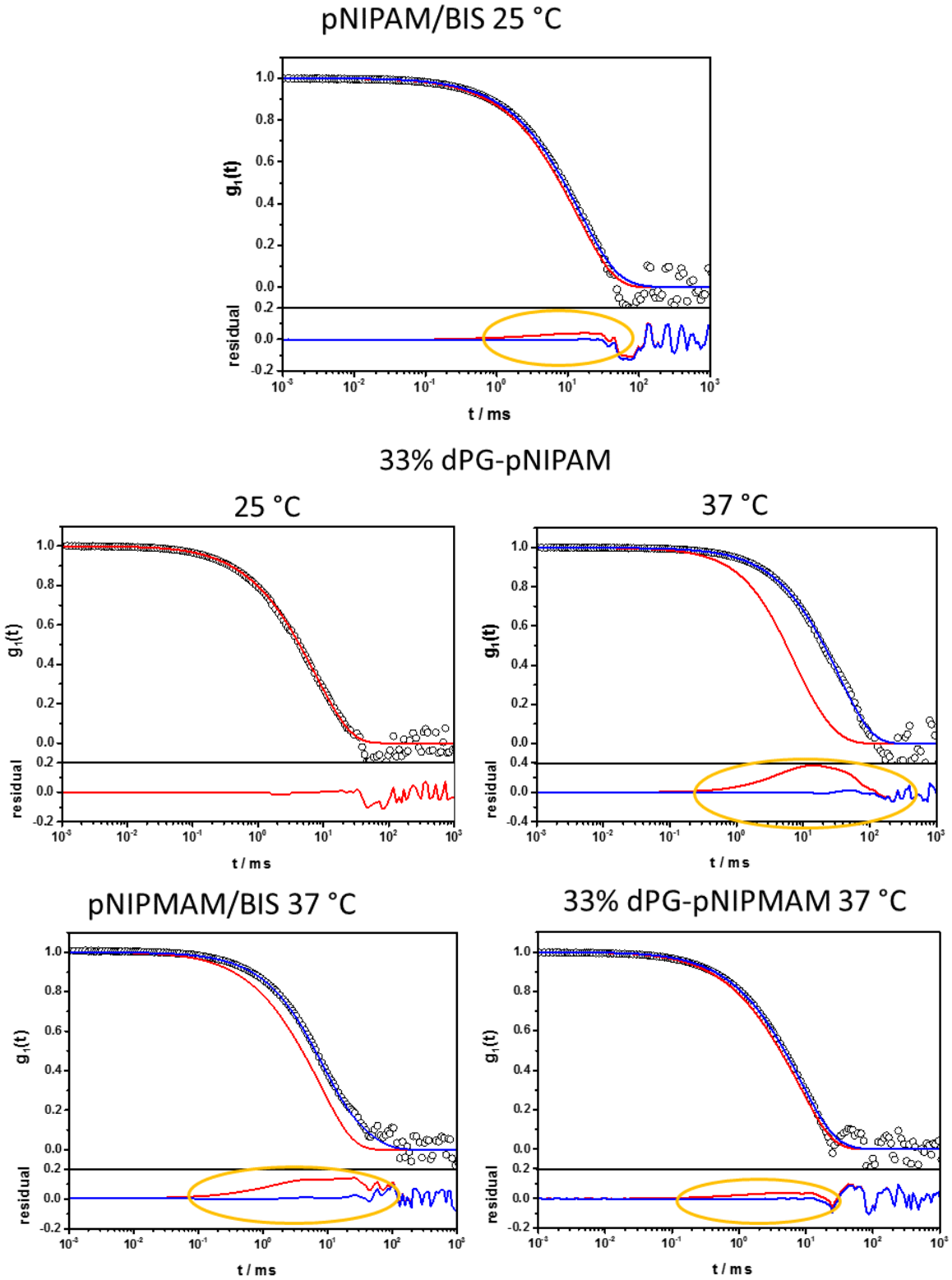

Fig. 2 Autocorrelation functions (ACFs) of thermoresponsive nanogels in concentrated human serum for an exemplary scattering angle of 30°. Upper graphs show the obtained data points (open circles) together with a force fit (red line) and a fit containing an additional aggregate term (blue line) where applicable. Lower graphs show the residuals between fits and data points and detected size increases (data cannot be described by the force fit) are highlighted with yellow circles.

Table 1. Summary of the multi-angle dynamic light scattering data acquired in human serum for thermoresponsive nanogels.

Sample	Particle size in H_2O (d.nm)	Aggregate size in serum (d.nm)	Aggregate intensity fraction (%)
pNIPAM / BIS 25 °C	250 ± 26	> 1000	10
33% dPG-pNIPAM 25 °C	276 ± 28	-	-
33% dPG-pNIPAM 37 °C	220 ± 22	> 1000	78
pNIPMAM / BIS 37 °C	190 ± 20	834 ± 84	27
33% dPG-pNIPMAM 37 °C	144 ± 14	374 ± 38	14

All NGs in their hydrophilic state showed moderate aggregate formation with aggregate intensity fractions of less than 30%. The size of the formed aggregates, however, was quite large for the NGs without dPG and a result of NG clustering. The presence of dPG decreased the aggregate intensity fraction in both cases, going from 10% to 0% for pNIPAM at 25 °C, and from 27% to 14% for pNIPMAM at 37 °C with a significantly reduced aggregate size. In contrast, 33% dPG-pNIPAM NGs showed pronounced, temperature-dependent aggregation in serum at 37 °C, even though no aggregation could be detected at 25 °C. The hydrophobic transition of pNIPAM in serum led to interparticle aggregation, resulting in micrometer-sized particles. This finding may corroborate what was observed by Obst et al., where the NGs showed flocculation in DLS in water, after their incubation in human plasma. [12] The same behavior was observed for NPs based on thermoresponsive poly(2-isopropyl-2-oxazoline), showing aggregation only above the polymer's LCST. [21]

In order to characterize the elusive protein coronae obtained around pNIPAM and pNIPMAM NGs with varying crosslinkers (dPG or BIS) and temperatures (25°C or 37°C), we used quantitative proteomics. By utilizing the $^{16}O/^{18}O$-labeling method we were able to quantify the relative changes in the protein coronae of four pairwise comparisons as highlighted in **Table 2**. Protein coronae were isolated by incubation of the NGs with human serum for 1 h followed by extensive washing using a 450 nm syringe filter. Proteins were eluted from the NGs by boiling in SDS sample buffer and a short SDS-PAGE was performed for protein clean-up, so that all proteins were contained in a single gel band. Subsequently, proteins from pairwise comparisons were in-gel digested with trypsin in the presence of "light" water ($H_2{}^{16}O$) or "heavy" water ($H_2{}^{18}O$). Peptides were extracted from the gel and corresponding "heavy" and "light" peptide samples were pooled and analyzed by LC-ECI-MS/MS. Each experiment was done in triplicate and about 40 proteins were reproducibly identified and quantified in each experiment (**Table S2-S5**, Supporting Information). The majority of proteins showed isotopic heavy-to-light (H/L) ratios around 1 (1:1), indicating that these proteins are of equal abundance in both

conditions/samples. Proteins that show reproducible relative enrichment in the heavy form (H/L ratio > 1.5) or in the light form (H/L ratios < 0.66) indicate specific binding to the corresponding nanogels (**Table 2**).

Table 2. Overview of the experimental settings for quantitative proteomics experiments and the number of proteins that were reproducibly identified and quantified (n=3) in the corona of thermoresponsive nanogels.

	Labeled light (^{16}O)	Labeled heavy (^{18}O)	# of proteins
Experiment 1	33% dPG-PNIPAM (37°C)	33% dPG-PNIPMAM (37 °C)	34
Experiment 2	33% dPG-PNIPAM (25°C)	33% dPG-PNIPAM (37°C)	35
Experiment 3	33% dPG-PNIPAM (25°C)	PNIPAM/BIS (25 °C)	46
Experiment 4	PNIPMAM/BIS (37°C)	33% dPG-PNIPMAM (37°C)	44

Table 3 summarizes the results of experiment 1, in which the protein coronae of 33% dPG-pNIPAM and 33% dPG-pNIPMAM were compared, both at 37 °C. Here, H/L ratios < 0.66 indicates preferential binding to dPG-pNIPAM, while H/L ratios > 1.5 indicate preferential binding to dPG-pNIPMAM. **Table 4** summarizes the results from experiment 2 in which the protein coronae of 33% dPG-pNIPAM were compared at 25°C (hydrophilic) and 37°C (hydrophobic). In this experiment, H/L ratios < 0.66 indicate preferential binding at 25°C, while H/L ratios > 1.5 indicate preferential binding at 37 °C. Whole datasets for experiments are provided in the Supporting Information.

Table 3. Excerpt from the proteomics analysis of protein coronae around 33 w/w% dPG-pNIPAM (L) and 33 w/w% dPG-pNIPMAM nanogels (H) incubated in human serum for 1 h at 37 °C. The top 10 most abundant proteins are ranked in order of their mean number of identified peptide sequences from three independent replicates. Below, proteins that show significant enrichment to 33 w/w% dPG-pNIPAM (mean H/L ratio < 0.66) and 33 w/w% dPG-pNIPMAM (mean H/L ratio > 1.5) are shown. Mean H/L ratios indicate the mean $^{18}O/^{16}O$ ratios from three independent experiments. Mean H/L ratios with *p*-values ≤ 0.05 were considered significant.

Top 10 Proteins	Accession number	Molecular Weight (kDa)	Mean Mascot score	Mean peptide count	Mean H/L ratio	*p*-value
Serum albumin	ALBU_HUMAN	71.3	3415	56	1.63	0.012
Apolipoprotein B-100	APOB_HUMAN	516.7	3861	49	0.26	0.003
Complement C3	CO3_HUMAN	188.6	2322	46	1.08	0.217
α-2-macroglobulin	A2MG_HUMAN	164.6	2160	42	0.63	0.010
Serotransferrin	TRFE_HUMAN	79.3	1524	31	1.50	0.015
Complement C4-A	CO4A_HUMAN	194.3	863	17	0.98	0.781
α-1-antitrypsin	A1AT_HUMAN	46.9	668	16	1.11	0.239
Complement C4-B	CO4B_HUMAN	194.2	859	16	1.00	0.980
Haptoglobin	HPT_HUMAN	45.9	620	14	0.74	0.255
Immunoglobulin heavy constant mu	IGHM_HUMAN	50.1	485	12	0.58	0.051
Enriched proteins	Accession number	Molecular Weight (kDa)	Mean Mascot score	Mean peptide count	Mean H/L ratio	*p*-value
Apolipoprotein B-100	APOB_HUMAN	516.7	3861	49	0.26	0.003
α-2-macroglobulin	A2MG_HUMAN	164.6	2160	42	0.63	0.010
Serotransferrin	TRFE_HUMAN	79.3	1524	31	1.50	0.015
Serum albumin	ALBU_HUMAN	71.3	3415	56	1.63	0.012
α-2-HS-glycoprotein	FETUA_HUMAN	40.1	68	2	1.82	0.013

Table 4. Excerpt from the proteomics analysis of protein coronae around 33 w/w% dPG-pNIPAM nanogels incubated for 1 h at 25 °C (L) and 37 °C (H). The top 10 most abundant proteins are ranked in order of their mean number of identified peptide sequences from three independent replicates. Below, proteins that show significant enrichment to 33 w/w% dPG-pNIPAM at 25 °C (mean H/L ratio < 0.66) and 37°C (mean H/L ratio > 1.5) are shown. Mean H/L ratios indicate the mean $^{18}O/^{16}O$ ratios from three independent experiments. Mean H/L ratios with *p*-values ≤ 0.05 were considered significant.

Top 10 Proteins	Accession number	Molecular Weight (kDa)	Mean Mascot score	Mean peptide count	Mean H/L ratio	*p*-value
Apolipoprotein B-100	APOB_HUMAN	516.7	2703	63	1.43	0.154
Serum albumin	ALBU_HUMAN	71.3	3443	62	0.93	0.304
Complement C3	CO3_HUMAN	188.6	2406	51	1.03	0.100
α-2-macroglobulin	A2MG_HUMAN	164.6	1947	43	1.10	0.378
Serotransferrin	TRFE_HUMAN	79.3	1273	27	0.96	0.424
Complement C4-B	CO4B_HUMAN	194.2	769	23	0.83	0.074
Complement C4-A	CO4A_HUMAN	194.3	713	23	0.81	0.082
α-1-antitrypsin	A1AT_HUMAN	46.9	703	16	0.96	0.147
Immunoglobulin heavy constant mu	IGHM_HUMAN	50.1	491	14	1.24	0.202
Haptoglobin	HPT_HUMAN	45.9	576	13	0.96	0.548
Enriched protein	Accession number	Molecular Weight (kDa)	Mean Mascot score	Mean peptide count	Mean H/L ratio	*p*-value
Immunoglobulin lambda-1 light chain	IGL1_HUMAN	23.1	120	3	1.64	0.026

For all samples in this study, Apolipoprotein B-100 (ApoB), dysopsonins (serum albumin, α-2-macroglobulin, transferrin) and complement proteins (C3 and C4) were identified among the most abundant proteins in the samples, indicating that they were bound in the corona (Tables 3, 4, and S2 – S5). ApoB is the main component of low density lipoprotein (LDL) and precursor of chylomicrons. In reported cases, the coating of NPs with ApoB was used to target lipoproteins for the treatment of hyperlipidemia. [26] Serum albumin is the most abundant serum protein. Together with α-2-macroglobulin and transferrin, their presence increases the bioavailability of NGs, by acting as dysopsonizing agents, prolonging the NG retention time in

blood. Complement proteins (mostly C3 and C4) and immunoglobulin mu were also found in a significant amount on the corona of all NGs. Complement proteins and immunoglobulins are part of the innate immune system. While their presence on the corona may signify an increased probability of immune response associated with opsonization, more information is still needed to assess this hypothesis. Previous reports revealed that the mere presence of complement proteins in the corona of Au NPs was not sufficient to activate the complement system, which required in turn a substantial depletion of complement proteins from blood plasma. [27] In this case, traces of proteins detected around NGs may not be enough to activate the complement system after all.

When comparing the protein coronae of hydrophilic 33% dPG-pNIPMAM NGs and hydrophobic 33% dPG-pNIPAM NGs at 37 °C (experiment 1), we observe a significant enrichment of ApoB and α-2-macroglobulin (A2MG), to pNIPAM. Dysopsonins like serum albumin, transferrin and α-2-HS-glycoprotein on the other hand were enriched in the corona of pNIPMAM. Taken together, the increased hydrophilicity of pNIPMAM was able to shift the corona composition from an ApoB-rich corona, towards a dysopsonin-enriched one, as shown in **Fig. 3** (left panel).

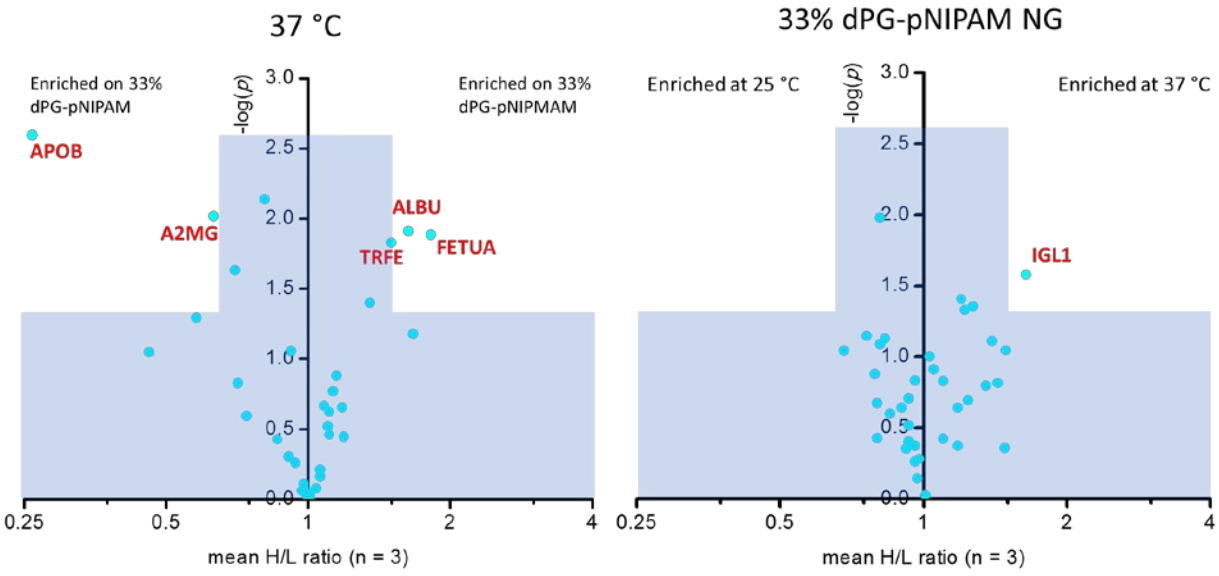

Fig. 3 Volcano plot of proteins identified in the coronae of 33 w/w% dPG-pNIPAM and 33 w/w% dPG-pNIPMAM nanogels after incubation with human serum for 1 h at 37 °C (left); Volcano plot of proteins identified in the coronae of 33 w/w% dPG-pNIPAM nanogels incubated for 1 h at 25 °C and 37 °C (right). Proteins were highlighted (red labels) if their mean H/L ratio (n=3) indicated more than 1.5-fold enrichment (mean H/L < 0.66 or mean H/L > 1.5). Mean H/L ratios with p-values ≤ 0.05 (-log(*p*) ≥ 1.3) were considered significant.

When comparing protein coronae of 33% dPG-pNIPAM NGs at 25 °C vs. 37 °C (experiment 2), above and below the LCST of pNIPAM, we observe a specific, temperature-dependent enrichment of immunoglobulin lambda light chain (IGL1) at 37 °C, when the NGs are in their hydrophobic state. This finding was in compliance with what observed by Zhang et al., for pNIPAM NPs in human plasma. [6] The hydrophobic transition underwent by pNIPAM was followed by aggregation of NGs in serum, as seen from DLS measurements (Fig. 2). The same phenomenon was observed by Koshkina et al., for poly(2-isopropyl-2-oxazoline) NPs, when incubated in serum above their LCST. [21] This might imply that the intrinsic hydrophobic shift, caused by heating of thermoresponsive polymers above their LCST, may promote protein-NG intercalation in blood, thereby compromising the NG's stability. Moreover, the observed NG aggregation can be correlated to the changes in protein corona composition in serum at 37 °C. A similar net enrichment of IgG in low abundances was responsible for polystyrene NP bridging, caused by IgG denaturation and resulting in NP aggregation. [18, 28]

Further experiments were performed, to understand whether dPG had an impact not only on the amount of bound protein, but also on the composition of the protein corona. Proteomics analysis revealed that dPG in the NGs increased their affinity for apolipoproteins. By comparing the compositions of the coronae of 33% dPG-pNIPAM and pNIPAM/BIS at 25 °C, we observed an increased affinity of the dPG-containing nanogel towards ApoB and haptoglobin. The control sample pNIPAM/BIS showed enrichment of several dysopsonins such as plasminogen, transferrin, and β-2-glycoprotein. Nevertheless, as accounted in **Fig. 1**, the overall amount of proteins on the coronae of pNIPAM/BIS was significantly higher. A similar comparison between 33% dPG-pNIPMAM and pNIPMAM/BIS NGs at 37 °C found a net enrichment of plasma protease C1 inhibitor in NGs with BIS. For a detailed listing of the components of all protein coronae, please refer to the supporting information (**Fig. S1 & S2** and **Tables S4 & S5**).

Overall, we observe distinct tendencies for the association of the main components ApoB and HSA, depending on the starting materials used for the synthesis of NGs. An increase in hydrophilicity of NGs, whether by decreasing the temperature in pNIPAM, or the use of pNIPMAM, led to a decrease in ApoB and increase in dysopsonin content. The composition of the protein corona was affected by the temperature of the system, as expected from thermoresponsive NGs.

Conclusions

The use of antifouling dPG proved to be essential for the inhibition of the protein absorption by NGs. Low protein amounts were found in all cases, however the presence of dPG allowed further decrease in a range of 10- to 13-fold. In order to isolate the elusive protein coronae around thermoresponsive NGs, we employed ultrafiltration that proved to be more efficient than the conventional centrifugation or size exclusion chromatography techniques.

An ApoB-rich corona found around all NGs, except dPG-pNIPMAM, may enhance the targeting of liver LDL receptors, for the treatment of hyperlipidemia or other cholesterol-related diseases. [26]

When used as nanogel components, pNIPMAM showed overall lower protein absorption than pNIPAM, especially when the latter was incubated in serum in its hydrophobic state, at 37 °C. dPG-pNIPAM NGs exhibited temperature-dependent protein coronae, with specific enrichment of Ig light chain above the pNIPAM LCST at 37 °C, together with interparticle aggregation in human serum as seen by DLS. This behavior reproduces what was observed by Koshkina et al. for poly(2-isopropyl-2-oxazoline) NPs showing pronounced aggregation in serum only above their LCST, [21] as well as resembling the IgG - driven bridging of polystyrene NPs, reported by Cukalevski et al. [28] An immunogenic response may originate from these features in the corona of dPG-pNIPAM NGs, such as triggering cytokine release from macrophages similar to what Obst et al. observed in a previous report regarding the same NGs. [12]

By designing thermoresponsive NGs, their recurring aggregation behavior in serum above their LCST [21] may be detrimental for their circulation in blood, and overall may increase the risk of thrombosis. However, smart thermoresponsive NGs that are able to switch to a hydrophobic conformation only upon external temperature regulation or an intrinsic temperature gradient, may increase their toxicity *in situ*, due to corona-dependent aggregation. In this way, one could boost the therapy efficacy. Analogously, the release of the protein corona upon sample cooling could be another strategy to deliver specific proteins, by applying external heating / cooling cycles.

By changing the nature of the thermoresponsive polymer to pNIPMAM, a safer profile in serum was observed for all samples, together with a more hydrophilic protein corona, with a depletion of ApoB and α-2-macroglobulin, and a specific enrichment of serum albumin, transferrin and α-2-HS-glycoprotein. The same samples showed overall diminished protein absorption compared to pNIPAM, and are considered optimal candidates for their application in systemic therapy.

Acknowledgements

We gratefully acknowledge financial support from the Bundesministerium für Bildung und Forschung (BMBF) through the NanoMatFutur award (ThermoNanogele, 13N12561), Helmholtz Virtual Institute (HVI), "Multifunctional Biomaterials for Medicine," and the Focus Area NanoScale of the Freie Universität Berlin (http://www.nanoscale.fu-berlin.de). Moreover, we would like to acknowledge the assistance of the Core Facility BioSupraMol supported by the Deutsche Forschungsgemeinschaft (DFG).

References

1. Molina, M., et al., *Stimuli-responsive nanogel composites and their application in nanomedicine.* Chem. Soc. Rev., 2015. **44**(17): p. 6161-6186.
2. Bergueiro, J. and M. Calderon, *Thermoresponsive nanodevices in biomedical applications.* Macromol Biosci, 2015. **15**(2): p. 183-99.
3. Fujishige, S., K. Kubota, and I. Ando, *Phase Transition of Aqueous Solutions of Poly(N-isopropylacrylamide) and Poly(N-isopropylmethacrylamide)* J. Phys. Chem., 1989. **93**: p. 3311-3313.
4. McPhee, W., K.C. Tam, and R. Pelton, *Poly(N-isopropylacrylamide) Latices Prepared with Sodium Dodecyl Sulfate.* Journal of Colloid and Interface Science, 1993. **156**(1): p. 24-30.
5. O'Brien, J. and K.J. Shea, *Tuning the Protein Corona of Hydrogel Nanoparticles: The Synthesis of Abiotic Protein and Peptide Affinity Reagents.* Acc Chem Res, 2016. **49**(6): p. 1200-1210.
6. Zhang, Y., et al., *Effects of thermosensitive poly(N-isopropylacrylamide) on blood coagulation.* J. Mater. Chem. B, 2016. **4**(21): p. 3733-3749.
7. Cuggino, J.C., et al., *Thermosensitive nanogels based on dendritic polyglycerol and N-isopropylacrylamide for biomedical applications.* Soft Matter, 2011. **7**(23): p. 11259.
8. Calderon, M., et al., *Dendritic polyglycerols for biomedical applications.* Adv Mater, 2010. **22**(2): p. 190-218.
9. Schöttler, S., et al., *Protein adsorption is required for stealth effect of poly(ethylene glycol)- and poly(phosphoester)-coated nanocarriers.* Nat Nanotechnol, 2016. **11**(4): p. 372-7.
10. Moyano, D.F., Saha, K.,, et al., *Fabrication of Corona-Free Nanoparticles with Tunable Hydrophobicity.* ACS Nano, 2014. **8**(7): p. 6748-6755.
11. Yang, S.T., et al., *Biosafety and bioapplication of nanomaterials by designing protein-nanoparticle interactions.* Small, 2013. **9**(9-10): p. 1635-53.

12. Obst, K., et al., *Protein Corona Formation on Colloidal Polymeric Nanoparticles and Polymeric Nanogels: Impact on Cellular Uptake, Toxicity, Immunogenicity, and Drug Release Properties.* Biomacromolecules, 2017. **18**(6): p. 1762-1771.
13. Palchetti, S., et al., *Nanoparticles-cell association predicted by protein corona fingerprints.* Nanoscale, 2016. **8**: p. 12755-12763.
14. Schöttler, S., K. Landfester, and V. Mailander, *Controlling the Stealth Effect of Nanocarriers through Understanding the Protein Corona.* Angew Chem Int Ed Engl, 2016. **55**(31): p. 8806-15.
15. Absolom, D.R., *Opsonins and dysopsonins: an overview.* Methods Enzymol., 1986. **132**: p. 281-318.
16. Miceli, E., M. Kar, and M. Calderón, *Interactions of organic nanoparticles with proteins in physiological conditions.* J. Mater. Chem. B, 2017. **5**(23): p. 4393-4405.
17. Vroman, L. and A.L. Adams, *Adsorption of proteins out of plasma and solutions in narrow spaces.* J Colloid Interface Sci, 1986. **111**(2): p. 391-402.
18. Müller, L.K., et al., *Pre-coating with protein fractions inhibits nano-carrier aggregation in human blood plasma.* RSC Adv., 2016. **6**(99): p. 96495-96509.
19. Hellstrand, E., et al., *Complete high-density lipoproteins in nanoparticle corona.* FEBS J, 2009. **276**(12): p. 3372-81.
20. Cedervall, T., et al., *Detailed identification of plasma proteins adsorbed on copolymer nanoparticles.* Angew Chem Int Ed Engl, 2007. **46**(30): p. 5754-6.
21. Koshkina, O., et al., *Temperature-Triggered Protein Adsorption on Polymer-Coated Nanoparticles in Serum.* Langmuir, 2015. **31**(32): p. 8873-81.
22. Kristiansen, T.Z., et al., *Differential Membrane Proteomics Using 18O-Labeling To Identify Biomarkers for Cholangiocarcinoma.* Journal of Proteome Research, 2008. **7**(11): p. 4670-4677.
23. Lange, S., et al., *Identification of Phosphorylation-Dependent Interaction Partners of the Adapter Protein ADAP using Quantitative Mass Spectrometry: SILAC vs 18O-Labeling.* Journal of Proteome Research, 2010. **9**(8): p. 4113-4122.
24. Rausch, K., et al., *Evaluation of Nanoparticle Aggregation in Human Blood Serum.* Biomacromolecules, 2010. **11**(11): p. 2836-2839.
25. Winzen, S., et al., *Complementary analysis of the hard and soft protein corona: sample preparation critically effects corona composition.* Nanoscale, 2015. **7**(7): p. 2992-3001.
26. Maximov, V.D., et al., *Protein-nanoparticle conjugates as potential therapeutic agents for the treatment of hyperlipidemia.* Nanotechnology, 2010. **21**(26): p. 265103.
27. Dobrovolskaia, M.A., et al., *Protein corona composition does not accurately predict hematocompatibility of colloidal gold nanoparticles.* Nanomedicine, 2014. **10**(7): p. 1453-63.

28. Cukalevski, R., et al., *IgG and fibrinogen driven nanoparticle aggregation.* Nano Research, 2015. **8**(8): p. 2733-2743.

Supporting Information

Temperature dependency of elusive protein corona around thermoresponsive nanogels: key interactions above the lower critical solution temperature

Enrico Miceli, Benno Kuropka, Christine Rosenauer, Ernesto Rafael Osorio Blanco, Loryn Fechner, Mrityunjoy Kar, Christoph Weise, Svenja Morsbach, Christian Freund, Marcelo Calderón

Table S1. Summarized data for the characterization of thermoresponsive pNIPAM and pNIPMAM nanogels according to nuclear magnetic resonance spectroscopy (a) and dynamic light scattering (b).

Monomer used	dPG content (w/w%)[a]	Size @ 25 °C, d.nm (PDI)[b]	Size @ 37 °C, d.nm (PDI)[b]					
NIPAM	0*	250 (0.048)	> 1000 (0.302)					
NIPAM	5	184 (0.223)	> 1000 (0.475)					
NIPAM	15	190 (0.190)	170 (0.143)					
NIPAM	33	276 (0.180)	220 (0.165)					
NIPMAM	0*	171 (0.051)	190 (0.042)					
NIPMAM	17	136 (0.226)	138 (0.206)					
NIPMAM	33	140 (0.176)	144 (0.180)					
NIPMAM	38	79 (0.186)	77 (0.190)					

*Samples having 0 dPG feed ratio were crosslinked with 4 mol% N,N'-methylenebisacrylamide. d.nm = hydrodynamic diameter, nm; PDI = polydispersity index.

Table S2. List of quantified proteins for Experiment 1 (Light = 33% dPG-PNIPAM (37°C), Heavy = 33% dPG-PNIPMAM (37 °C) , ^{18}O-ratios according to the Mascot Distiller software (version 2.6.1.0 [Matrix Science Ltd, London, UK]).

Description	Accession	Molecular weight (Da)	Ratio H/L normalized A	LOG2 Ratio H/L normalized A	Mascot Score A	# A (Count)	Ratio H/L normalized B	LOG2 Ratio H/L normalized B	Mascot Score B	# B (Count)
Apolipoprotein B-100 OS=Homo sapiens GN=APOB PE=1 SV=2	APOB_HUMAN	516651	0.29	-1.8	4225	50	0.24	-2.0	3444	50
Serum albumin OS=Homo sapiens GN=ALB PE=1 SV=2	ALBU_HUMAN	71317	1.45	0.5	2935	48	1.61	0.7	3026	61
Alpha-2-macroglobulin OS=Homo sapiens GN=A2M PE=1 SV=3	A2MG_HUMAN	164613	0.60	-0.7	2006	46	0.59	-0.8	2291	41
Complement C3 OS=Homo sapiens GN=C3 PE=1 SV=2	CO3_HUMAN	188569	1.13	0.2	2274	42	1.02	0.0	2213	40
Serotransferrin OS=Homo sapiens GN=TF PE=1 SV=3	TRFE_HUMAN	79294	1.47	0.6	1394	30	1.38	0.5	1603	31
Alpha-1-antitrypsin OS=Homo sapiens GN=SERPINA1 PE=1 SV=3	A1AT_HUMAN	46878	1.19	0.3	532	15	1.09	0.1	734	17
Haptoglobin OS=Homo sapiens GN=HP PE=1 SV=1	HPT_HUMAN	45861	0.49	-1.0	574	15	0.83	-0.3	626	13
Apolipoprotein A-I OS=Homo sapiens GN=APOA1 PE=1 SV=1	APOA1_HUMAN	30759	0.93	-0.1	508	13	1.08	0.1	399	9
Immunoglobulin heavy constant mu OS=Homo sapiens GN=IGHM PE=1 SV=4	IGHM_HUMAN	50093	0.68	-0.6	496	13	0.46	-1.1	448	12
Complement C4-A OS=Homo sapiens GN=C4A PE=1 SV=2	CO4A_HUMAN	194261	0.86	-0.2	762	12	1.04	0.1	713	18
Complement C4-B OS=Homo sapiens GN=C4B PE=1 SV=2	CO4B_HUMAN	194170	0.91	-0.1	749	11	1.03	0.0	726	16
Immunoglobulin heavy constant alpha 1 OS=Homo sapiens GN=IGHA1 PE=1 SV=2	IGHA1_HUMAN	38486	1.13	0.2	221	8	0.88	-0.2	318	8
C4b-binding protein alpha chain OS=Homo sapiens GN=C4BPA PE=1 SV=2	C4BPA_HUMAN	69042	0.83	-0.3	471	7	0.69	-0.5	528	8
Ceruloplasmin OS=Homo sapiens GN=CP PE=1 SV=1	CERU_HUMAN	122983	0.93	-0.1	360	6	1.11	0.1	461	14
Immunoglobulin gamma-1 heavy chain OS=Homo sapiens PE=1 SV=1	IGG1_HUMAN	49926	1.12	0.2	331	6	0.94	-0.1	439	9
Immunoglobulin heavy constant gamma 3 OS=Homo sapiens GN=IGHG3 PE=1 SV=2	IGHG3_HUMAN	42287	1.27	0.3	268	6	0.86	-0.2	310	10
Immunoglobulin heavy constant gamma 2 OS=Homo sapiens GN=IGHG2 PE=1 SV=2	IGHG2_HUMAN	36505	0.89	-0.2	161	5	0.89	-0.2	286	8
Immunoglobulin heavy constant gamma 4 OS=Homo sapiens GN=IGHG4 PE=1 SV=1	IGHG4_HUMAN	36431	0.75	-0.4	170	5	0.83	-0.3	215	4
Immunoglobulin kappa light chain OS=Homo sapiens PE=1 SV=1	IGK_HUMAN	23650	1.15	0.2	337	5	1.24	0.3	440	5
Immunoglobulin kappa constant OS=Homo sapiens GN=IGKC PE=1 SV=2	IGKC_HUMAN	11929	1.08	0.1	261	5	1.24	0.3	295	5
Alpha-1B-glycoprotein OS=Homo sapiens GN=A1BG PE=1 SV=4	A1BG_HUMAN	54790	1.30	0.4	233	4	0.99	0.0	220	4
Alpha-1-antichymotrypsin OS=Homo sapiens GN=SERPINA3 PE=1 SV=2	AACT_HUMAN	47792	1.40	0.5	287	4	1.20	0.3	411	6
Complement factor H OS=Homo sapiens GN=CFH PE=1 SV=4	CFAH_HUMAN	143680	1.04	0.1	526	4	0.76	-0.4	412	8
Hemopexin OS=Homo sapiens GN=HPX PE=1 SV=2	HEMO_HUMAN	52385	1.05	0.1	235	4	1.05	0.1	302	10
Antithrombin-III OS=Homo sapiens GN=SERPINC1 PE=1 SV=1	ANT3_HUMAN	53025	0.96	-0.1	242	3	1.06	0.1	263	2
Immunoglobulin alpha-2 heavy chain OS=Homo sapiens PE=1 SV=1	IGA2_HUMAN	49817	1.32	0.4	138	3	0.90	-0.1	236	5
Inter-alpha-trypsin inhibitor heavy chain H1 OS=Homo sapiens GN=ITIH1 PE=1 SV=3	ITIH1_HUMAN	101782	0.65	-0.6	334	3	0.95	-0.1	354	3
Inter-alpha-trypsin inhibitor heavy chain H2 OS=Homo sapiens GN=ITIH2 PE=1 SV=2	ITIH2_HUMAN	106853	0.71	-0.5	216	3	0.63	-0.7	229	5
Inter-alpha-trypsin inhibitor heavy chain H4 OS=Homo sapiens GN=ITIH4 PE=1 SV=4	ITIH4_HUMAN	103521	1.54	0.6	346	3	1.06	0.1	411	2
Vitamin D-binding protein OS=Homo sapiens GN=GC PE=1 SV=1	VTDB_HUMAN	54526	2.07	1.0	206	3	1.34	0.4	102	2
Alpha-1-acid glycoprotein 1 OS=Homo sapiens GN=ORM1 PE=1 SV=1	A1AG1_HUMAN	23725	0.70	-0.5	70	2	0.99	0.0	250	3
Alpha-2-HS-glycoprotein OS=Homo sapiens GN=AHSG PE=1 SV=1	FETUA_HUMAN	40098	1.80	0.9	43	2	1.60	0.7	91	2
Kininogen-1 OS=Homo sapiens GN=KNG1 PE=1 SV=2	KNG1_HUMAN	72996	0.89	-0.2	188	2	1.01	0.0	93	2
Transthyretin OS=Homo sapiens GN=TTR PE=1 SV=1	TTHY_HUMAN	15991	0.30	-1.7	71	2	0.74	-0.4	94	4

Table S2 (follows). List of quantified proteins for Experiment 1 (Light = 33% dPG-PNIPAM (37°C), Heavy = 33% dPG-PNIPMAM (37 °C) , 18O-ratios according to the Mascot Distiller software (version 2.6.1.0 [Matrix Science Ltd, London, UK]).

Description	Accession	Ratio H/L normalized C	LOG2 Ratio H/L normalized C	Mascot score C	# C (Count)	Mean H/L ratio	p-value	-LOG(P-value)
Apolipoprotein B-100 OS=Homo sapiens GN=APOB PE=1 SV=2	APOB_HUMAN	0.24	-2.1	3913	47	0.26	0.002	2.796
Serum albumin OS=Homo sapiens GN=ALB PE=1 SV=2	ALBU_HUMAN	1.80	0.9	4284	59	1.61	0.017	1.759
Alpha-2-macroglobulin OS=Homo sapiens GN=A2M PE=1 SV=3	A2MG_HUMAN	0.69	-0.5	2182	39	0.62	0.010	2.010
Complement C3 OS=Homo sapiens GN=C3 PE=1 SV=2	CO3_HUMAN	1.06	0.1	2480	55	1.07	0.155	0.809
Serotransferrin OS=Homo sapiens GN=TF PE=1 SV=3	TRFE_HUMAN	1.62	0.7	1575	31	1.48	0.014	1.860
Alpha-1-antitrypsin OS=Homo sapiens GN=SERPINA1 PE=1 SV=3	A1AT_HUMAN	1.00	0.0	739	16	1.09	0.214	0.669
Haptoglobin OS=Homo sapiens GN=HP PE=1 SV=1	HPT_HUMAN	0.96	-0.1	661	14	0.73	0.264	0.579
Apolipoprotein A-I OS=Homo sapiens GN=APOA1 PE=1 SV=1	APOA1_HUMAN	0.72	-0.5	396	5	0.90	0.456	0.342
Immunoglobulin heavy constant mu OS=Homo sapiens GN=IGHM PE=1 SV=4	IGHM_HUMAN	0.60	-0.7	512	10	0.57	0.041	1.391
Complement C4-A OS=Homo sapiens GN=C4A PE=1 SV=2	CO4A_HUMAN	1.04	0.1	1012	21	0.97	0.707	0.151
Complement C4-B OS=Homo sapiens GN=C4B PE=1 SV=2	CO4B_HUMAN	1.03	0.0	1101	20	0.99	0.816	0.089
Immunoglobulin heavy constant alpha 1 OS=Homo sapiens GN=IGHA1 PE=1 SV=2	IGHA1_HUMAN	1.00	0.0	251	6	1.00	0.958	0.019
C4b-binding protein alpha chain OS=Homo sapiens GN=C4BPA PE=1 SV=2	C4BPA_HUMAN	1.08	0.1	434	8	0.85	0.339	0.470
Ceruloplasmin OS=Homo sapiens GN=CP PE=1 SV=1	CERU_HUMAN	1.30	0.4	602	11	1.10	0.434	0.363
Immunoglobulin gamma-1 heavy chain OS=Homo sapiens PE=1 SV=1	IGG1_HUMAN	0.89	-0.2	425	9	0.98	0.787	0.104
Immunoglobulin heavy constant gamma 3 OS=Homo sapiens GN=IGHG3 PE=1 SV=2	IGHG3_HUMAN	0.81	-0.3	296	8	0.96	0.801	0.096
Immunoglobulin heavy constant gamma 2 OS=Homo sapiens GN=IGHG2 PE=1 SV=2	IGHG2_HUMAN	0.96	-0.1	276	7	0.91	0.073	1.135
Immunoglobulin heavy constant gamma 4 OS=Homo sapiens GN=IGHG4 PE=1 SV=1	IGHG4_HUMAN	0.83	-0.3	199	4	0.80	0.019	1.717
Immunoglobulin kappa light chain OS=Homo sapiens PE=1 SV=1	IGK_HUMAN	1.02	0.0	529	6	1.13	0.150	0.823
Immunoglobulin kappa constant OS=Homo sapiens GN=IGKC PE=1 SV=2	IGKC_HUMAN	0.96	-0.1	477	6	1.09	0.361	0.443
Alpha-1B-glycoprotein OS=Homo sapiens GN=A1BG PE=1 SV=4	A1BG_HUMAN	1.22	0.3	155	4	1.16	0.204	0.691
Alpha-1-antichymotrypsin OS=Homo sapiens GN=SERPINA3 PE=1 SV=2	AACT_HUMAN	1.42	0.5	427	4	1.34	0.032	1.501
Complement factor H OS=Homo sapiens GN=CFH PE=1 SV=4	CFAH_HUMAN	1.40	0.5	637	10	1.03	0.880	0.056
Hemopexin OS=Homo sapiens GN=HPX PE=1 SV=2	HEMO_HUMAN	1.26	0.3	278	9	1.12	0.210	0.677
Antithrombin-III OS=Homo sapiens GN=SERPINC1 PE=1 SV=1	ANT3_HUMAN	0.79	-0.3	356	4	0.93	0.487	0.313
Immunoglobulin alpha-2 heavy chain OS=Homo sapiens PE=1 SV=1	IGA2_HUMAN	0.97	0.0	216	5	1.05	0.716	0.145
Inter-alpha-trypsin inhibitor heavy chain H1 OS=Homo sapiens GN=ITIH1 PE=1 SV=3	ITIH1_HUMAN	0.56	-0.8	435	5	0.70	0.150	0.825
Inter-alpha-trypsin inhibitor heavy chain H2 OS=Homo sapiens GN=ITIH2 PE=1 SV=2	ITIH2_HUMAN	0.73	-0.4	217	7	0.69	0.016	1.800
Inter-alpha-trypsin inhibitor heavy chain H4 OS=Homo sapiens GN=ITIH4 PE=1 SV=4	ITIH4_HUMAN	1.00	0.0	484	4	1.18	0.351	0.455
Vitamin D-binding protein OS=Homo sapiens GN=GC PE=1 SV=1	VTDB_HUMAN	1.62	0.7	231	8	1.65	0.058	1.239
Alpha-1-acid glycoprotein 1 OS=Homo sapiens GN=ORM1 PE=1 SV=1	A1AG1_HUMAN	1.43	0.5	81	2	1.00	0.989	0.005
Alpha-2-HS-glycoprotein OS=Homo sapiens GN=AHSG PE=1 SV=1	FETUA_HUMAN	2.00	1.0	70	3	1.80	0.012	1.931
Kininogen-1 OS=Homo sapiens GN=KNG1 PE=1 SV=2	KNG1_HUMAN	1.29	0.4	203	5	1.05	0.702	0.153
Transthyretin OS=Homo sapiens GN=TTR PE=1 SV=1	TTHY_HUMAN	0.42	-1.3	107	3	0.46	0.095	1.022

Table S3. List of quantified proteins for Experiment 2 (Light = 33% dPG-PNIPAM (25°C), Heavy = 33% dPG-PNIPAM (37°C), ^{18}O-ratios according to the Mascot Distiller software (version 2.6.1.0 [Matrix Science Ltd, London, UK]).

Description	Accession	Molecular weight (Da)	Ratio H/L normalized A	LOG2 Ratio H/L normalized A	Mascot score A	# A (Count)	Ratio H/L normalized B	LOG2 Ratio H/L normalized B	Mascot score B	# B (Count)
Apolipoprotein B-100 OS=Homo sapiens GN=APOB PE=1 SV=2	APOB_HUMAN	516651	1.92	0.9	3113	74	1.12	0.2	2664	49
Serum albumin OS=Homo sapiens GN=ALB PE=1 SV=2	ALBU_HUMAN	71317	0.84	-0.3	3794	64	0.95	-0.1	2961	56
Complement C3 OS=Homo sapiens GN=C3 PE=1 SV=2	CO3_HUMAN	188569	1.05	0.1	2307	43	1.02	0.0	2014	49
Alpha-2-macroglobulin OS=Homo sapiens GN=A2M PE=1 SV=3	A2MG_HUMAN	164613	1.28	0.4	2077	41	0.96	-0.1	1928	39
Serotransferrin OS=Homo sapiens GN=TF PE=1 SV=3	TRFE_HUMAN	79294	0.90	-0.2	1162	28	0.99	0.0	1286	29
Complement C4-A OS=Homo sapiens GN=C4A PE=1 SV=2	CO4A_HUMAN	194261	0.73	-0.4	839	26	0.79	-0.3	607	21
Complement C4-B OS=Homo sapiens GN=C4B PE=1 SV=2	CO4B_HUMAN	194170	0.78	-0.4	900	26	0.78	-0.4	658	20
Immunoglobulin heavy constant mu OS=Homo sapiens GN=IGHM PE=1 SV=4	IGHM_HUMAN	50093	1.56	0.6	707	17	1.08	0.1	332	12
Alpha-1-antitrypsin OS=Homo sapiens GN=SERPINA1 PE=1 SV=3	A1AT_HUMAN	46878	1.14	0.2	679	13	0.91	-0.1	764	18
Haptoglobin OS=Homo sapiens GN=HP PE=1 SV=1	HPT_HUMAN	45861	0.96	-0.1	552	13	0.87	-0.2	512	13
Apolipoprotein A-I OS=Homo sapiens GN=APOA1 PE=1 SV=1	APOA1_HUMAN	30759	1.41	0.5	442	9	1.19	0.3	371	8
C4b-binding protein alpha chain OS=Homo sapiens GN=C4BPA PE=1 SV=2	C4BPA_HUMAN	69042	1.41	0.5	554	9	1.01	0.0	445	9
Immunoglobulin gamma-1 heavy chain OS=Homo sapiens PE=1 SV=1	IGG1_HUMAN	49926	1.68	0.7	306	9	1.22	0.3	344	8
Hemopexin OS=Homo sapiens GN=HPX PE=1 SV=2	HEMO_HUMAN	52385	0.76	-0.4	285	8	0.97	0.0	196	7
Immunoglobulin heavy constant gamma 3 OS=Homo sapiens GN=IGHG3 PE=1 SV=2	IGHG3_HUMAN	42287	1.29	0.4	239	8	1.12	0.2	319	9
Complement factor H OS=Homo sapiens GN=CFH PE=1 SV=4	CFAH_HUMAN	143680	0.64	-0.6	471	7	0.79	-0.3	272	5
Inter-alpha-trypsin inhibitor heavy chain H1 OS=Homo sapiens GN=ITIH1 PE=1 SV=3	ITIH1_HUMAN	101782	0.94	-0.1	524	7	1.03	0.0	488	6
Inter-alpha-trypsin inhibitor heavy chain H2 OS=Homo sapiens GN=ITIH2 PE=1 SV=2	ITIH2_HUMAN	106853	0.93	-0.1	313	7	0.80	-0.3	357	5
Alpha-1-antichymotrypsin OS=Homo sapiens GN=SERPINA3 PE=1 SV=2	AACT_HUMAN	47792	0.98	0.0	317	6	0.98	0.0	307	6
Antithrombin-III OS=Homo sapiens GN=SERPINC1 PE=1 SV=1	ANT3_HUMAN	53025	0.92	-0.1	197	6	1.27	0.3	266	7
Ceruloplasmin OS=Homo sapiens GN=CP PE=1 SV=1	CERU_HUMAN	122983	0.81	-0.3	415	6	1.02	0.0	516	10
Plasma protease C1 inhibitor OS=Homo sapiens GN=SERPING1 PE=1 SV=2	IC1_HUMAN	55347	0.66	-0.6	432	6	0.75	-0.4	242	3
Immunoglobulin heavy constant alpha 1 OS=Homo sapiens GN=IGHA1 PE=1 SV=2	IGHA1_HUMAN	38486	1.02	0.0	311	6	1.09	0.1	219	7
Alpha-1B-glycoprotein OS=Homo sapiens GN=A1BG PE=1 SV=4	A1BG_HUMAN	54790	0.69	-0.5	227	5	0.95	-0.1	117	4
Haptoglobin-related protein OS=Homo sapiens GN=HPR PE=2 SV=2	HPTR_HUMAN	39518	1.07	0.1	246	5	0.90	-0.2	150	4
Immunoglobulin heavy constant gamma 2 OS=Homo sapiens GN=IGHG2 PE=1 SV=2	IGHG2_HUMAN	36505	1.16	0.2	203	5	1.15	0.2	238	6
Apolipoprotein E OS=Homo sapiens GN=APOE PE=1 SV=1	APOE_HUMAN	36246	1.63	0.7	269	4	0.95	-0.1	150	2
Immunoglobulin alpha-2 heavy chain OS=Homo sapiens PE=1 SV=1	IGA2_HUMAN	49817	1.19	0.2	164	4	1.03	0.0	216	6
Immunoglobulin kappa light chain OS=Homo sapiens PE=1 SV=1	IGK_HUMAN	23650	1.14	0.2	252	4	1.22	0.3	198	3
Kininogen-1 OS=Homo sapiens GN=KNG1 PE=1 SV=2	KNG1_HUMAN	72996	0.59	-0.8	117	3	1.14	0.2	85	4
Protein AMBP OS=Homo sapiens GN=AMBP PE=1 SV=1	AMBP_HUMAN	39886	0.54	-0.9	167	2	0.73	-0.5	104	2
Immunoglobulin lambda-1 light chain OS=Homo sapiens PE=1 SV=1	IGL1_HUMAN	23101	1.92	0.9	112	2	1.48	0.6	58	2
Immunoglobulin kappa variable 3-20 OS=Homo sapiens GN=IGKV3-20 PE=1 SV=2	KV320_HUMAN	12663	1.22	0.3	107	2	1.44	0.5	123	2
Vitamin D-binding protein OS=Homo sapiens GN=GC PE=1 SV=1	VTDB_HUMAN	54526	0.83	-0.3	123	2	0.82	-0.3	168	3
Vitronectin OS=Homo sapiens GN=VTN PE=1 SV=1	VTNC_HUMAN	55069	0.66	-0.6	186	2	0.87	-0.2	200	2

Table S3 (follows). List of quantified proteins for Experiment 2 (Light = 33% dPG-PNIPAM (25°C), Heavy = 33% dPG-PNIPAM (37°C), ^{18}O-ratios according to the Mascot Distiller software (version 2.6.1.0 [Matrix Science Ltd, London, UK]).

Description	Accession	Ratio H/L normalized C	LOG2 Ratio H/L normalized C	Mascot score C	# C (Count)	Mean H/L ratio	p-value	-LOG(P-value)
Apolipoprotein B-100 OS=Homo sapiens GN=APOB PE=1 SV=2	APOB_HUMAN	1.35	0.4	2333	65	1.44	0.157	0.805
Serum albumin OS=Homo sapiens GN=ALB PE=1 SV=2	ALBU_HUMAN	1.01	0.0	3574	65	0.94	0.282	0.550
Complement C3 OS=Homo sapiens GN=C3 PE=1 SV=2	CO3_HUMAN	1.02	0.0	2898	60	1.04	0.180	0.744
Alpha-2-macroglobulin OS=Homo sapiens GN=A2M PE=1 SV=3	A2MG_HUMAN	1.08	0.1	1837	48	1.11	0.371	0.430
Serotransferrin OS=Homo sapiens GN=TF PE=1 SV=3	TRFE_HUMAN	1.01	0.0	1372	24	0.97	0.423	0.374
Complement C4-A OS=Homo sapiens GN=C4A PE=1 SV=2	CO4A_HUMAN	0.92	-0.1	693	21	0.81	0.068	1.165
Complement C4-B OS=Homo sapiens GN=C4B PE=1 SV=2	CO4B_HUMAN	0.92	-0.1	748	23	0.83	0.061	1.215
Immunoglobulin heavy constant mu OS=Homo sapiens GN=IGHM PE=1 SV=4	IGHM_HUMAN	1.13	0.2	433	12	1.25	0.209	0.680
Alpha-1-antitrypsin OS=Homo sapiens GN=SERPINA1 PE=1 SV=3	A1AT_HUMAN	0.87	-0.2	667	17	0.97	0.797	0.099
Haptoglobin OS=Homo sapiens GN=HP PE=1 SV=1	HPT_HUMAN	0.98	0.0	664	14	0.94	0.224	0.650
Apolipoprotein A-I OS=Homo sapiens GN=APOA1 PE=1 SV=1	APOA1_HUMAN	1.23	0.3	286	7	1.28	0.052	1.281
C4b-binding protein alpha chain OS=Homo sapiens GN=C4BPA PE=1 SV=2	C4BPA_HUMAN	1.16	0.2	327	5	1.19	0.230	0.637
Immunoglobulin gamma-1 heavy chain OS=Homo sapiens PE=1 SV=1	IGG1_HUMAN	1.30	0.4	374	12	1.40	0.084	1.078
Hemopexin OS=Homo sapiens GN=HPX PE=1 SV=2	HEMO_HUMAN	1.04	0.1	421	10	0.92	0.442	0.355
Immunoglobulin heavy constant gamma 3 OS=Homo sapiens GN=IGHG3 PE=1 SV=2	IGHG3_HUMAN	1.25	0.3	349	10	1.23	0.048	1.317
Complement factor H OS=Homo sapiens GN=CFH PE=1 SV=4	CFAH_HUMAN	0.99	0.0	449	8	0.80	0.202	0.694
Inter-alpha-trypsin inhibitor heavy chain H1 OS=Homo sapiens GN=ITIH1 PE=1 SV=3	ITIH1_HUMAN	0.97	0.0	416	7	0.99	0.677	0.170
Inter-alpha-trypsin inhibitor heavy chain H2 OS=Homo sapiens GN=ITIH2 PE=1 SV=2	ITIH2_HUMAN	0.99	0.0	317	8	0.91	0.240	0.620
Alpha-1-antichymotrypsin OS=Homo sapiens GN=SERPINA3 PE=1 SV=2	AACT_HUMAN	0.93	-0.1	404	7	0.97	0.329	0.483
Antithrombin-III OS=Homo sapiens GN=SERPINC1 PE=1 SV=1	ANT3_HUMAN	0.88	-0.2	209	7	1.02	0.897	0.047
Ceruloplasmin OS=Homo sapiens GN=CP PE=1 SV=1	CERU_HUMAN	0.97	0.0	547	9	0.94	0.405	0.393
Plasma protease C1 inhibitor OS=Homo sapiens GN=SERPING1 PE=1 SV=2	IC1_HUMAN	0.87	-0.2	264	5	0.76	0.061	1.216
Immunoglobulin heavy constant alpha 1 OS=Homo sapiens GN=IGHA1 PE=1 SV=2	IGHA1_HUMAN	1.04	0.1	248	8	1.06	0.097	1.013
Alpha-1B-glycoprotein OS=Homo sapiens GN=A1BG PE=1 SV=4	A1BG_HUMAN	0.93	-0.1	190	4	0.85	0.245	0.612
Haptoglobin-related protein OS=Homo sapiens GN=HPR PE=2 SV=2	HPTR_HUMAN	0.92	-0.1	306	6	0.97	0.660	0.180
Immunoglobulin heavy constant gamma 2 OS=Homo sapiens GN=IGHG2 PE=1 SV=2	IGHG2_HUMAN	1.29	0.4	244	6	1.21	0.024	1.617
Apolipoprotein E OS=Homo sapiens GN=APOE PE=1 SV=1	APOE_HUMAN	1.06	0.1	247	2	1.19	0.420	0.377
Immunoglobulin alpha-2 heavy chain OS=Homo sapiens PE=1 SV=1	IGA2_HUMAN	1.10	0.1	203	5	1.11	0.158	0.802
Immunoglobulin kappa light chain OS=Homo sapiens PE=1 SV=1	IGK_HUMAN	1.78	0.8	319	4	1.36	0.139	0.856
Kininogen-1 OS=Homo sapiens GN=KNG1 PE=1 SV=2	KNG1_HUMAN	0.77	-0.4	111	4	0.81	0.382	0.417
Protein AMBP OS=Homo sapiens GN=AMBP PE=1 SV=1	AMBP_HUMAN	0.82	-0.3	40	2	0.69	0.083	1.080
Immunoglobulin lambda-1 light chain OS=Homo sapiens PE=1 SV=1	IGL1_HUMAN	1.54	0.6	190	4	1.65	0.030	1.523
Immunoglobulin kappa variable 3-20 OS=Homo sapiens GN=IGKV3-20 PE=1 SV=2	KV320_HUMAN	1.90	0.9	196	2	1.50	0.077	1.111
Vitamin D-binding protein OS=Homo sapiens GN=GC PE=1 SV=1	VTDB_HUMAN	0.77	-0.4	210	3	0.81	0.021	1.675
Vitronectin OS=Homo sapiens GN=VTN PE=1 SV=1	VTNC_HUMAN	0.87	-0.2	219	2	0.80	0.123	0.911

Table S4. List of quantified proteins for Experiment 3 (Light = 33% dPG-PNIPAM (25°C), Heavy = PNIPAM/BIS (25 °C), ^{18}O-ratios according to the Mascot Distiller software (version 2.6.1.0 [Matrix Science Ltd, London, UK]).

Description	Accession	Molecular weight (Da)	Ratio H/L normalized A	LOG2 Ratio H/L normalized A	Mascot score A	# A (Count)	Ratio H/L normalized B	LOG2 Ratio H/L normalized B	Mascot score B	# B (Count)
Serum albumin OS=Homo sapiens GN=ALB PE=1 SV=2	ALBU_HUMAN	71317	1.67	0.7	5636	82	1.31	0.4	3983	57
Apolipoprotein B-100 OS=Homo sapiens GN=APOB PE=1 SV=2	APOB_HUMAN	516651	0.32	-1.7	3697	64	0.45	-1.2	2188	56
Complement C3 OS=Homo sapiens GN=C3 PE=1 SV=2	CO3_HUMAN	188569	0.68	-0.6	2356	53	1.03	0.0	1728	48
Serotransferrin OS=Homo sapiens GN=TF PE=1 SV=3	TRFE_HUMAN	79294	2.12	1.1	1513	46	1.52	0.6	1436	40
Alpha-2-macroglobulin OS=Homo sapiens GN=A2M PE=1 SV=3	A2MG_HUMAN	164613	0.32	-1.7	2459	41	0.64	-0.6	2067	39
Alpha-1-antitrypsin OS=Homo sapiens GN=SERPINA1 PE=1 SV=3	A1AT_HUMAN	46878	1.11	0.1	883	21	0.83	-0.3	726	18
Complement C4-B OS=Homo sapiens GN=C4B PE=1 SV=2	CO4B_HUMAN	194170	0.82	-0.3	1148	21	1.00	0.0	803	18
Complement C4-A OS=Homo sapiens GN=C4A PE=1 SV=2	CO4A_HUMAN	194261	0.76	-0.4	1071	20	0.99	0.0	775	16
Ceruloplasmin OS=Homo sapiens GN=CP PE=1 SV=1	CERU_HUMAN	122983	1.30	0.4	702	19	1.24	0.3	660	16
Immunoglobulin heavy constant mu OS=Homo sapiens GN=IGHM PE=1 SV=4	IGHM_HUMAN	50093	0.09	-3.4	867	17	0.59	-0.8	375	9
Haptoglobin OS=Homo sapiens GN=HP PE=1 SV=1	HPT_HUMAN	45861	0.68	-0.6	714	15	0.56	-0.8	417	8
Immunoglobulin gamma-1 heavy chain OS=Homo sapiens PE=1 SV=1	IGG1_HUMAN	49926	1.41	0.5	329	12	1.12	0.2	368	10
Apolipoprotein A-I OS=Homo sapiens GN=APOA1 PE=1 SV=1	APOA1_HUMAN	30759	0.44	-1.2	471	11	0.39	-1.4	375	10
Hemopexin OS=Homo sapiens GN=HPX PE=1 SV=2	HEMO_HUMAN	52385	1.72	0.8	324	11	1.37	0.5	244	8
Immunoglobulin heavy constant alpha 1 OS=Homo sapiens GN=IGHA1 PE=1 SV=2	IGHA1_HUMAN	38486	0.90	-0.2	373	10	1.25	0.3	196	7
Immunoglobulin heavy constant gamma 3 OS=Homo sapiens GN=IGHG3 PE=1 SV=2	IGHG3_HUMAN	42287	1.19	0.3	321	9	0.96	-0.1	296	8
Inter-alpha-trypsin inhibitor heavy chain H2 OS=Homo sapiens GN=ITIH2 PE=1 SV=2	ITIH2_HUMAN	106853	0.65	-0.6	372	9	0.78	-0.4	254	9
Vitamin D-binding protein OS=Homo sapiens GN=GC PE=1 SV=1	VTDB_HUMAN	54526	2.87	1.5	352	9	1.41	0.5	314	8
Alpha-1B-glycoprotein OS=Homo sapiens GN=A1BG PE=1 SV=4	A1BG_HUMAN	54790	0.91	-0.1	257	8	1.20	0.3	191	6
Complement factor H OS=Homo sapiens GN=CFH PE=1 SV=4	CFAH_HUMAN	143680	0.86	-0.2	748	8	0.87	-0.2	562	12
Haptoglobin-related protein OS=Homo sapiens GN=HPR PE=2 SV=2	HPTR_HUMAN	39518	0.86	-0.2	210	8	0.60	-0.7	220	6
Immunoglobulin kappa constant OS=Homo sapiens GN=IGKC PE=1 SV=2	IGKC_HUMAN	11929	1.00	0.0	436	8	0.61	-0.7	212	3
C4b-binding protein alpha chain OS=Homo sapiens GN=C4BPA PE=1 SV=2	C4BPA_HUMAN	69042	0.32	-1.6	519	7	0.66	-0.6	433	9
Plasma protease C1 inhibitor OS=Homo sapiens GN=SERPING1 PE=1 SV=2	IC1_HUMAN	55347	0.82	-0.3	353	7	0.75	-0.4	317	6
Immunoglobulin lambda-1 light chain OS=Homo sapiens PE=1 SV=1	IGL1_HUMAN	23101	1.36	0.4	259	7	0.83	-0.3	167	2
Inter-alpha-trypsin inhibitor heavy chain H4 OS=Homo sapiens GN=ITIH4 PE=1 SV=4	ITIH4_HUMAN	103521	1.13	0.2	412	7	0.99	0.0	396	7
Kininogen-1 OS=Homo sapiens GN=KNG1 PE=1 SV=2	KNG1_HUMAN	72996	1.44	0.5	339	7	1.13	0.2	160	4
Alpha-1-antichymotrypsin OS=Homo sapiens GN=SERPINA3 PE=1 SV=2	AACT_HUMAN	47792	1.27	0.3	285	6	1.05	0.1	234	8
Antithrombin-III OS=Homo sapiens GN=SERPINC1 PE=1 SV=1	ANT3_HUMAN	53025	1.20	0.3	429	6	1.03	0.0	292	8
Immunoglobulin heavy constant gamma 4 OS=Homo sapiens GN=IGHG4 PE=1 SV=1	IGHG4_HUMAN	36431	1.24	0.3	186	6	1.00	0.0	154	6
Inter-alpha-trypsin inhibitor heavy chain H1 OS=Homo sapiens GN=ITIH1 PE=1 SV=3	ITIH1_HUMAN	101782	0.39	-1.4	583	6	0.68	-0.6	506	9
Complement factor B OS=Homo sapiens GN=CFB PE=1 SV=2	CFAB_HUMAN	86847	1.16	0.2	383	5	1.10	0.1	308	6
Afamin OS=Homo sapiens GN=AFM PE=1 SV=1	AFAM_HUMAN	70963	1.61	0.7	250	4	1.56	0.6	181	5
Plasminogen OS=Homo sapiens GN=PLG PE=1 SV=2	PLMN_HUMAN	93247	1.81	0.9	249	4	1.78	0.8	186	4
Vitronectin OS=Homo sapiens GN=VTN PE=1 SV=1	VTNC_HUMAN	55069	0.98	0.0	161	4	1.15	0.2	187	5
Alpha-1-acid glycoprotein 1 OS=Homo sapiens GN=ORM1 PE=1 SV=1	A1AG1_HUMAN	23725	1.35	0.4	148	3	0.96	-0.1	106	3
Gelsolin OS=Homo sapiens GN=GSN PE=1 SV=1	GELS_HUMAN	86043	1.39	0.5	216	3	1.04	0.1	155	6
Alpha-1-acid glycoprotein 2 OS=Homo sapiens GN=ORM2 PE=1 SV=2	A1AG2_HUMAN	23873	1.05	0.1	74	2	0.90	-0.2	69	3
Protein AMBP OS=Homo sapiens GN=AMBP PE=1 SV=1	AMBP_HUMAN	39886	0.43	-1.2	199	2	0.85	-0.2	110	2
Angiotensinogen OS=Homo sapiens GN=AGT PE=1 SV=1	ANGT_HUMAN	53406	1.00	0.0	292	2	1.09	0.1	305	4
Apolipoprotein E OS=Homo sapiens GN=APOE PE=1 SV=1	APOE_HUMAN	36246	0.45	-1.2	152	2	0.52	-1.0	146	2
Beta-2-glycoprotein 1 OS=Homo sapiens GN=APOH PE=1 SV=3	APOH_HUMAN	39584	1.97	1.0	113	2	1.82	0.9	95	5
Heparin cofactor 2 OS=Homo sapiens GN=SERPIND1 PE=1 SV=3	HEP2_HUMAN	57205	0.97	0.0	134	2	1.46	0.5	109	3
Histidine-rich glycoprotein OS=Homo sapiens GN=HRG PE=1 SV=1	HRG_HUMAN	60510	0.90	-0.1	112	2	1.34	0.4	160	3
Immunoglobulin alpha-2 heavy chain OS=Homo sapiens PE=1 SV=1	IGA2_HUMAN	49817	0.98	0.0	183	2	1.31	0.4	86	5
Prothrombin OS=Homo sapiens GN=F2 PE=1 SV=2	THRB_HUMAN	71475	1.08	0.1	116	2	0.89	-0.2	125	2

Table S4 (follows). List of quantified proteins for Experiment 3 (Light = 33% dPG-PNIPAM (25°C), Heavy = PNIPAM/BIS (25 °C), ^{18}O-ratios according to the Mascot Distiller software (version 2.6.1.0 [Matrix Science Ltd, London, UK]).

Description	Accession	Ratio H/L normalized C	LOG2 Ratio H/L normalized C	Mascot score C	# C (Count)	Mean H/L ratio	p-value	-LOG(P-value)
Serum albumin OS=Homo sapiens GN=ALB PE=1 SV=2	ALBU_HUMAN	1.33	0.4	3775	58	1.43	0.045	1.343
Apolipoprotein B-100 OS=Homo sapiens GN=APOB PE=1 SV=2	APOB_HUMAN	0.41	-1.3	2493	53	0.39	0.012	1.926
Complement C3 OS=Homo sapiens GN=C3 PE=1 SV=2	CO3_HUMAN	0.96	-0.1	2274	52	0.88	0.411	0.386
Serotransferrin OS=Homo sapiens GN=TF PE=1 SV=3	TRFE_HUMAN	1.45	0.5	1549	30	1.67	0.050	1.304
Alpha-2-macroglobulin OS=Homo sapiens GN=A2M PE=1 SV=3	A2MG_HUMAN	0.67	-0.6	2269	40	0.51	0.114	0.945
Alpha-1-antitrypsin OS=Homo sapiens GN=SERPINA1 PE=1 SV=3	A1AT_HUMAN	1.20	0.3	859	18	1.04	0.780	0.108
Complement C4-B OS=Homo sapiens GN=C4B PE=1 SV=2	CO4B_HUMAN	0.93	-0.1	921	20	0.91	0.273	0.564
Complement C4-A OS=Homo sapiens GN=C4A PE=1 SV=2	CO4A_HUMAN	0.88	-0.2	928	19	0.87	0.213	0.671
Ceruloplasmin OS=Homo sapiens GN=CP PE=1 SV=1	CERU_HUMAN	1.11	0.2	738	13	1.21	0.053	1.274
Immunoglobulin heavy constant mu OS=Homo sapiens GN=IGHM PE=1 SV=4	IGHM_HUMAN	0.56	-0.8	533	9	0.31	0.193	0.714
Haptoglobin OS=Homo sapiens GN=HP PE=1 SV=1	HPT_HUMAN	0.77	-0.4	477	11	0.66	0.046	1.341
Immunoglobulin gamma-1 heavy chain OS=Homo sapiens PE=1 SV=1	IGG1_HUMAN	0.90	-0.1	373	11	1.13	0.454	0.343
Apolipoprotein A-I OS=Homo sapiens GN=APOA1 PE=1 SV=1	APOA1_HUMAN	0.86	-0.2	344	5	0.53	0.123	0.910
Hemopexin OS=Homo sapiens GN=HPX PE=1 SV=2	HEMO_HUMAN	1.45	0.5	303	9	1.51	0.026	1.579
Immunoglobulin heavy constant alpha 1 OS=Homo sapiens GN=IGHA1 PE=1 SV=2	IGHA1_HUMAN	0.93	-0.1	192	8	1.01	0.901	0.045
Immunoglobulin heavy constant gamma 3 OS=Homo sapiens GN=IGHG3 PE=1 SV=2	IGHG3_HUMAN	0.78	-0.4	418	8	0.96	0.776	0.110
Inter-alpha-trypsin inhibitor heavy chain H2 OS=Homo sapiens GN=ITIH2 PE=1 SV=2	ITIH2_HUMAN	0.61	-0.7	320	5	0.67	0.033	1.487
Vitamin D-binding protein OS=Homo sapiens GN=GC PE=1 SV=1	VTDB_HUMAN	1.57	0.7	213	6	1.86	0.107	0.971
Alpha-1B-glycoprotein OS=Homo sapiens GN=A1BG PE=1 SV=4	A1BG_HUMAN	1.56	0.6	203	5	1.19	0.374	0.427
Complement factor H OS=Homo sapiens GN=CFH PE=1 SV=4	CFAH_HUMAN	0.93	-0.1	645	13	0.89	0.035	1.456
Haptoglobin-related protein OS=Homo sapiens GN=HPR PE=2 SV=2	HPTR_HUMAN	0.72	-0.5	311	5	0.72	0.085	1.070
Immunoglobulin kappa constant OS=Homo sapiens GN=IGKC PE=1 SV=2	IGKC_HUMAN	0.72	-0.5	232	4	0.76	0.204	0.690
C4b-binding protein alpha chain OS=Homo sapiens GN=C4BPA PE=1 SV=2	C4BPA_HUMAN	0.77	-0.4	659	9	0.55	0.155	0.809
Plasma protease C1 inhibitor OS=Homo sapiens GN=SERPING1 PE=1 SV=2	IC1_HUMAN	0.91	-0.1	332	8	0.82	0.070	1.158
Immunoglobulin lambda-1 light chain OS=Homo sapiens PE=1 SV=1	IGL1_HUMAN	0.97	0.0	135	3	1.03	0.849	0.071
Inter-alpha-trypsin inhibitor heavy chain H4 OS=Homo sapiens GN=ITIH4 PE=1 SV=4	ITIH4_HUMAN	1.67	0.7	373	6	1.23	0.321	0.494
Kininogen-1 OS=Homo sapiens GN=KNG1 PE=1 SV=2	KNG1_HUMAN	1.11	0.1	165	4	1.22	0.142	0.848
Alpha-1-antichymotrypsin OS=Homo sapiens GN=SERPINA3 PE=1 SV=2	AACT_HUMAN	1.03	0.0	295	6	1.11	0.264	0.578
Antithrombin-III OS=Homo sapiens GN=SERPINC1 PE=1 SV=1	ANT3_HUMAN	1.16	0.2	265	8	1.13	0.126	0.899
Immunoglobulin heavy constant gamma 4 OS=Homo sapiens GN=IGHG4 PE=1 SV=1	IGHG4_HUMAN	0.84	-0.3	196	6	1.01	0.921	0.036
Inter-alpha-trypsin inhibitor heavy chain H1 OS=Homo sapiens GN=ITIH1 PE=1 SV=3	ITIH1_HUMAN	0.59	-0.8	478	5	0.54	0.068	1.167
Complement factor B OS=Homo sapiens GN=CFB PE=1 SV=2	CFAB_HUMAN	1.24	0.3	336	9	1.16	0.049	1.312
Afamin OS=Homo sapiens GN=AFM PE=1 SV=1	AFAM_HUMAN	1.51	0.6	163	4	1.56	0.002	2.758
Plasminogen OS=Homo sapiens GN=PLG PE=1 SV=2	PLMN_HUMAN	1.42	0.5	255	4	1.66	0.022	1.651
Vitronectin OS=Homo sapiens GN=VTN PE=1 SV=1	VTNC_HUMAN	1.22	0.3	110	4	1.11	0.256	0.592
Alpha-1-acid glycoprotein 1 OS=Homo sapiens GN=ORM1 PE=1 SV=1	A1AG1_HUMAN	1.69	0.8	166	4	1.30	0.256	0.592
Gelsolin OS=Homo sapiens GN=GSN PE=1 SV=1	GELS_HUMAN	1.42	0.5	127	2	1.27	0.143	0.844
Alpha-1-acid glycoprotein 2 OS=Homo sapiens GN=ORM2 PE=1 SV=2	A1AG2_HUMAN	1.64	0.7	93	2	1.16	0.509	0.293
Protein AMBP OS=Homo sapiens GN=AMBP PE=1 SV=1	AMBP_HUMAN	1.37	0.5	171	3	0.79	0.562	0.250
Angiotensinogen OS=Homo sapiens GN=AGT PE=1 SV=1	ANGT_HUMAN	1.27	0.3	211	4	1.11	0.269	0.571
Apolipoprotein E OS=Homo sapiens GN=APOE PE=1 SV=1	APOE_HUMAN	0.86	-0.2	211	2	0.58	0.112	0.953
Beta-2-glycoprotein 1 OS=Homo sapiens GN=APOH PE=1 SV=3	APOH_HUMAN	2.00	1.0	103	4	1.93	0.002	2.672
Heparin cofactor 2 OS=Homo sapiens GN=SERPIND1 PE=1 SV=3	HEP2_HUMAN	1.23	0.3	163	3	1.20	0.256	0.593
Histidine-rich glycoprotein OS=Homo sapiens GN=HRG PE=1 SV=1	HRG_HUMAN	1.16	0.2	103	3	1.12	0.428	0.369
Immunoglobulin alpha-2 heavy chain OS=Homo sapiens PE=1 SV=1	IGA2_HUMAN	0.87	-0.2	149	5	1.03	0.807	0.093
Prothrombin OS=Homo sapiens GN=F2 PE=1 SV=2	THRB_HUMAN	0.93	-0.1	91	2	0.96	0.592	0.228

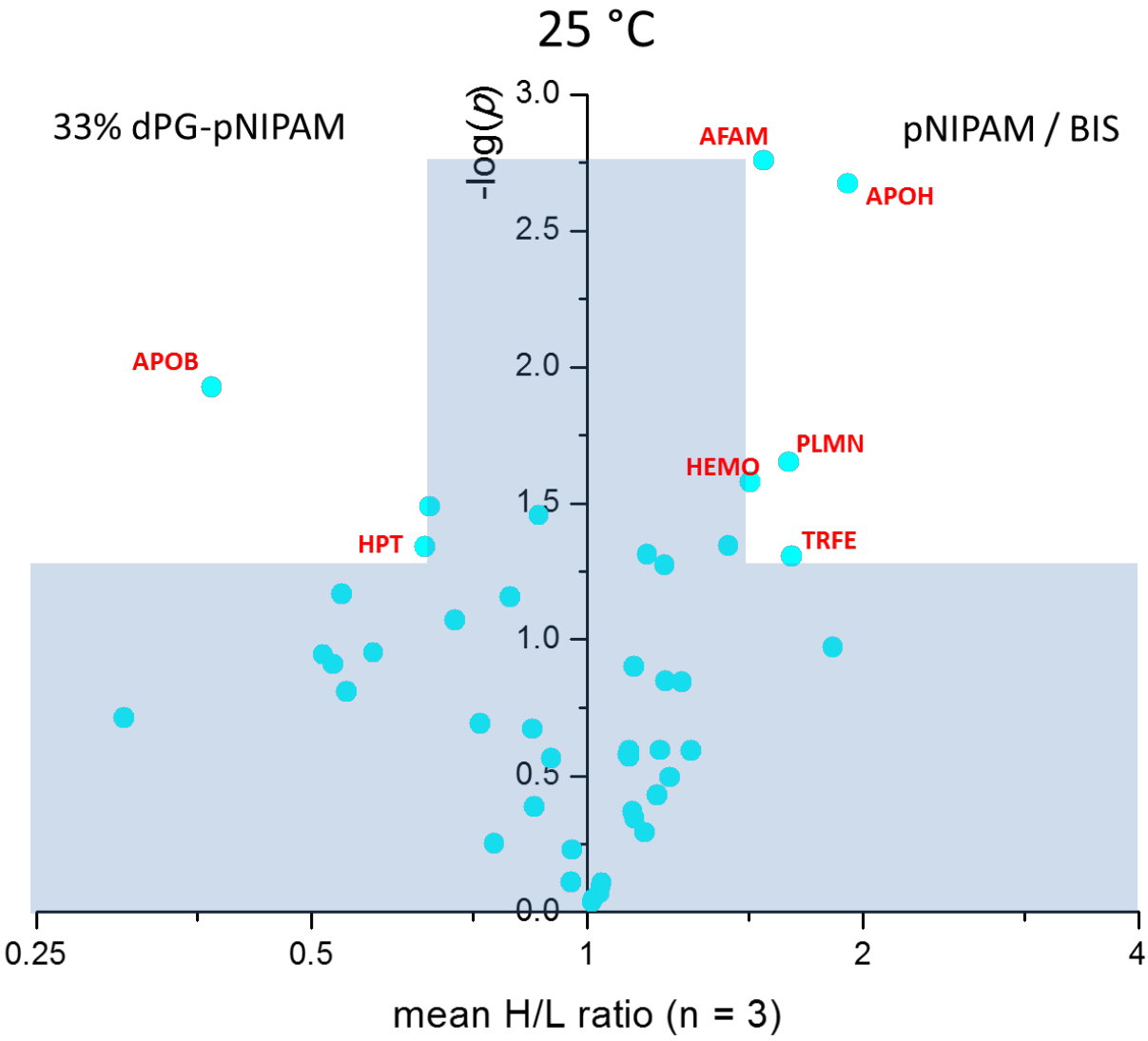

Fig. S1 Volcano plot for the enriched proteins found in the protein coronae around 33 w/w% dPG – pNIPAM and pNIPAM/BIS nanogels incubated in human serum for 1 h at 25 °C. Proteins were highlighted (red labels) if their mean H/L ratio (n=3) indicated more than 1.5-fold enrichment (mean H/L < 0.66 or mean H/L > 1.5). Mean H/L ratios with p-values ≤ 0.05 (-log(p) ≥ 1.3) were considered significant.

Table S5. List of quantified proteins for Experiment 4 (Light = PNIPMAM/BIS (37°C), Heavy = 33% dPG-PNIPMAM (37°C), ^{18}O-ratios according to the Mascot Distiller software (version 2.6.1.0 [Matrix Science Ltd, London, UK]).

Description	Accession	Molecular weight (Da)	Ratio H/L normalized A	LOG2 Ratio H/L normalized A	Mascot score A	# A (Count)	Ratio H/L normalized B	LOG2 Ratio H/L normalized B	Mascot score B	# B (Count)
Complement C3 OS=Homo sapiens GN=C3 PE=1 SV=2	CO3_HUMAN	188569	1.10	0.1	3159	67	1.05	0.1	2969	63
Serum albumin OS=Homo sapiens GN=ALB PE=1 SV=2	ALBU_HUMAN	71317	1.22	0.3	4737	60	1.21	0.3	4189	52
Apolipoprotein B-100 OS=Homo sapiens GN=APOB PE=1 SV=2	APOB_HUMAN	516651	0.73	-0.4	3210	46	0.48	-1.0	3272	38
Serotransferrin OS=Homo sapiens GN=TF PE=1 SV=3	TRFE_HUMAN	79294	1.14	0.2	2323	42	1.01	0.0	1592	36
Alpha-2-macroglobulin OS=Homo sapiens GN=A2M PE=1 SV=3	A2MG_HUMAN	164613	0.80	-0.3	2273	40	0.79	-0.3	2359	40
Complement C4-A OS=Homo sapiens GN=C4A PE=1 SV=2	CO4A_HUMAN	194261	1.00	0.0	1115	24	0.94	-0.1	893	21
Complement C4-B OS=Homo sapiens GN=C4B PE=1 SV=2	CO4B_HUMAN	194170	1.02	0.0	1090	24	0.94	-0.1	933	21
Alpha-1-antitrypsin OS=Homo sapiens GN=SERPINA1 PE=1 SV=3	A1AT_HUMAN	46878	1.10	0.1	769	22	1.04	0.1	608	22
Ceruloplasmin OS=Homo sapiens GN=CP PE=1 SV=1	CERU_HUMAN	122983	0.96	-0.1	682	21	1.05	0.1	580	17
Haptoglobin OS=Homo sapiens GN=HP PE=1 SV=1	HPT_HUMAN	45861	0.61	-0.7	674	14	0.77	-0.4	632	15
Complement factor H OS=Homo sapiens GN=CFH PE=1 SV=4	CFAH_HUMAN	143680	0.77	-0.4	709	12	0.61	-0.7	659	9
Apolipoprotein A-I OS=Homo sapiens GN=APOA1 PE=1 SV=1	APOA1_HUMAN	30759	1.32	0.4	501	11	1.30	0.4	432	11
Immunoglobulin heavy constant mu OS=Homo sapiens GN=IGHM PE=1 SV=4	IGHM_HUMAN	50093	0.80	-0.3	442	11	1.02	0.0	341	12
Immunoglobulin heavy constant gamma 3 OS=Homo sapiens GN=IGHG3 PE=1 SV=2	IGHG3_HUMAN	42287	1.30	0.4	288	10	0.92	-0.1	232	9
Inter-alpha-trypsin inhibitor heavy chain H2 OS=Homo sapiens GN=ITIH2 PE=1 SV=2	ITIH2_HUMAN	106853	0.69	-0.5	482	10	0.63	-0.7	488	8
Hemopexin OS=Homo sapiens GN=HPX PE=1 SV=2	HEMO_HUMAN	52385	0.99	0.0	430	9	0.85	-0.2	355	9
Immunoglobulin heavy constant alpha 1 OS=Homo sapiens GN=IGHA1 PE=1 SV=2	IGHA1_HUMAN	38486	1.00	0.0	416	9	0.99	0.0	279	8
Immunoglobulin gamma-1 heavy chain OS=Homo sapiens PE=1 SV=1	IGG1_HUMAN	49926	1.26	0.3	320	8	1.06	0.1	260	10
Immunoglobulin mu heavy chain OS=Homo sapiens PE=1 SV=1	IGM_HUMAN	64244	0.82	-0.3	404	8	0.93	-0.1	280	9
Inter-alpha-trypsin inhibitor heavy chain H4 OS=Homo sapiens GN=ITIH4 PE=1 SV=4	ITIH4_HUMAN	103521	0.98	0.0	614	8	1.02	0.0	437	2
Haptoglobin-related protein OS=Homo sapiens GN=HPR PE=2 SV=2	HPTR_HUMAN	39518	0.80	-0.3	350	7	0.54	-0.9	441	7
Immunoglobulin alpha-2 heavy chain OS=Homo sapiens PE=1 SV=1	IGA2_HUMAN	49817	1.29	0.4	197	7	1.31	0.4	164	4
Immunoglobulin kappa constant OS=Homo sapiens GN=IGKC PE=1 SV=2	IGKC_HUMAN	11929	0.93	-0.1	321	7	1.07	0.1	272	5
Alpha-1B-glycoprotein OS=Homo sapiens GN=A1BG PE=1 SV=4	A1BG_HUMAN	54790	0.84	-0.2	233	6	0.98	0.0	118	3
Alpha-1-antichymotrypsin OS=Homo sapiens GN=SERPINA3 PE=1 SV=2	AACT_HUMAN	47792	1.28	0.4	341	6	1.18	0.2	492	8
C4b-binding protein alpha chain OS=Homo sapiens GN=C4BPA PE=1 SV=2	C4BPA_HUMAN	69042	1.08	0.1	461	6	1.03	0.0	359	5
Immunoglobulin kappa light chain OS=Homo sapiens PE=1 SV=1	IGK_HUMAN	23650	0.90	-0.1	294	6	0.91	-0.1	310	4
Inter-alpha-trypsin inhibitor heavy chain H1 OS=Homo sapiens GN=ITIH1 PE=1 SV=3	ITIH1_HUMAN	101782	0.82	-0.3	577	6	0.68	-0.6	592	10
Vitamin D-binding protein OS=Homo sapiens GN=GC PE=1 SV=1	VTDB_HUMAN	54526	0.89	-0.2	209	6	1.06	0.1	485	7
Antithrombin-III OS=Homo sapiens GN=SERPINC1 PE=1 SV=1	ANT3_HUMAN	53025	0.91	-0.1	313	5	1.28	0.4	560	7
Alpha-2-HS-glycoprotein OS=Homo sapiens GN=AHSG PE=1 SV=1	FETUA_HUMAN	40098	1.31	0.4	133	5	0.83	-0.3	225	5
Plasma protease C1 inhibitor OS=Homo sapiens GN=SERPING1 PE=1 SV=2	IC1_HUMAN	55347	0.62	-0.7	365	5	0.57	-0.8	426	6
Immunoglobulin lambda-1 light chain OS=Homo sapiens PE=1 SV=1	IGL1_HUMAN	23101	1.10	0.1	215	5	1.18	0.2	116	3
Immunoglobulin heavy constant gamma 2 OS=Homo sapiens GN=IGHG2 PE=1 SV=2	IGHG2_HUMAN	36505	1.19	0.3	268	4	0.99	0.0	265	8
Afamin OS=Homo sapiens GN=AFM PE=1 SV=1	AFAM_HUMAN	70963	0.35	-1.5	142	3	1.31	0.4	87	2
Angiotensinogen OS=Homo sapiens GN=AGT PE=1 SV=1	ANGT_HUMAN	53406	0.97	-0.1	372	3	0.89	-0.2	338	3
Complement factor B OS=Homo sapiens GN=CFB PE=1 SV=2	CFAB_HUMAN	86847	0.67	-0.6	310	3	0.98	0.0	339	6
Immunoglobulin heavy constant gamma 4 OS=Homo sapiens GN=IGHG4 PE=1 SV=1	IGHG4_HUMAN	36431	1.19	0.3	236	3	1.05	0.1	221	6
Kininogen-1 OS=Homo sapiens GN=KNG1 PE=1 SV=2	KNG1_HUMAN	72996	1.23	0.3	253	3	0.55	-0.9	207	3
Vitronectin OS=Homo sapiens GN=VTN PE=1 SV=1	VTNC_HUMAN	55069	1.21	0.3	135	3	0.95	-0.1	234	2
Alpha-1-acid glycoprotein 1 OS=Homo sapiens GN=ORM1 PE=1 SV=1	A1AG1_HUMAN	23725	1.88	0.9	181	2	1.28	0.4	149	2
Apolipoprotein A-IV OS=Homo sapiens GN=APOA4 PE=1 SV=3	APOA4_HUMAN	45371	1.26	0.3	232	2	1.61	0.7	192	2
Histidine-rich glycoprotein OS=Homo sapiens GN=HRG PE=1 SV=1	HRG_HUMAN	60510	1.30	0.4	188	2	1.03	0.0	161	2
Plasminogen OS=Homo sapiens GN=PLG PE=1 SV=2	PLMN_HUMAN	93247	1.44	0.5	320	2	1.09	0.1	263	2

Table S5 (follows). List of quantified proteins for Experiment 4 (Light = PNIPMAM/BIS (37°C), Heavy = 33% dPG-PNIPMAM (37°C), ^{18}O-ratios according to the Mascot Distiller software (version 2.6.1.0 [Matrix Science Ltd, London, UK]).

Description	Accession	Ratio H/L normalized C	LOG2 Ratio H/L normalized C	Mascot score C	# C (Count)	Mean H/L ratio	p-value	-LOG(P-value)
Complement C3 OS=Homo sapiens GN=C3 PE=1 SV=2	CO3_HUMAN	1.13	0.2	3096	62	1.09	0.061	1.215
Serum albumin OS=Homo sapiens GN=ALB PE=1 SV=2	ALBU_HUMAN	1.34	0.4	5046	60	1.25	0.022	1.657
Apolipoprotein B-100 OS=Homo sapiens GN=APOB PE=1 SV=2	APOB_HUMAN	0.66	-0.6	3733	51	0.62	0.061	1.217
Serotransferrin OS=Homo sapiens GN=TF PE=1 SV=3	TRFE_HUMAN	1.08	0.1	2349	32	1.07	0.195	0.711
Alpha-2-macroglobulin OS=Homo sapiens GN=A2M PE=1 SV=3	A2MG_HUMAN	1.10	0.1	1860	39	0.89	0.383	0.417
Complement C4-A OS=Homo sapiens GN=C4A PE=1 SV=2	CO4A_HUMAN	0.94	-0.1	1178	27	0.96	0.188	0.725
Complement C4-B OS=Homo sapiens GN=C4B PE=1 SV=2	CO4B_HUMAN	0.95	-0.1	1181	27	0.97	0.329	0.483
Alpha-1-antitrypsin OS=Homo sapiens GN=SERPINA1 PE=1 SV=3	A1AT_HUMAN	1.04	0.1	1002	27	1.06	0.103	0.989
Ceruloplasmin OS=Homo sapiens GN=CP PE=1 SV=1	CERU_HUMAN	1.12	0.2	818	17	1.04	0.500	0.301
Haptoglobin OS=Homo sapiens GN=HP PE=1 SV=1	HPT_HUMAN	0.80	-0.3	829	13	0.72	0.060	1.219
Complement factor H OS=Homo sapiens GN=CFH PE=1 SV=4	CFAH_HUMAN	0.94	-0.1	824	12	0.76	0.159	0.800
Apolipoprotein A-I OS=Homo sapiens GN=APOA1 PE=1 SV=1	APOA1_HUMAN	1.42	0.5	494	9	1.35	0.007	2.136
Immunoglobulin heavy constant mu OS=Homo sapiens GN=IGHM PE=1 SV=4	IGHM_HUMAN	0.86	-0.2	371	12	0.89	0.235	0.629
Immunoglobulin heavy constant gamma 3 OS=Homo sapiens GN=IGHG3 PE=1 SV=2	IGHG3_HUMAN	1.11	0.2	258	8	1.10	0.447	0.349
Inter-alpha-trypsin inhibitor heavy chain H2 OS=Homo sapiens GN=ITIH2 PE=1 SV=2	ITIH2_HUMAN	0.68	-0.6	426	8	0.67	0.005	2.279
Hemopexin OS=Homo sapiens GN=HPX PE=1 SV=2	HEMO_HUMAN	0.96	-0.1	372	10	0.93	0.277	0.558
Immunoglobulin heavy constant alpha 1 OS=Homo sapiens GN=IGHA1 PE=1 SV=2	IGHA1_HUMAN	0.89	-0.2	390	7	0.96	0.394	0.405
Immunoglobulin gamma-1 heavy chain OS=Homo sapiens PE=1 SV=1	IGG1_HUMAN	1.15	0.2	302	10	1.15	0.098	1.008
Immunoglobulin mu heavy chain OS=Homo sapiens PE=1 SV=1	IGM_HUMAN	0.85	-0.2	320	10	0.86	0.055	1.262
Inter-alpha-trypsin inhibitor heavy chain H4 OS=Homo sapiens GN=ITIH4 PE=1 SV=4	ITIH4_HUMAN	1.01	0.0	432	6	1.00	0.959	0.018
Haptoglobin-related protein OS=Homo sapiens GN=HPR PE=2 SV=2	HPTR_HUMAN	1.36	0.4	425	10	0.84	0.575	0.241
Immunoglobulin alpha-2 heavy chain OS=Homo sapiens PE=1 SV=1	IGA2_HUMAN	0.98	0.0	149	5	1.18	0.209	0.680
Immunoglobulin kappa constant OS=Homo sapiens GN=IGKC PE=1 SV=2	IGKC_HUMAN	1.48	0.6	304	5	1.14	0.442	0.354
Alpha-1B-glycoprotein OS=Homo sapiens GN=A1BG PE=1 SV=4	A1BG_HUMAN	1.37	0.5	254	7	1.04	0.800	0.097
Alpha-1-antichymotrypsin OS=Homo sapiens GN=SERPINA3 PE=1 SV=2	AACT_HUMAN	0.99	0.0	532	9	1.14	0.212	0.675
C4b-binding protein alpha chain OS=Homo sapiens GN=C4BPA PE=1 SV=2	C4BPA_HUMAN	0.87	-0.2	625	9	0.99	0.896	0.048
Immunoglobulin kappa light chain OS=Homo sapiens PE=1 SV=1	IGK_HUMAN	1.28	0.4	305	4	1.02	0.904	0.044
Inter-alpha-trypsin inhibitor heavy chain H1 OS=Homo sapiens GN=ITIH1 PE=1 SV=3	ITIH1_HUMAN	0.84	-0.3	766	13	0.77	0.059	1.232
Vitamin D-binding protein OS=Homo sapiens GN=GC PE=1 SV=1	VTDB_HUMAN	1.09	0.1	494	8	1.01	0.887	0.052
Antithrombin-III OS=Homo sapiens GN=SERPINC1 PE=1 SV=1	ANT3_HUMAN	0.98	0.0	505	6	1.04	0.734	0.135
Alpha-2-HS-glycoprotein OS=Homo sapiens GN=AHSG PE=1 SV=1	FETUA_HUMAN	1.11	0.2	175	5	1.07	0.678	0.169
Plasma protease C1 inhibitor OS=Homo sapiens GN=SERPING1 PE=1 SV=2	IC1_HUMAN	0.63	-0.7	423	8	0.61	0.004	2.396
Immunoglobulin lambda-1 light chain OS=Homo sapiens PE=1 SV=1	IGL1_HUMAN	1.32	0.4	163	3	1.20	0.077	1.114
Immunoglobulin heavy constant gamma 2 OS=Homo sapiens GN=IGHG2 PE=1 SV=2	IGHG2_HUMAN	1.08	0.1	156	6	1.08	0.279	0.555
Afamin OS=Homo sapiens GN=AFM PE=1 SV=1	AFAM_HUMAN	0.94	-0.1	133	2	0.76	0.550	0.260
Angiotensinogen OS=Homo sapiens GN=AGT PE=1 SV=1	ANGT_HUMAN	0.96	-0.1	367	5	0.94	0.134	0.873
Complement factor B OS=Homo sapiens GN=CFB PE=1 SV=2	CFAB_HUMAN	0.96	-0.1	347	11	0.86	0.341	0.468
Immunoglobulin heavy constant gamma 4 OS=Homo sapiens GN=IGHG4 PE=1 SV=1	IGHG4_HUMAN	0.95	-0.1	196	3	1.06	0.481	0.318
Kininogen-1 OS=Homo sapiens GN=KNG1 PE=1 SV=2	KNG1_HUMAN	0.56	-0.8	255	4	0.72	0.347	0.460
Vitronectin OS=Homo sapiens GN=VTN PE=1 SV=1	VTNC_HUMAN	1.10	0.1	229	4	1.08	0.387	0.412
Alpha-1-acid glycoprotein 1 OS=Homo sapiens GN=ORM1 PE=1 SV=1	A1AG1_HUMAN	1.22	0.3	207	3	1.43	0.122	0.913
Apolipoprotein A-IV OS=Homo sapiens GN=APOA4 PE=1 SV=3	APOA4_HUMAN	1.16	0.2	192	2	1.33	0.100	1.001
Histidine-rich glycoprotein OS=Homo sapiens GN=HRG PE=1 SV=1	HRG_HUMAN	0.82	-0.3	230	3	1.03	0.825	0.084
Plasminogen OS=Homo sapiens GN=PLG PE=1 SV=2	PLMN_HUMAN	1.13	0.2	400	2	1.21	0.163	0.789

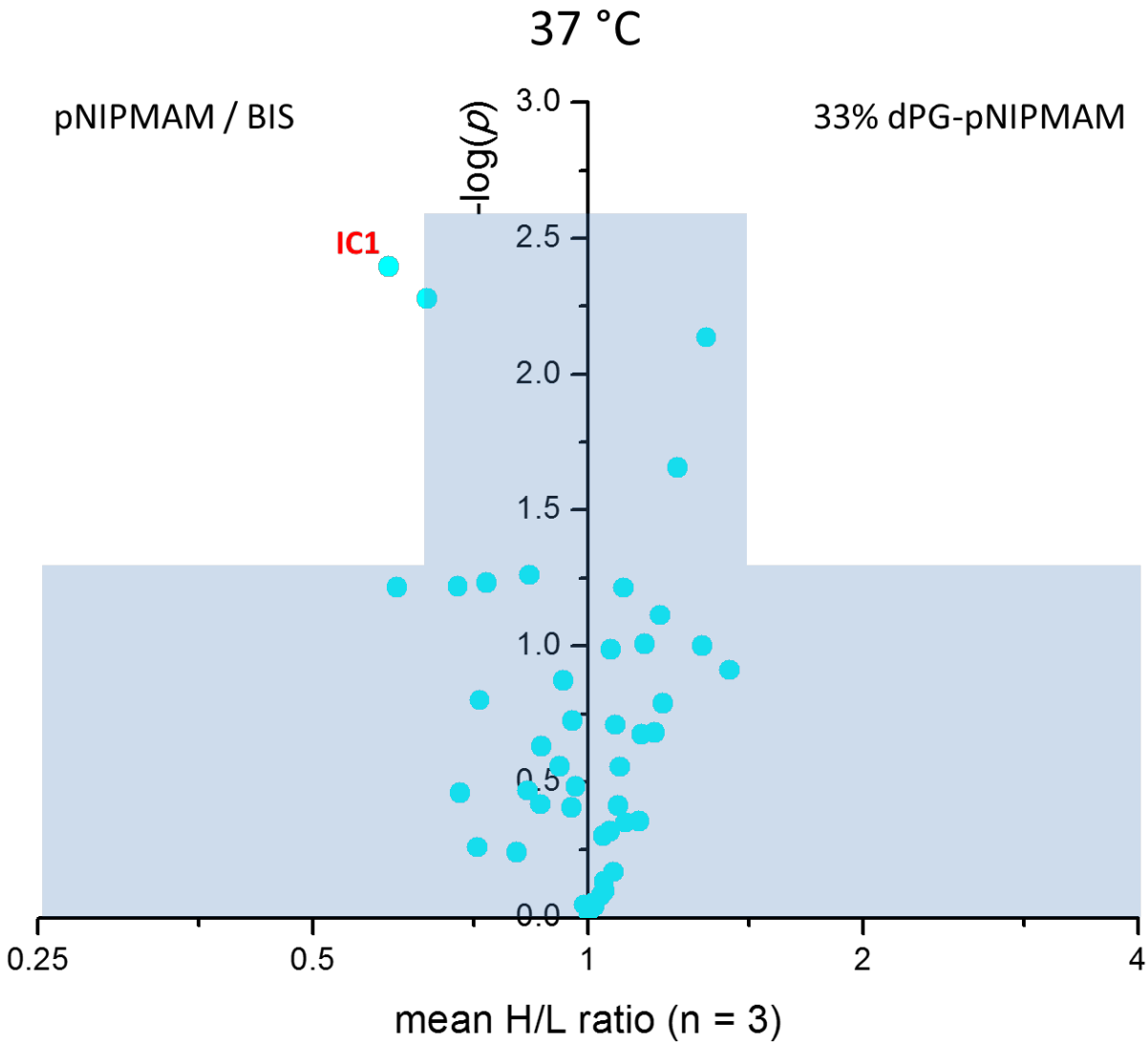

Fig. S2. Volcano plot for the enriched proteins found in the protein coronae around pNIPMAM/BIS and 33 w/w% dPG – pNIPMAM nanogels incubated in human serum for 1 h at 37 °C. Proteins were highlighted (red labels) if their mean H/L ratio (n=3) indicated more than 1.5-fold enrichment (mean H/L < 0.66 or mean H/L > 1.5). Mean H/L ratios with p-values ≤ 0.05 (-log(p) ≥ 1.3) were considered significant.

3.2 Protein Corona Formation on Colloidal Polymeric Nanoparticles and Polymeric Nanogels: Impact on Cellular Uptake, Toxicity, Immunogenicity, and Drug Release Properties

K. Obst, G. Yealland, B. Balzus, **E. Miceli**, M. Dimde, C. Weise, M. Eravci, R. Bodmeier, R. Haag, M. Calderón, N. Charbaji, S. Hedtrich, *Biomacromolecules* **2017**, *18*, 1762.

https://doi.org/10.1021/acs.biomac.7b00158

Author contribution: In this work, the author carried out the synthesis and characterization of thermoresponsive dPG-pNIPAM nanogels, as well as contributing to the data analysis, scientific discussion and the writing of a section of the manuscript.

3.3 Semi-interpenetrated, dendritic, dual-responsive nanogels with cytochrome *c* corona induce controlled apoptosis in HeLa cells

E. Miceli, S. Wedepohl, E. R. Osorio Blanco, G. N. Rimondino, M. Martinelli, M. Strumia, M. Molina, M. Kar, M. Calderón, *manuscript submitted.*

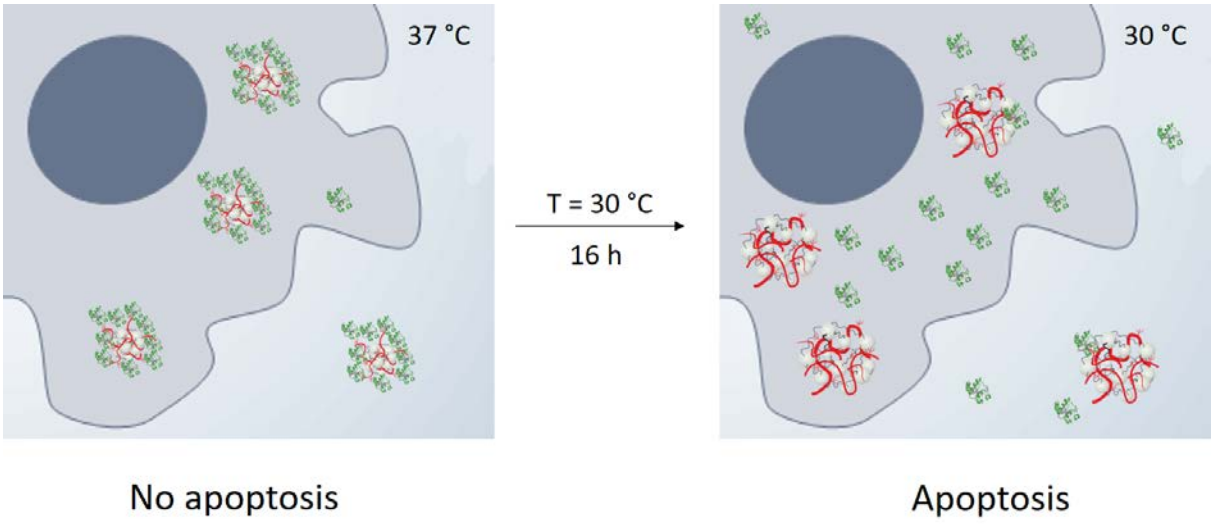

Fig. 3.3 A preassembled cytochrome *c* corona may be released upon nanogel swelling at 30 °C, inducing apoptosis in HeLa cells under controlled conditions.

Author contribution: The author was responsible for the overall concept, for the syntheses, characterizations, protein corona formation, *in vitro* release studies of cytochrome *c*, and sample preparation for apoptosis study on HeLa cells.

Abstract: Poly(N-isopropylacrylamide) (pNIPAM)-based NGs were involved in the release of a therapeutic protein corona by temperature decrease. NGs based on dendritic polyglycerol (dPG) and thermoresponsive pNIPAM were semi-interpenetrated with poly(4-acryloylamine-4-(carboxyethyl)heptanodioic acid) (pABC). The resulting semi-interpenetrated NGs retain the thermoresponsive properties of pNIPAM, together with pH-responsive, dendritic pABC as a secondary network, in one single nanoparticle. A cytochrome *c* (cyt *c*) corona was formed on SIPN NGs in their collapsed state (37 °C). Upon cooling of the samples to room temperature, the swelling of the NG effectively boosted the release of cyt c, as compared with the same kept at constant 37 °C. These responsive SIPN NGs were able to deliver cyt c to cancer cells and specifically induce apoptosis at 30 °C, while the cells remained largely unaffected at 37 °C.

Semi-interpenetrated, dendritic, dual-responsive nanogels with cytochrome c corona induce controlled apoptosis in HeLa cells

Enrico Miceli[ab], Stefanie Wedepohl[a], Ernesto Rafael Osorio Blanco[a], Guido Noé Rimondino[c,d], Marisa Martinelli[d], Miriam Strumia[d], Maria Molina[a], Mrityunjoy Kar[a], Marcelo Calderón[ab]*

a) Freie Universität Berlin, Institute of Chemistry and Biochemistry, Takustr. 3, 14195 Berlin, Germany.

b) Helmholtz Virtual Institute ‘‘Multifunctional Biomaterials for Medicine’’, Kantstr. 55, 14513 Teltow, Germany

c) Instituto de Investigaciones en Físico Química de (INFIQC), CONICET. Departamento de Físico-Química. Facultad de Ciencias Químicas, Universidad Nacional de Córdoba. Córdoba, Argentina.

d) LaMaP Laboratorio de Materiales Poliméricos, IPQA-CONICET, Departamento de Química, Facultad de Ciencias Químicas, Universidad Nacional de Córdoba, Haya de la Torre y Medina Allende, X5000HUA Córdoba, Argentina.

*E-mail: marcelo.calderon@fu-berlin.de

Abstract Poly(N-isopropylacrylamide) (pNIPAM)-based NGs were involved in the release of a therapeutic protein corona by temperature decrease. NGs based on dendritic polyglycerol (dPG) and thermoresponsive pNIPAM were semi-interpenetrated with poly(4-acryloylamine-4-(carboxyethyl)heptanodioic acid) (pABC). The resulting semi-interpenetrated NGs retain the thermoresponsive properties of pNIPAM, together with pH-responsive, dendritic pABC as a secondary network, in one single nanoparticle. A cytochrome c (cyt *c*) corona was formed on SIPN NGs in their collapsed state (37 °C). Upon cooling of the samples to room temperature, the swelling of the NG effectively boosted the release of cyt *c*, as compared with the same kept at constant 37 °C. These responsive SIPN NGs were able to deliver cyt *c* to cancer cells and specifically induce apoptosis at 30 °C, while the cells remained largely unaffected at 37 °C. In this way, we show therapeutic efficacy of thermoresponsive NGs as protein carriers and their efficacy triggered by temperature decrease. We envision the use of such thermal trigger as relevant for the treatment of superficial tumors, in which induction of apoptosis can be controlled by the application of local cooling agents.

Introduction

Nanogels (NGs) are three-dimensional crosslinked nanoparticles that are able to absorb a large amount of water. They constitute a powerful class of new nanocarriers for the loading and improved release *in situ* of hydrophilic cargoes (both small molecules or macromolecules) in controlled conditions. Their ease of functionalization with dyes or inorganic imaging agents allows them to be used as powerful diagnostic agents, in an effort to combine therapeutic efficacy and diagnostics in one single theranostic macromolecule. [1] Their nanosized dimensions allow for an increased residence time in the bloodstream by avoiding excretion from the kidneys, [2] as well as for enhanced skin [3] and follicular penetration [4] or improved mucosal adhesion. [5] Stimuli-responsive NGs are capable of changing their physicochemical properties upon exposure to external conditions such as temperature, pH, reducing conditions, light, and magnetic field, among others. These „smart" materials offer new promising perspectives for the development of next generation agents for the controlled delivery of drugs. [6] Thermoresponsive polymers exhibit a reversible phase transition, caused by the hydrophobic aggregation upon heating of their aqueous solutions to temperatures above their lower critical solution temperature (LCST). Poly(N-isopropylacrylamide) (pNIPAM) undergoes this phase transition at around 33 °C. [7] Thermoresponsive NGs based on N-isopropylacrylamide (NIPAM) are one of the main candidates for biomedical research due to their reversible phase transition at a temperature of 33 °C, close to the body temperature. [8] pNIPAM NGs crosslinked with dendritic polyglycerol (dPG), [9] were published by our group, showing a versatility for their use in biomedical applications. The copolymerization of pNIPAM with poly(N-isopropylmethacrylamide) (pNIPMAM) or hydrophilic comonomers, such as acrylamide or acrylic acid, helps tuning the LCST values to a more desired transition temperature, closer to 37 °C. [10] The use of dPG as a macromolecular crosslinker helps improving the biocompatibility of pNIPAM, as well as avoiding the pNIPAM-driven NG aggregation above the LCST, thus ensuring the colloidal stability of dPG-pNIPAM NGs under physiological conditions. [9] The high swelling abilities of NGs can be exploited to achieve high loadings of bioactives. [11] This property, combined with the abrupt shrinkage of the thermoresponsive network upon temperature change, gives NGs unique properties for the controlled release of small drugs, as well as biomacromolecules, in a controlled fashion.

Dendrons are molecules with regular branching points and symmetrical tree-like structures. At their extremity, the repeated end groups may induce multivalency, leading to an exponential increase in binding affinities. [12] In some cases though, multivalency is counteracted by steric crowding which may hinder the multivalent effects, leading to a binding saturation point, in an anti-cooperative fashion. [13] The tuning of the generation (number of repeated branchings) allows the regulation of the hydrophilic/hydrophobic balance of the dendron. [14] In this way,

one can tune the binding affinity towards guest molecules, whether these are small molecules, proteins, dendrons, or polymers. [15] Newkome-type dendrons / dendrimers are a class of molecules that are biocompatible, non-toxic and are used to create polymers with multifunctional acidic units, useful for promoting host-guest interactions with therapeutic relevant moieties. [16] Among this class of dendrons, 4-acryloylamine-4-(carboxyethyl)heptanodioic acid (ABC) and its copolymer NGs with pNIPAM have been developed by our group and have been proven to provide sustained release of cisplatin at lysosomal conditions. [17] Following a similar approach, we used ABC in this study to generate semi-interpenetrated NGs with dendritic multifunctional units that can be used as anchoring points for the binding of therapeutic proteins. Semi-interpenetrated polymer networks (SIPNs) are composed by more than one polymeric network that are physically entangled, although not covalently bound to each other. As a result, the different networks cannot be separated by simple mechanical stress, but rather only by chemical reactions. This approach is useful for the fabrication of polymer composites that retain the physicochemical properties of the individual networks. SIPN NGs can be synthesized by a two-step process, in which the secondary network is being polymerized inside the preformed NG. By controlling the synthetic parameters of the polymerization, the resulting SIPN concentrations can be optimized in order to get chain lengths that can be exposed to the NG surface ideally only upon shrinkage of the thermoresponsive NG scaffolds. Our group has developed dPG-pNIPAM SIPN NGs with polymerized 2- acrylamido- 2- methylpropane sulfonic acid (AMPS) or dimethylaminoethylmethacrylate (DMAEM) as vectors for the efficient delivery of doxorubicin to the resistant KB-V1 cell line. [18] Their incorporation into honeycomb films for controlled bovine serum albumin (BSA) delivery was also investigated and described by our group in a follow-up study. [19] Their copolymeric NG analogues were reported in another case study for the sustained delivery of doxorubicin and methotrexate. [20] In another report, we employed dPG-PNIPAM SIPN NGs with poly(aniline) as secondary network, a near infrared - active polymer to add photothermal reactivity to the NGs. [21] Several other examples of SIPN NGs can be found in literature, showing a broad range of applications for this synthetic approach, for the development of next generation nanoparticles for biomedical applications. [22]

The use of protein drugs has advantages over conventional chemotherapy agents, due to their inherent lower toxicities combined with high specificities. The presence of a protein corona has a profound impact on the biological efficacy of nanoparticles, and by designing tailor-made protein corona one could boost the therapeutic efficacy of the nanoparticle, [23] in a synergistic effort to combine efficient nanosized vectors to therapeutic proteins. [24] Cytochrome *c* (cyt *c*) is a small, 12 kDa heme protein with an isoelectric point (pI) of 10 and is therefore positively charged at a physiological pH of 7.4. In cells, cyt *c* is loosely associated to the inner membrane of the mitochondria and is involved as an intermediate in the electron transport chain. If

released into the cytosol, cyt *c* triggers apoptosis by binding to apoptosis activating factor-1 (Apaf-1). This in turn is responsible for the activation of caspase-9 to initiate the intrinsic apoptotic cascade. [25] While cyt *c* itself is membrane-impermeable, recent studies involved the use of nanoparticles (NPs) for sustained cytosolic release of cyt *c*. Different nanoparticle-based systems have been evaluated for the activation of apoptosis following cyt *c* release: mesoporous SiO_2 NPs [26] or a combination of end-capped cyt *c* and encapsulated doxorubicin, [27] crosslinked cyt *c* – based NPs [28] or redox-sensitive hyaluronic acid NGs. [29] To our knowledge however, none of these studies investigate the temperature-dependent cyt *c* activation for controlled induction of apoptosis.

In this work, we describe the synthesis of dendritic SIPN NGs, based on thermoresponsive dPG-pNIPAM NGs, with pABC as a SIPN (Fig. 1). This arrangement forms NGs which maintain the original thermoresponsiveness of pNIPAM, together with dPG to provide colloidal stability at a temperature higher than the pNIPAM LCST (33 °C), combined with pH-sensitive dendritic pABC or monofunctional control poly(acrylic acid) (pAA) as SIPN. We characterized the NGs via UV-VIS, nuclear magnetic resonance spectroscopy (NMR), and dynamic light scattering (DLS). These NGs were loaded with cyt *c* at 37 °C, to form a corona around the collapsed NG, by binding pABC or pAA on the NG surface. The subsequent swelling of the NGs at 25 °C was investigated in relation with its ability to disrupt the corona, thereby triggering the release of cyt *c*. The temperature-controlled delivery of cyt *c* was evaluated *in vitro* in HeLa cells, where the ability of the cyt *c*-laden NGs to induce apoptosis by controlled intracellular delivery of cyt *c* was probed. In this way, we combined dendritic NG design with the use of a thermal trigger in order to achieve full control on the reactivity of a therapeutic protein. Thus, we introduce a model system for the development of NG-based therapeutics for the treatment of superficial tumors or skin diseases, where local cooling may be efficiently applied.

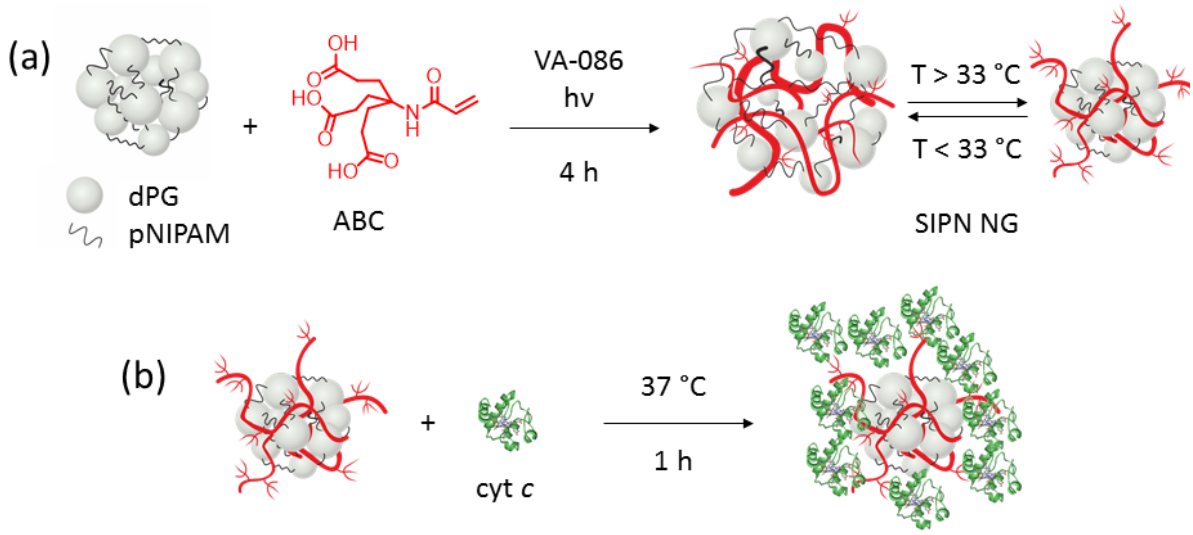

Fig. 1 (a) Schematic representation of the polymerization of 4-acryloylamine-4-(carboxyethyl)heptanodioic acid inside the preformed dendritic polyglycerol - poly(N-isopropylacrylamide) nanogels (b) Formation of cytochrome *c* corona.

Materials and Methods

All materials were purchased by Sigma, except 2,2-azobis(2-methyl-N-(2-hydroxyethyl)-propionamide) (VA-086), which was purchased by Wako Ltd.

The syntheses of dPG-PNIPAM NGs and ABC have been previously published.[9, 17] The synthesis of SIPN NGs proceeded as follows: 50 mg of lyophilized dPG-PNIPAM NG were soaked in a 5 mL solution of ABC or AA in a concentration range of 0.3-2.6 mg mL^{-1} at 0 °C for 16 h. The solution was then purified by ultrafiltration (molecular weight cut-off MWCO = 1 MDa), then 2 mg VA-086 were added and the solution was purged for 30 min under Ar flow. The polymerization was then initiated by light irradiation for 1 min and kept running for 4 h in an ice bath. The solution was dialyzed (MWCO = 50 kDa) against water and ultimately freeze-dried, to obtain NGs as a cotton-like powder.

The cyt *c* corona formation was done by mixing 200 µL of a 20 mg mL^{-1} solution of SIPN NG and 200 µL of a 20 mg mL^{-1} cyt *c* solution both in phosphate buffered saline (PBS), for 4 h at 37 °C. The solution was then purified by ultrafiltration (MWCO = 1 MDa), by short centrifugation cycles at 5000 x g of maximum 10 s, in order to not cool down the sample, to prevent NG swelling. Repeated centrifugation and warming cycles are needed in order to wash with 2 mL PBS volume through the cartridge. The cyt *c* amount was quantified by UV-VIS spectroscopy, by measuring absorbance at λ = 530 nm.

Hydrodynamic diameters were measured by dynamic light scattering (DLS) in a Malvern Zetasizer instrument with a He–Ne laser (λ = 633 nm) and scattering angle of 173°. All the samples were prepared at 1 mg mL^{-1} in 10 mM PBS at pH 7.4 and a 150 mM ionic strength.

For ζ-potential measurements, the NGs' electrophoretic mobility was analyzed following application of a 20 V cm^{-1} electric field and converted into the ζ-potential according to the Helmholtz-Smoluchowski equation.

Nuclear magnetic resonance spectra (NMR) were recorded on a Bruker AVANCE III 700, 700 MHz at 25 °C or 45 °C in deuterated water. Data were analyzed using the MestreNova software package.

Transition temperatures were measured on a Cary 100 Bio UV-vis spectrophotometer equipped with a temperature-controlled, six-position sample holder. Buffer NG solutions (1 mg mL^{-1}) were heated at 0.2 °C min^{-1} while monitoring both the transmittance at 500 nm (1 cm path length) and the solution temperature (from 15 to 65 °C), as determined by the internal temperature probe. The cloud point temperature (T_{cp}) of each NG was determined using the minimum of the first derivative of the graph % transmittance vs. temperature.

Release studies were conducted inside an ultrafiltration cartridge (MWCO = 1 MDa). Fast repeated centrifugation cycles (10s at 5000 xg) were used in order to avoid sample cooling. The collection of the filtrate at different times and quantifiying cyt *c* by means of absorbance measurement at λ = 530 nm, led to the quantification of the released cyt *c*. Repeated experiments at 37 °C and 25 °C were performed by the identical procedure.

For the apoptosis assay, $1x10^5$ HeLa cells mL^{-1} were seeded into 96 well plates and incubated overnight. The next day, the supernatant was discarded and replaced by 100 µL/well fresh medium with dilutions of compounds. The cyt *c* concentration served as the basis for dilution calculations and equal volumes of the respective unloaded NGs were applied. Samples and cells were kept at temperatures above 37 °C using a heating block and a heating plate. 10-fold serial dilutions were prepared in a 96-well plate placed on the heat plate at 40 °C. Dilutions for duplicate wells were prepared independently. Two identical plates were prepared. Incubations were done in two regular cell culture incubators set to 37 °C or 30 °C and 5% CO_2. One plate was incubated in at 37 °C for 2 h (presumed uptake phase), then at 30 °C over night (release phase), then 4 h @37 °C (apoptosis induction phase). The other identical plate was incubated in parallel but at 37 °C only. Induction of Caspase 3/7 activity was measured using the Caspase-Glo® 3/7 Assay System (Promega) according to the instructions of the manufacturer.

Results and discussion

Synthesis and characterization of SIPN nanogels

The dPG-pNIPAM NGs and ABC were synthesized according to procedures published previously by our group. [9, 17] To perform semi-interpenetration, the lyophilized NGs were soaked in a concentrated aqueous solution of ABC or acrylic acid (AA). ABC or AA were present in a concentration range of 0.3 - 2.6 mg mL^{-1} in the NGs solution (10 mg mL^{-1}). After purification by ultracentrifugation, the SIPN formation occurred *via* radical polymerization of the acrylic monomer inside the NGs. The light activation of 0.3 mg mL^{-1} 2,2'-azobis(2-methyl-N-(2-hydroxyethyl)propionamide) (VA-086) was used to initiate the radical polymerization of the SIPN. After 4 h of polymerization, the conversion of pABC or pAA in the resulting SIPN NGs was found to be in the range of 12% - 26%, as determined by NMR. These low values may indicate a lack of affinity between ABC or AA and dPG-pNIPAM NG scaffolds to boost their encapsulation, combined with the porous conformation of the NGs. **Table 1** shows the values obtained from characterization of a panel of SIPN NGs. Different ratios were screened to obtain SIPN with increasing concentrations inside the NGs.

Table 1. Summary of the data for the characterization of the screened conditions for semi-interpenetrated nanogels.

SIPN polymer	SIPN concentration, mol%[a)]	Size[b)], nm (PDI)	ζ-potential[b)], mV	Size[b)], nm (PDI)	ζ-potential[b)], mV
Temperature		25 °C		45 °C	
	0.2	137 (0.187)	-1.3	104 (0.096)	-3.1
	0.5	130 (0.200)	+0.4	97 (0.076)	-2.4
pABC	0.9	128 (0.193)	-1.0	92 (0.076)	-5.5
	1.4	138 (0.179)	-0.3	107 (0.096)	-8.1
	2.7	127 (0.211)	-2.3	86 (0.043)	-17.2
	1.3	132 (0.187)	-1.1	98 (0.086)	-3.4
pAA	1.9	133 (0.210)	-0.6	107 (0.085)	-5.1
	5.1	130 (0.165)	-2.0	123 (0.195)	-10.2

[a)] ratio normalized to poly(N-isopropylacrylamide) content, quantified *via* pH titration.

[b)] measured in PBS (10 mM , pH 7.4)

The NGs were monodisperse and maintained the typical thermoresponsive behavior of pNIPAM, showing a shrinkage in volume of about 67% at 45 °C. UV-VIS spectroscopy revealed cloud point temperature (T_{cp}) values of 33 °C for all samples, in agreement with the values

obtained by dPG-pNIPAM NGs prior to semi-interpenetration. As expected from the synthetic approach, the semi-interpenetration was not affecting the thermoresponsive behavior of the NGs. After semi-interpenetration with both pABC (pKa = 5) and pAA (pKa = 4.2), NGs exhibit temperature-dependent ζ-potential variations at a neutral pH of 7.4. By increasing the temperature above the LCST of pNIPAM (33 °C), NGs turned from neutral to negatively charged. This finding was interpreted as an indication for pABC or pAA being exposed at the NGs surface after NG shrinkage. Sharp, reversible ζ-potential transitions with changing temperature were observed, for samples with at least 1.4 mol% pABC or 1.9 mol% pAA, as shown in Fig. 2. The inflection of the data points was highest at 32 °C, compatible with the LCST of pNIPAM, while the Δζ values between 25 °C and 45 °C were proportional to the SIPN concentrations. In this way, the SIPN provided new temperature-dependent charge density fluctuations in the NGs, which were then exploited as on-demand switchable protein binding moieties.

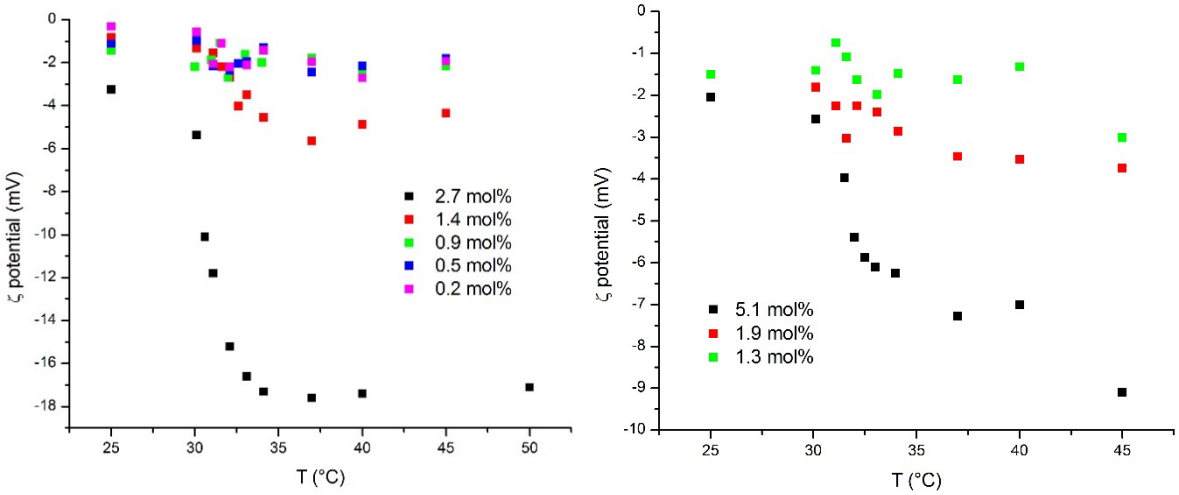

Fig. 2 Evolution of ζ-potential values with temperature, measured at pH 7.4 in a 10 mM sodium phosphate buffer for semi-interpenetrated poly(4-acryloylamine-4-(carboxyethyl)heptanodioic acid) (left) and poly(acrylic acid) (right) nanogels.

By comparing ^{1}H-NMR spectra of pABC SIPN NGs at 25 °C and 45 °C, both above and below the LCST of pNIPAM, the spectra revealed significant changes in the peak intensities of the different polymers. In **Fig. 3** it can be visualized how the peaks representing pNIPAM (δ = 0.8 – 2.1; δ = 3.8 ppm) are strongly decreasing at 45 °C as compared to those detected at 25 °C. The peak intensities for dPG (δ = 3.4 – 3.7; δ = 3.9 ppm) and pABC at δ = 2.3 ppm remained in turn mostly constant after temperature increase. This observation corroborates the previous finding that pABC chains and dPG are surface-active after the collapse of pNIPAM.

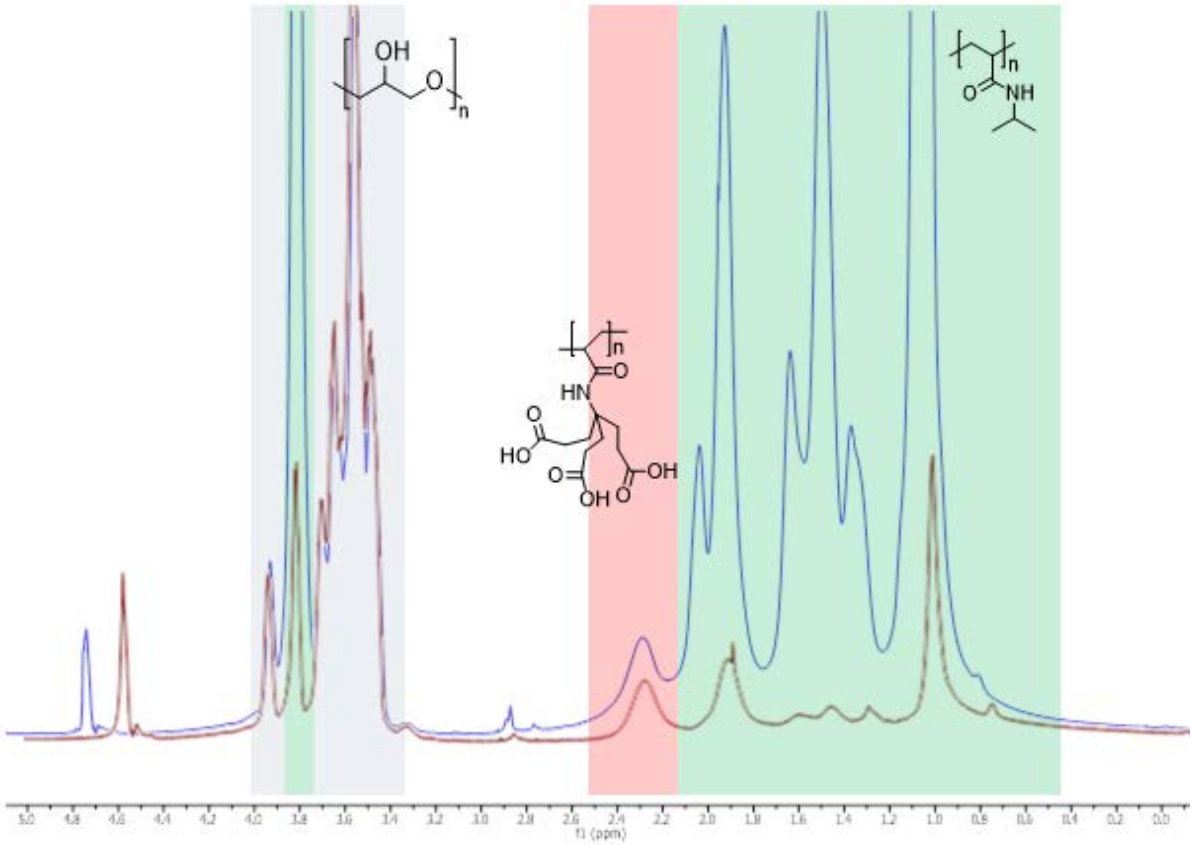

Fig. 3 ^{1}H-NMR spectra in D_2O of 2.7 mol% poly(4-acryloylamine-4-(carboxyethyl)heptanodioic acid) semi-interpenetrated nanogels at 25 °C (blue line) vs 45 °C (red line).

Cyt *c* corona formation and *in vitro* release kinetics

The ability to expose charges on the surface of the NGs triggered by temperature change allowed the use of SIPN NGs as agents for reversible electrostatic binding of proteins. At 37 °C and pH 7.4 the NGs achieve maximum exposure of negatively charged pABC (or pAA), an ideal setting for the binding of basic proteins. A cyt *c* corona was thus easily formed by electrostatic pairing of the positively charged protein with negatively charged pABC (or pAA) on the NG surface. Although the collapsed NGs were ideally not contributing to encapsulation, loading capacities were found to be high, with values found in a range of 50-70 wt% for SIPN pABC NGs and 70-80 wt% for SIPN pAA NGs, starting from an initial 1:1 w/w cyt c/NG ratio. After the cyt *c* corona formation, release kinetics were determined both at a constant temperature of 37 °C and by cooling down to 25 °C, to investigate whether the swelling of NGs would lead to the disruption of the corona and thereby cause cyt *c* release. The kinetics data is shown in **Fig. 4**.

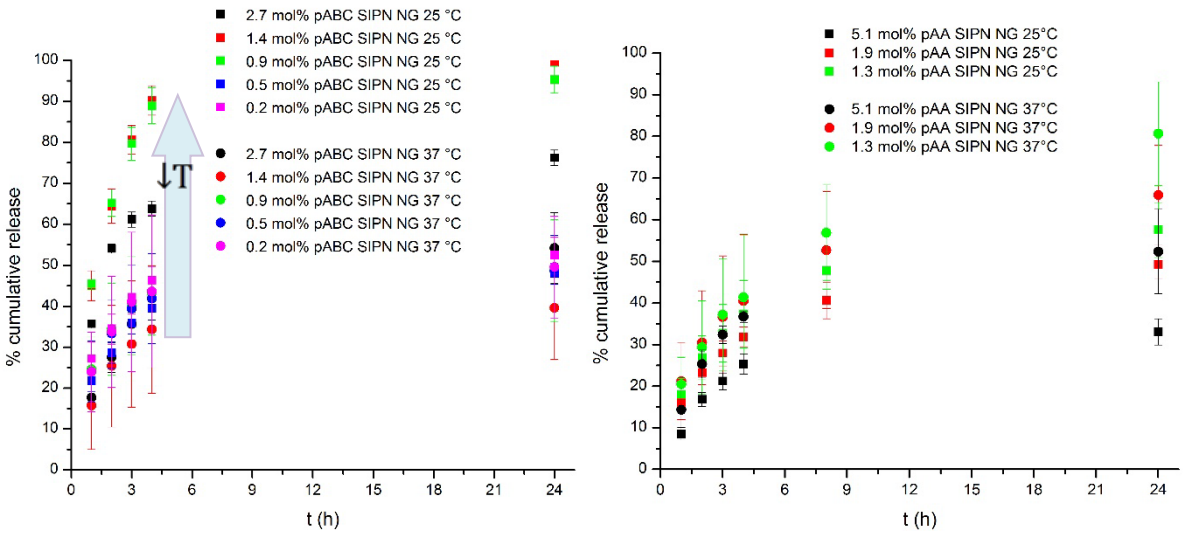

Fig. 4 Cytochrome *c* release kinetics for semi-interpenetrated poly(4-acryloylamine-4-(carboxyethyl)heptanodioic acid) nanogels (left), semi-interpenetrated poly(acrylic acid) nanogels (right).

For pABC SIPN NGs, a distinct boost in the release was observed by cooling down the samples to 25 °C, as compared to the release values obtained at 37 °C, in samples with at least 0.9 mol% pABC. In this case, the swelling of the NGs efficiently boosted the release of cyt *c*, thereby acting as a trigger. For samples having less than 0.9 mol% pABC, the SIPN concentration might have been too low to observe any difference in release kinetics, just as they did not show strong ζ-potential changes above and below 32 °C (see Fig. 2). The release kinetics for pAA SIPN NGs however were almost independent from the experimental temperature, with a slight increase at 37 °C. Although a sustained release in a 24 h interval was still present in this case, the kinetics curves resemble those observed for cyt *c* alone, although with increasing half - lives. Thus, the driving force for cyt *c* release by AA SIPN NGs may be attributed to simple diffusion, with no contribution from NG swelling. For pAA-cyt *c* samples, a slower release and 25% higher loadings might indicate a stronger binding than in pABC-cyt *c* samples, with comparable SIPN polymer concentrations / -COOH groups. Therefore, these findings suggest an anti-cooperative effect for the binding of cyt *c* by dendritic pABC, that ultimately yielded an optimal reactivity for the reversible binding of cyt *c*. Control non-SIPN NGs had a lower cyt *c* loading (16 wt%) and a very fast release behavior, with more than 70% cyt *c* released within 4 h, independently from the experimental temperature (see SI). Furthermore, cyt *c*'s structural integrity was confirmed after release by circular dichroism measurements (see SI).

Induction of apoptosis in HeLa cells

To confirm the controlled binding and triggered release of cyt *c* in a biological context, we investigated the ability of the loaded SIPN NGs to induce apoptosis in HeLa cells. The NGs,

both loaded with cyt *c* and unloaded as a control, were first incubated at 37 °C for 2 h with HeLa cells to allow cellular uptake of the NG at the physiologically optimal temperature. Then the temperature was lowered to 30 °C, allowing a prolonged release of cyt *c* for 16 h, while a parallel sample set was kept at 37 °C, where release of cyt *c* should be strongly sustained. In the last step, all samples were incubated at 37 °C for 4 h, in order to allow sufficient time at physiologically optimal temperature for the induction of apoptosis, which was measured by quantifying caspase 3/7 activation (**Fig. 5**).

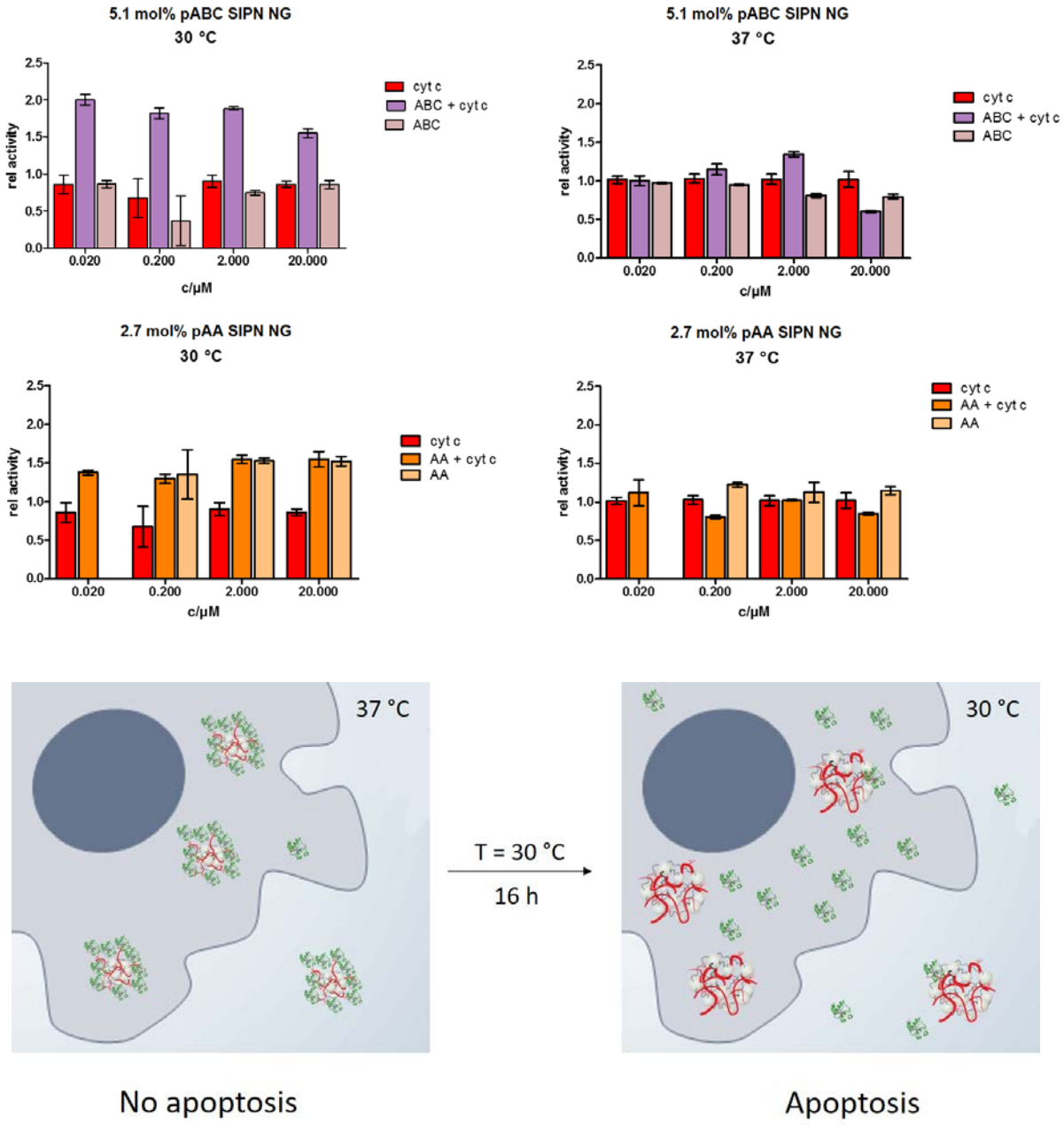

Fig. 5 Apoptosis assay on HeLa cells after incubation with semi-interpenetrated 2.7 mol% pABC (top) and 5.1 mol% pAA nanogels (middle). The release of cytochrome *c* from 2.7 mol% pABC nanogels was efficiently boosted by swelling of the nanogels at 30 °C, thereby activating apoptosis in HeLa cells (bottom).

We could clearly observe that apoptosis was promoted only in presence of cyt *c*-loaded 2.7 mol% pABC NG, and the effect was greatly amplified at 30°C, where full NG swelling occurred. This effect of the NG swelling had an impact on the cyt *c* release *in vitro*, which activated apoptosis in HeLa cells. 2.7 mol% pABC SIPN NG with cyt *c* concentrations as low as 20 nM were promoting apoptosis at 30 °C, while no significant effect was observed by increasing cyt *c* concentration. At 37 °C, a minimum cyt *c* concentration of 200 nM was necessary to observe any effect on apoptosis, which was slightly enhanced by increasing towards 2 μM cyt *c*. While a slight increase in apoptosis was generated by 5.1 mol% pAA SIPN NG, independently from the cyt *c* loading, no effect was detected in combination with cyt *c*. In this case, no efficient cytosolic delivery of cyt *c* might have occurred, possibly due to a too strong pAA-cyt *c* binding. Again, the careful choice of SIPN polymer showed an impact on the therapeutic efficacy of SIPN NGs as cyt *c* carriers for controlled apoptosis.

Conclusions

In this work, we synthesized SIPN NGs by a simple one-pot strategy, with the aid of free-radical polymerization, where the previously synthesized NGs were used as scaffold to hold the resulting SIPN. The polymerization of ABC monomer achieved SIPN NGs with repetitive dendritic charged units, which were found to be exposed to the NG surface above 33 °C, as shown by DLS and ^{1}H-NMR spectroscopy. By exposing charges at 37 °C, we were able to form a cyt *c* corona by electrostatic pairing between pABC and cyt *c*. An identical procedure was employed for the synthesis of pAA SIPN NGs and subsequent cyt *c* corona formation, in order to compare the protein binding behavior between monovalent and dendritic SIPNs. The stability of the cyt *c* corona was investigated in relation with the NG swelling *in vitro*, where a boost in the release of cyt *c* was observed for SIPN pABC NGs when cooled down to room temperature. By maintaining a higher temperature of 37 °C, the cyt *c* corona was in fact more stable and the cyt *c* release was decreased. For monofunctional control pAA SIPN NGs, we could not observe any relevant contribution from NG swelling on the release, as the cyt *c* release mechanism appeared as simple diffusion. Moreover, the pAA SIPN NGs showed a stronger binding of cyt *c* than pABC SIPN NGs, as seen by 25% higher loadings and overall slower cyt *c* release kinetics. The use of a dendritic polymer (pABC) helped decreasing the binding affinity to an extent that was optimal for compensating the mechanical forces arisen from NG swelling, thus achieving full on-demand control of loading / release of cyt *c* upon thermal trigger. In order to demonstrate their potential for controlled delivery applications, a cyt *c* corona was assembled on SIPN NGs, which could successfully promote apoptosis in HeLa cells. The activation of the intrinsic apoptotic pathway following cyt *c* cytosolic delivery was observed only in presence of cyt *c*-loaded 2.7 mol% pABC SIPN NG, the effect being strongly enhanced by full NG swelling, induced by applying moderate cooling to 30 °C. Overall, these

findings showed that the choice of dendritic SIPN polymer and concentration was crucial for the modulation of the cyt *c* binding / release. We therefore achieved full controlled reactivity of dendritic SIPN NGs as carriers for the apoptotic reagent cyt *c*, its activation being regulated by a simple thermal trigger. By performing a similar set of experiments with SIPN NGs binding the acidic protein asparaginase (pI = 5.5), we unfortunately observed aggregation of all samples. Nevertheless, a similar approach may show potential for the reversible binding of other proteins of interest.

Overall, we believe that the use of localized cooling agents in combination with thermoresponsive NGs and a preassembled protein corona may show promising uses for the treatment of superficial tumors as well as skin diseases. The use of therapeutic proteins, combined with dendritic thermoresponsive NGs as macromolecular agents, may be beneficial in order to reduce side effects of conventional therapeutics as well as to improve the therapy specificity.

Acknowledgements

We gratefully acknowledge financial support from the Bundesministerium für Bildung und Forschung (BMBF) through the NanoMatFutur award (ThermoNanogele, 13N12561), Helmholtz Virtual Institute (HVI), "Multifunctional Biomaterials for Medicine," DFG-CONICET, CONICET, Alexander von Humboldt foundation, the Focus Area NanoScale of the Freie Universität Berlin (http://www.nanoscale.fu-berlin.de), the Sonderforschungsbereich 1112 (http://www.sfb1112.de), Projects A04 and B02.

References

[1] a) D. Li, C. F. van Nostrum, E. Mastrobattista, T. Vermonden, W. E. Hennink, *J. Control. Release* **2016**, *259*, 16; b) M. Kar, M. Molina, M. Calderon, *Nanomedicine* **2017**, *12*, 1627.

[2] M. Calderon, A. Sosnik, *Biotechnol. Adv.* **2015**, *33*, 1277.

[3] M. Asadian-Birjand, J. Bergueiro, F. Rancan, J. C. Cuggino, R. C. Mutihac, K. Achazi, J. Dernedde, U. Blume-Peytayi, A. Vogt, M. Calderón, *Polym. Chem.* **2015**, *6*, 5827.

[4] F. F. Sahle, M. Giulbudagian, J. Bergueiro, J. Lademann, M. Calderon, *Nanoscale* **2017**, *9*, 172.

[5] A. Sosnik, J. das Neves, B. Sarmento, *Prog. Polym. Sci.* **2014**, *39*, 2030.

[6] a) M. Molina, M. Asadian-Birjand, J. Balach, J. Bergueiro, E. Miceli, M. Calderón, *Chem. Soc. Rev.* **2015**, *44*, 6161; b) R. Cheng, F. Meng, C. Deng, Z. Zhong, *Nano Today* **2015**, *10*, 656.

[7] S. Fujishige, K. Kubota, I. Ando, *J. Phys. Chem.* **1989**, *93*, 3311.

[8] J. Bergueiro, M. Calderon, *Macromol. Biosci.* **2015**, *15*, 183.

[9] J. C. Cuggino, C. I. Alvarez I, M. C. Strumia, P. Welker, K. Licha, D. Steinhilber, R.-C. Mutihac, M. Calderón, *Soft Matter* **2011**, *7*, 11259.

[10] a) J. Shen, T. Ye, A. Chang, W. Wu, S. Zhou, *Soft Matter* **2012**, *8*, 12034; b) Y. Wang, H. Xu, J. Wang, L. Ge, J. Zhu, *J. Pharm. Sci.* **2014**, *103*, 2012.

[11] Y. Chen, X. Zheng, H. Qian, Z. Mao, D. Ding, X. Jiang, *ACS Appl. Mater. Interfaces* **2010**, *2*, 3532.

[12] a) C. Fasting, C. A. Schalley, M. Weber, O. Seitz, S. Hecht, B. Koksch, J. Dernedde, C. Graf, E. W. Knapp, R. Haag, *Angew. Chem.* **2012**, *124*, 10622; *Angew. Chem. Int. Ed. Engl.* **2012**, *51*, 10472; b) M. Martinelli, M. Strumia, *Molecules* **2017**, *22*, 243.

[13] a) J. W. Jones, W. S. Bryant, A. W. Bosman, R. A. J. Janssen, E. W. Meijer, H. W. Gibson, *J. Org. Chem.* **2003**, *68*, 2385; b) I. Porcar, H. Cottet, P. Gareil, C. Tribet, *Macromolecules* **1999**, *32*, 3922; c) S. Bhatia, D. Lauster, M. Bardua, K. Ludwig, S. Angioletti-Uberti, N. Popp, U. Hoffmann, F. Paulus, M. Budt, M. Stadtmuller, T. Wolff, A. Hamann, C. Bottcher, A. Herrmann, R. Haag, *Biomaterials* **2017**, *138*, 22.

[14] B. Devarakonda, R. A. Hill, M. M. de Villiers, *Int. J. Pharm.* **2004**, *284*, 133.

[15] J. I. Paez, M. Martinelli, V. Brunetti, M. C. Strumia, *Polymers* **2012**, *4*, 355.

[16] a) L. Fernandez, M. Calderón, M. Martinelli, M. Strumia, H. Cerecetto, M. González, J. J. Silber, M. Santo, *J. Phys. Org. Chem.* **2008**, *21*, 1079; b) I. P. Julieta, B. Veronica, A. C. Eduardo, C. S. Miriam, *Curr. Org. Chem.* **2013**, *17*, 943; c) N. Dib, L. Fernández, L. Otero, M. Santo, M. Calderón, M. Martinelli, M. Strumia, *J. Incl. Phenom. Macro.* **2015**, *82*, 351; d) A. A. Aldana, B. Barrios, M. Strumia, S. Correa, M. Martinelli, *React. Funct. Polym.* **2016**, *100*, 18.

[17] G. N. Rimondino, E. Miceli, M. Molina, S. Wedepohl, S. Thierbach, E. Rühl, M. Strumia, M. Martinelli, M. Calderón, *J. Mater. Chem. B* **2017**, *5*, 866.

[18] M. Molina, S. Wedepohl, E. Miceli, M. Calderón, *Nanomedicine* **2016**, *12*, 117.

[19] A. S. De Leon, M. Molina, S. Wedepohl, A. Munoz-Bonilla, J. Rodriguez-Hernandez, M. Calderon, *Langmuir* **2016**, *32*, 1854.

[20] M. Molina, M. Giulbudagian, M. Calderón, *Macromol. Chem. Phys.* **2014**, *215*, 2414.

[21] M. Molina, S. Wedepohl, M. Calderon, *Nanoscale* **2016**, *8*, 5852.

[22] a) M. Du, D. Lu, Z. Liu, *J. Mol. Catal. B – Enzym.* **2013**, *88*, 60; b) X. Liu, H. Guo, L. Zha, *Polym. Int.* **2012**, *61*, 1144; c) V. Koul, R. Mohamed, D. Kuckling, H. J. Adler, V. Choudhary, *Colloid Surface B* **2011**, *83*, 204; d) Y. Chen, D. Ding, Z. Mao, Y. He, Y. Hu, W. Wu, X. Jiang, *Biomacromolecules* **2008**, *9*, 2609; e) N. Sahiner, W. T. Godbey, G. L. McPherson, V. T. John, *Colloid Polym. Sci.* **2006**, *284*, 1121.

[23] a) E. Miceli, M. Kar, M. Calderon, *J. Mat. Chem. B* **2017**, *5*, 4393; b) K. Obst, G. Yealland, B. Balzus, E. Miceli, M. Dimde, C. Weise, M. Eravci, R. Bodmeier, R. Haag, M. Calderon, N. Charbaji, S. Hedtrich, *Biomacromolecules* **2017**, *18*, 1762.

[24] Z. Gu, A. Biswas, M. Zhao, Y. Tang, *Chem. Soc. Rev.* **2011**, *40*, 3638.

[25] a) X. Liu, C. N. Kim, J. Yang, R. Jemmerson, X. Wang, *Cell* **1996**, *86*, 147; b) A. Matapurkar, Y. Lazebnik, *Cell Death Differ.* **2006**, *13*, 2062.

[26] J. Mendez, M. Morales Cruz, Y. Delgado, C. M. Figueroa, E. A. Orellano, M. Morales, A. Monteagudo, K. Griebenow, *Mol. Pharm.* **2014**, *11*, 102.

[27] B. Zhang, Z. Luo, J. Liu, X. Ding, J. Li, K. Cai, *J. Control. Release* **2014**, *192*, 192.

[28] M. Morales-Cruz, C. M. Figueroa, T. González-Robles, Y. Delgado, A. Molina, J. Méndez, M. Morales, K. Griebenow, *J. Nanobiotechnol.* **2014**, *12*, 33.

[29] a) S. Li, J. Zhang, C. Deng, F. Meng, L. Yu, Z. Zhong, *ACS Appl. Mater. Inter.* **2016**, *8*, 21155; b) J. Chen, Y. Zou, C. Deng, F. Meng, J. Zhang, Z. Zhong, *Chem. Mater.* **2016**, *28*, 8792.

Supporting Information

Semi-interpenetrated, dendritic, dual-responsive nanogels with cytochrome c corona induce controlled apoptosis in HeLa cells

Enrico Miceli, Stefanie Wedepohl, Ernesto Rafael Osorio Blanco, Guido Noé Rimondino, Marisa Martinelli, Miriam Strumia, Maria Molina, Mrityunjoy Kar, Marcelo Calderón

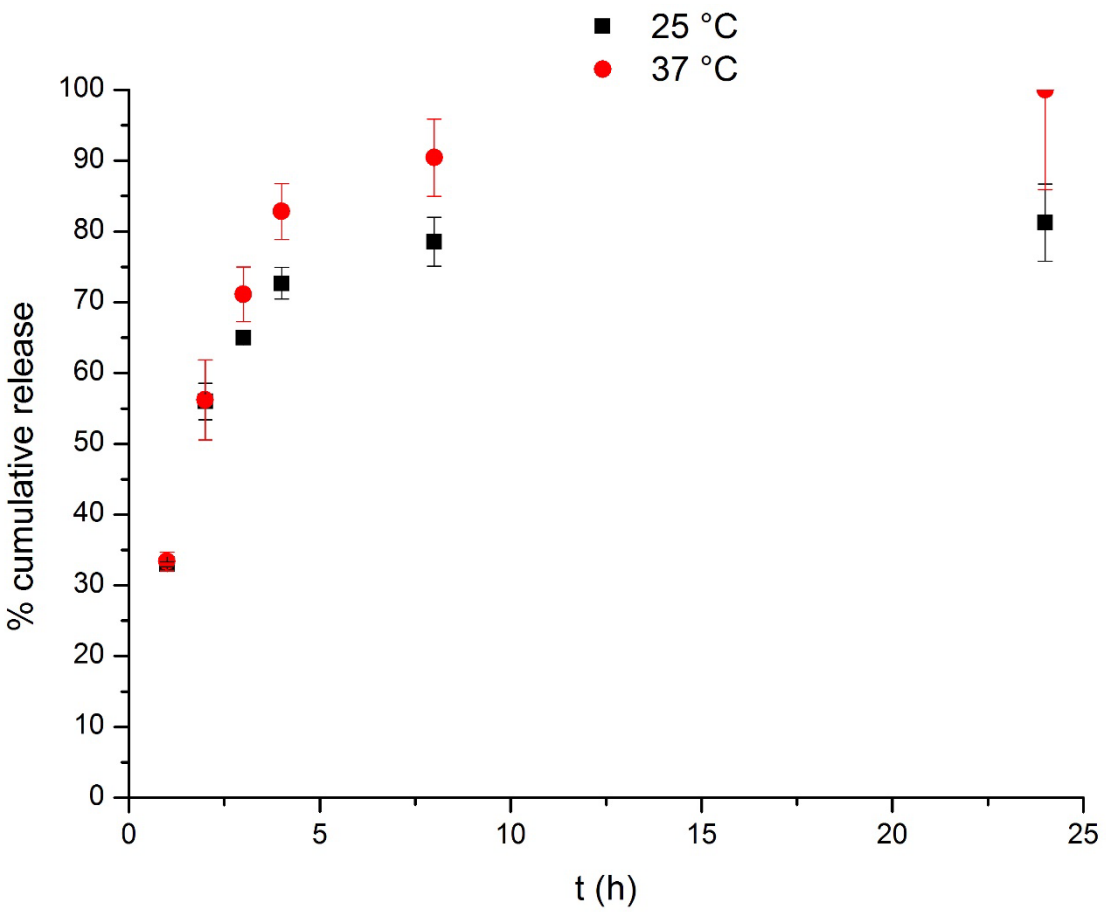

Fig. S1. Cytochrome c release kinetics for non-interpenetrated dPG-pNIPAM nanogels.

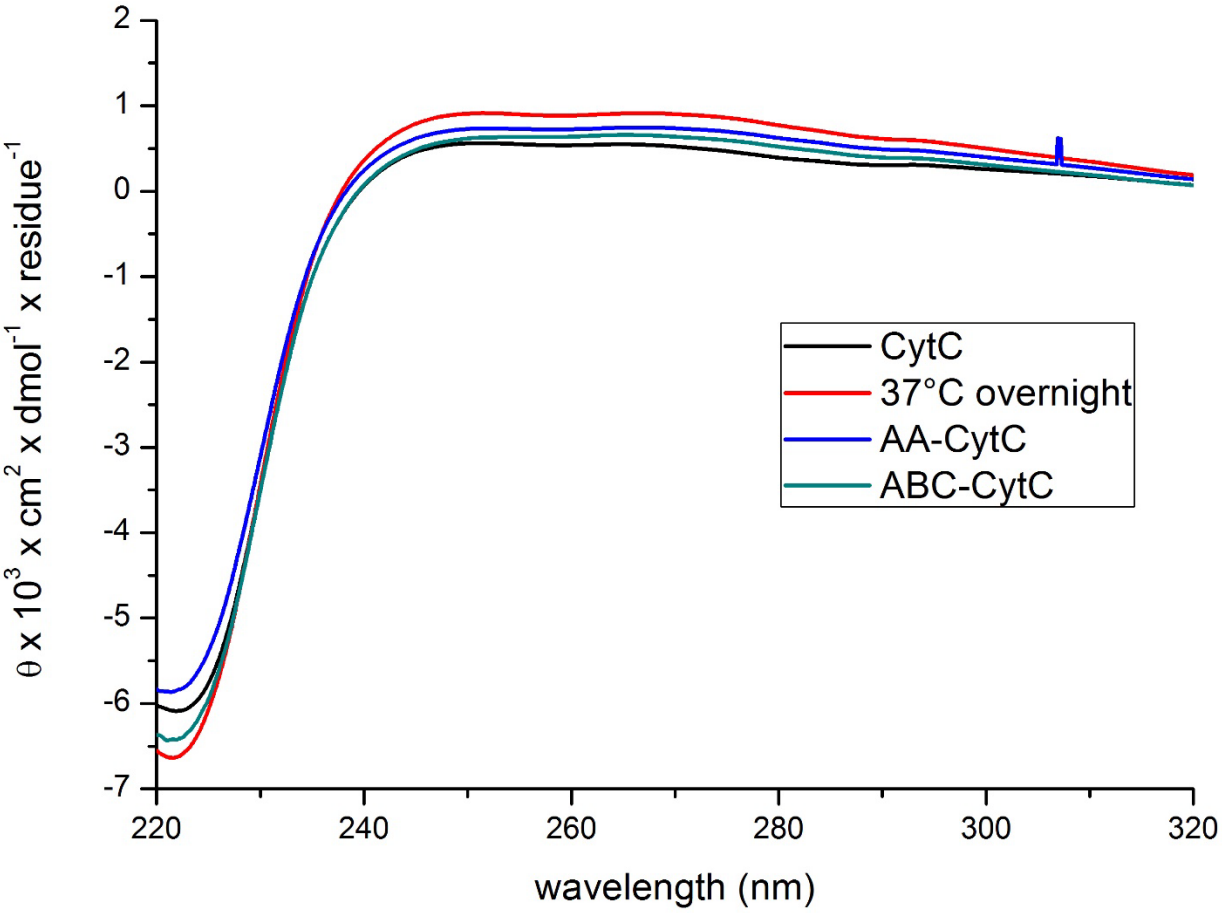

Fig. S2. Circular dichroism spectra of released cytochrome c from nanogels.

3.4 Rational Design of Dendritic Thermoresponsive Nanogels that Undergo Phase Transition under Endolysosomal Conditions

G. N. Rimondino,[‡] **E. Miceli**,[‡] M. Molina, S. Wedepohl, S. Thierbach, E. Rühl, M. Strumia, M. Martinelli, M. Calderón, *Journal of Materials Chemistry B*, **2017**, *5*, 866.

[‡]Both authors contributed equally to this work.

https://doi.org/10.1039/c6tb02001a

Author contribution: In this work, the author provided the synthesis of nanogels, together with the screening of the synthetic conditions, the overall nanogel characterization, their loading with cisplatin drug, the *in vitro* cisplatin release studies, and the nanogel-cisplatin sample preparation for the biological essays.

3.5 Overcoming Drug Resistance with On-demand Charged Thermoresponsive Dendritic Nanogels

M. Molina, S. Wedepohl, **E. Miceli**, M. Calderón, *Nanomedicine (Lond.)*, **2017**, *12*, 117.

https://doi.org/10.2217/nnm-2016-0308

Author contribution: The author was responsible for the synthesis and characterization of doxorubicin-loaded SIPN nanogels for *in vivo* studies, and the related doxorubicin *in vitro* release studies.

4. Summary and Conclusion

This work explored different modalities for the optimization of the properties of thermoresponsive nanogels, with regard to their application as drug carriers in anticancer therapy. The ability of nanogels to reversibly bind different chemotherapeutic drugs was investigated, following different strategies. The main focus was the implementation of synthetic procedures that allowed the incorporation of dendritic structures into nanogels, together with the design of multicompartimental nanogels as drug carriers with improved versatility. In order to successfully translate these synthetic efforts into nanogels showing good *in vivo* compatibility, thermoresponsive nanogels were investigated for their ability to interact with blood proteins in physiological conditions. The assessment of the protein corona around thermoresponsive nanogels, after their incubation in human serum and plasma, was described in **Section 3.1 - 3.2** of the present thesis. These studies focused on the understanding of polymer – protein associations in physiological conditions with regard to the role of the single constituents of thermoresponsive nanogels in the interaction with proteins, namely thermoresponsive polymers and dPG. In order to direct the drug carrier to the desired target *in vivo* and prevent its sequestration from the bloodstream, unwanted interactions with opsonins at a protein corona level should be avoided. The analysis of such interactions help understanding the biocompatibility of thermoresponsive nanogels that are designed for intravenous administration, ideally to bridge a gap between *in vitro* and *in vivo* assays. While both nanogel constituents, dPG and pNIPAM, are regarded as polymers with very low protein affinities,[28, 65] their incorporation into nanogels leads to a relevant size increase, which is a common factor associated with increased protein binding.[56] An in-depth analysis of the protein corona of dPG-based thermoresponsive nanogels is thus revealed in this thesis in **Section 3.1 - 3.2**. Following the need to optimize nanogels to adjust the biological responses they will evoke, the ability to resist unwanted surface interactions with proteins was proven to be enhanced in the presence of dPG, as expected from its neutral, hydrophilic character. dPG provided colloidal stability to thermoresponsive nanogels, without drastically altering the key thermoresponsive properties,[71] as well as inhibiting the unspecific absorption of proteins onto the nanogels' surface. The inhibition of the protein binding was so successful that only traces of protein were found for these nanogel systems (3 – 7 µg / m^2 nanogel). Nevertheless, a protein-dependent aggregation for dPG-pNIPAM nanogels was found above their VPTT, as revealed by DLS measurements in full human serum at 37 °C. The traces of immunoglobulin light chains, found specifically enriched at 37 °C, may signal an immunoglobulin bridging between nanogels as driving force for their aggregation, analogous to what was found for polystyrene nanoparticle systems in the literature.[128] This temperature-dependent protein corona study proved the need to optimize the polymer choice for their use in biology, where

unspecific protein binding is ruling the final polymer / nanoparticle distribution and blood availability. In fact, by changing the polymer from pNIPAM to pNIPMAM, the nanogels were found to be safe to use in physiological conditions at 37 °C, as they do not aggregate in serum and reach their hydrophobic transition at a higher VPTT of 46 °C.

The generation of innovative nanogel systems for different applications as responsive drug carriers for anticancer therapy is disclosed in **Section 3.3 - 3.5** of this thesis. The core of this section is the optimization of the synthesis of pH- and / or thermoresponsive nanogels, by tuning the dendron / pNIPAM comonomer ratio in copolymer nanogels (**Section 3.4**) or by screening polymer concentrations to obtain an optimal binding strength for the loading and sustained release of therapeutic molecules by SIPN nanogels (**Sections 3.3, 3.5**). Nanogels with tunable reactivities are designed using dendritic polymers. Dendritic structures allow for a high density of functional groups, that improve nanogel solubility and may mediate multivalent effects. The use of dPG as macromolecular crosslinker helped in previous reports to improve the biocompatibility of thermoresponsive pNIPAM.[71] Linear polymers with tunable responsive functionalities / concentrations were used in combination with dendritic moieties, in a synergistic effort for the optimization of the nanogels' biological behavior. The use of the nanogels as drug delivery systems was demonstrated for small chemotherapeutic drugs (cisplatin and DOX), as well as for cytochrome *c* as a therapeutic protein.

The changes in nanogel morphology upon chemical modification were thoroughly investigated, in relation with the nanogel's ability to weakly interact with therapeutic molecules (small drugs or proteins). In this way, an optimal tuning of the binding and release kinetics of the loaded molecule for efficient drug delivery could be achieved. SIPN nanogels were developed as powerful agents for the rational tuning of the interactions between nanogels and the desired therapeutic cargo. Most importantly, the introduction of a secondary network to give SIPN does not directly interfere with the key responsive properties of nanogels, but rather adds new physicochemical responsive modalities. dPG-pNIPAM nanogels were employed as starting materials for the generation of SIPN within the nanogel scaffold. In this way, the advantageous properties of dPG-pNIPAM nanogels were further tuned, with pABC as dendritic secondary polymeric network to achieve SIPN nanogels, which allow the assembly of a therapeutic cytochrome *c* corona. The loaded nanogels showed therapeutic potency against HeLa cells which could be specifically triggered by a temperature shift. Here, the swelling of thermoresponsive nanogels was used as the mechanical force helping the disruption of the supramolecular protein corona and its intracellular delivery into HeLa cells (**Section 3.3**). The use of dendritic ABC was further investigated as comonomer for the synthesis of pABC-co-pNIPAM nanogels, which introduced pH-responsiveness in addition to the thermoresponsive behavior of nanogels. This allowed a sustained release of cisplatin only upon reaching acidic

compartments (like lysosomes) of cells (**Section 3.4**). The copolymerization with ABC drastically altered the thermoresponsiveness of the copolymer compared to pNIPAM, to give nanogels with VPTT behavior only in acidic conditions (pH < 5), with VPTT values decreasing in an ABC concentration-dependent manner. The decrease in the VPTT was related to increased intermolecular pABC hydrogen bonding, when pABC was in its protonated state. The loading of the nanogels with cisplatin at pH 7.4 resulted in stable ABC-Pt bonds, which may be disrupted in acidic conditions, as a consequence of H-bond driven nanogel aggregation and subsequent release of the previously bound cisplatin.

In an analogous approach to that of **Section 3.3**, SIPN nanogels showed increased affinity towards the chemotherapeutic drug DOX, with the aid of p(AMPS) as secondary polymeric network within the nanogels, and achieved *in vivo* anticancer activity in DOX-resistant conditions (**Section 3.5**). The use of AMPS SIPN nanogels could tune the electrostatic binding of DOX to the carrier and thereby enable the drug to successfully bypass the resistance mechanisms of multidrug resistant tumor cells *in vitro* and *in vivo*.

All areas of the research discussed in this thesis help to unveil relevant discoveries for the optimization the properties of soft, stimuli-responsive nanogels, for their application as innovative drug carriers. The discoveries published in this work help to push forward the implementation of next generation nanogels and to disclose further information about the modalities of actions of stimuli-responsive nanogels and their translation into clinical therapies. There is no limit for the design of new nanoparticles exhibiting moderate polymer - drug interactions for sustained drug release, as long as the polymer - protein interactions are identified and show compatibility with the envisioned therapeutic purpose.

5. Outlook

In order to push the application of the core findings of this work further, a strong effort is currently made to pursue the synthesis of biocompatible soft nanogels that are capable to undergo controlled degradation at physiological conditions, to achieve effective clearance from the body after accomplishing their therapeutic purpose. To achieve this, disulfide bonds or proteolytically cleavable bonds are usually introduced within the core nanogel structure, that are susceptible to degradation, to give smaller polymer chains / particles that may be excreted ultimately by the kidneys. A strong synthetic effort is needed in this sense to prevent nanoparticle accumulation in the body, which may result in long-term toxicity issues.

At the same time, the findings about the protein corona published in this thesis do not cover the interaction between a self-assembled corona and the release kinetics of a loaded biomolecule from the nanogels. In a way, the presence of a protein corona may counteract a too fast release of cargo and meliorate the overall nanogel performance in specific cases, due to the steric crowding of nanogels by protein coating layers. Nevertheless, a sustained release kinetics *in vitro* in absence of proteins may signify a too slow release in presence of a protein corona. It is thus strongly suggested to perform drug release studies in presence of a protein corona, as it reflects more closely the physiological conditions in which nanogels are designed to perform.[124, 125, 171]

An example of a preassembled protein corona with therapeutic efficacy shown in **Section 3.3** opens a range of new unanswered questions, regarding the intrinsic therapeutic potency of protein coronae that are spontaneously formed around nanogels, and their potential as stand-alone drugs. A protein corona-dependent aggregation of dPG-pNIPAM above its VPTT observed in **Section 3.1** may be a model case study to generate localized toxicity upon temperature-induced aggregation by thermoresponsive nanogels.

The systematic studies about the characterization of protein coronae may be further extended to SIPN or copolymer nanogels in future studies. As the presence of a SIPN shows increased stiffness of nanogels, this may influence the protein corona composition unpredictably, upon incubation of nanogels in blood plasma and / or serum. The presence of a hydrophobic or charged SIPN polymer may lead to an increase in protein absorption and change in composition of the corona, thus it should be considered as a direct follow-up study from this thesis.

The wise choice of polymer structure, nanogel architecture and interactions with environmental conditions are the main requirements for the successful development of macromolecular therapeutic agents. The tailoring of these properties synergistically helps to define the protein corona structure that is expected upon contact with any biological fluid, and translates the

nanoparticle’s chemical structure to its *in vivo* behavior. The synthetic strategies employed in this work may be further optimized through their protein coronae outcomes, to give performing nanogels structures with improved therapeutic responses.

6. Kurzzusammenfassung und Ausblick

Die Grundlage dieser Arbeit war die Untersuchung verschiedener Modalitäten zur Optimierung der Eigenschaften von thermoresponsiven Nanogelen hinsichtlich ihrer Anwendung als Wirkstoffträger in der Krebstherapie. Die Fähigkeit von Nanogelen verschiedene Chemotherapeutika reversibel zu binden wurde mit verschiedenen Strategien untersucht. Das Hauptaugenmerk lag auf der Implementierung von Synthesemethoden, die den Einbau von dendritischen Strukturen in Nanogele ermöglichten, sowie das Design multikompartimenteller Nanogele als Wirkstoffträger mit verbesserter Anpassungsfähigkeit. Um diese synthetischen Anstrengungen erfolgreich in Nanogele mit guter *In-vivo*-Kompatibilität umzusetzen, wurde die Interaktion von thermoresponsiven Nanogelen mit Blutproteinen unter physiologischen Bedingungen untersucht. Die Untersuchung der Proteinkorona, die sich um thermoresponsive Nanogele nach ihrer Inkubation in Humanserum und Plasma bildet, wurde in **Abschnitt 3.1 - 3.2** der vorliegenden Arbeit beschrieben. Diese Studien konzentrierten sich auf das Verständnis von Polymer-Protein-Assoziationen unter physiologischen Bedingungen in Bezug auf die Rolle der einzelnen Bestandteile thermoresponsiver Nanogele bei der Wechselwirkung mit Proteinen, nämlich thermoresponsive Polymere und dPG. Damit der Wirkstoffträger *in viv*o das gewünschte Ziel erreicht und um dessen Sequestrierung aus dem Blutstrom zu verhindern, sollten unerwünschte Wechselwirkungen mit Opsoninen vermieden werden. Die Analyse solcher Wechselwirkungen hilft, die Biokompatibilität von thermoresponsiven Nanogelen zu verstehen, die für intravenöse Verabreichungen konzipiert sind und idealerweise schließen sie damit die Lücke zwischen *In-vitro*- und *In-vivo*-Assays. Während beide Nanogel-Bestandteile, dPG und pNIPAM, als Polymere mit sehr geringen Proteinaffinitäten angesehen werden, [28, 65] führt ihr Einbau in Nanogele zu einer relevanten Größenzunahme, welche häufig auf eine erhöhte Proteinbindung hinweist.[56] Es konnte gezeigt werden, dass unerwünschte Oberflächenwechselwirkungen mit Proteinen in Gegenwart von dPG verringert werden, was durch den neutralen, hydrophilen Charakter zu erwarten ist. dPG vermittelt kolloidale Stabilität der thermoresponsiven Nanogele ohne die wichtigen thermoresponsiven Eigenschaften drastisch zu verändern[71] und hemmt die unspezifische Anlagerung von Proteinen an die Oberfläche der Nanogele. Die Hemmung der Proteinbindung war so erfolgreich, dass für diese Nanogelsysteme nur Spuren von Proteinen (3 - 7 µg/m^2 Nanogel) gefunden wurden. Nichtsdestotrotz wurde eine Protein-abhängige Aggregation für dPG-pNIPAM-Nanogele oberhalb ihrer VPTT gefunden, wie durch DLS-Messungen in vollem Humanserum bei 37 ° C beobachtet wurde. Die Spuren leichter Ketten des Immunglobulins, die bei 37 °C spezifisch angereichert wurden, weisen auf eine Quervernetzung mit Immunoglobulinen zwischen Nanogelen als Triebkraft für deren Aggregation hin; analog zu dem, was in der Literatur für Polystyrol-Nanopartikelsysteme gefunden wurde. [128] Diese

temperaturabhängige der Proteinkorona hat die Notwendigkeit aufgezeigt, die Wahl des Polymers für die Verwendung in der Biologie zu optimieren, wo die unspezifische Proteinbindung die Serumverfügbarkeit und endgültige systemische Verteilung von Polymer/Nanopartikeln bestimmt. Tatsächlich erwiesen sich die Nanogele durch die Veränderung des Polymers von pNIPAM zu pNIPMAM als sicherer für die Anwendung unter physiologischen Bedingungen bei 37 °C, da sie nicht im Serum aggregieren und ihren hydrophoben Übergang bei einer höheren VPTT von 46 °C erreichen.

Die Erzeugung von innovativen Nanogelsystemen für verschiedene Anwendungen als responsive Wirkstoffträger für die Krebstherapie ist in **Abschnitt 3.3 - 3.5** dieser Arbeit beschrieben. Der Kern dieses Abschnitts ist die Optimierung der Synthese von pH- und/oder thermoresponsiven Nanogelen durch Abstimmen des Dendron/pNIPAM-Comonomer Verhältnisses in Copolymer-Nanogelen **(Abschnitt 3.4)** und durch Untersuchung einer systematischen Reihe verschiedener Polymerkonzentrationen, um eine optimale Bindungsstärke für die Beladung und kontinuierliche Freisetzung von therapeutischen Molekülen durch SIPN-Nanogele **(Abschnitte 3.3, 3.5**) zu erhalten. Nanogele mit abstimmbaren Reaktivitäten werden hierbei mit dendritischen Polymeren konzipiert. Dendritische Strukturen erlauben eine hohe Dichte an funktionellen Gruppen, die die Löslichkeit von Nanogelen verbessern und multivalente Effekte vermitteln können. Die Verwendung von dPG als makromolekularer Vernetzer half in früheren Berichten die Biokompatibilität von thermoresponsivem pNIPAM zu verbessern.[71] Lineare Polymere mit abstimmbaren reaktiven Funktionalitäten/Konzentrationen wurden in Kombination mit dendritischen Einheiten verwendet, um in einer synergistischen Anstrengung das biologische Verhalten der Nanogele zu optimieren. Die Verwendbarkeit der Nanogele als Wirkstofftransportsystem wurde für kleine Chemotherapeutika (Cisplatin und DOX) sowie für Cytochrom c als therapeutisches Protein belegt.

Die Veränderungen der Nanogel-Morphologie während der chemischen Modifikation wurden eingehend untersucht, insbesondere im Zusammenhang mit der Fähigkeit des Nanogels mit therapeutischen Molekülen (kleinen Wirkstoffen oder Proteinen) schwach zu interagieren. Auf diese Weise konnte eine optimale Abstimmung der Bindungs- und Freisetzungskinetik des geladenen Moleküls für eine effiziente Wirkstoffabgabe erreicht werden. SIPN-Nanogele wurden als leistungsstarke Kandidaten für die rationale Abstimmung der Wechselwirkungen zwischen Nanogelen und den gewünschten eingelagerten Wirkstoffe entwickelt. Ein bedeutender Punkt war die Einführung eines sekundären Netzwerkes, um das SIPN zu erhalten und dabei nicht direkt mit den responsiven Eigenschaften der Nanogelen zu interferieren, sondern vielmehr neue physikochemisch responsive Modalitäten hinzuzufügen. dPG-pNIPAM-Nanogele wurden als Ausgangsstoffe für die Erzeugung von SIPN im Nanogel-

Gerüst eingesetzt. Auf diese Weise wurden die vorteilhaften Eigenschaften von dPG-pNIPAM-Nanogelen weiter abgestimmt, wobei pABC als dendritisches sekundäres polymeres Netzwerk zum Aufbau von SIPN-Nanogelen diente, das die Anlagerung einer therapeutischen Cytochrom-c-Korona ermöglichte. Die beladenen Nanogele zeigten eine therapeutische Wirksamkeit gegen HeLa-Zellen, die spezifisch durch eine Temperaturverschiebung ausgelöst werden konnte. Hier wurde das Aufquellen von thermoresponsiven Nanogelen als mechanische Kraft verwendet, um die Auflösung der supramolekularen Proteinkorona und deren intrazelluläre Freisetzung in HeLa-Zellen zu unterstützen **(Abschnitt 3.3)**. Weiterhin wurde die Verwendung von dendritischem ABC als Comonomer für die Synthese von pABC-co-pNIPAM-Nanogelen untersucht, die zusätzlich zum thermoresponsiven Verhalten von Nanogelen eine Sensitivität gegenüber Änderung des pH-Wertes einführten. Dies ermöglichte eine kontinuierliche Freisetzung von Cisplatin erst bei Erreichen von sauren Kompartimenten (wie Lysosomen) in den Zellen **(Abschnitt 3.4)**. Die Copolymerisation mit ABC veränderte die Thermoresponsivität des Copolymers im Vergleich zu pNIPAM drastisch. Die erhaltenen Nanogele zeigten ihr typisches VPTT-Verhalten nur unter sauren Bedingungen (pH <5), wobei die VPTT-Werte in Abhängigkeit der ABC-Konzentration abnahmen. Die Abnahme der VPTT war auf erhöhte intermolekulare pABC-Wasserstoffbrücken zurückzuführen, wenn sich pABC im protonierten Zustand befand. Die Beladung der Nanogele mit Cisplatin bei pH 7,4 führte zu stabilen ABC-Pt-Bindungen, die unter sauren Bedingungen als Folge der durch Wasserstoffbrücken induzierten Nanogelaggregation gebrochen wurden, und anschließender Freisetzung des zuvor gebundenen Cisplatin.

In einem analogen Ansatz wie in **Abschnitt 3.3** zeigten SIPN Nanogele mit Hilfe von p(AMPS) als sekundäres polymeres Netzwerk innerhalb der Nanogele eine erhöhte Affinität gegenüber dem chemotherapeutischen Wirkstoff DOX und waren somit in der Lage, antitumorale Wirkung gegenüber DOX-resistenten Tumorzellen *in vitro* und *in vivo* zu vermitteln **(Abschnitt 3.5)**.

Die in dieser Arbeit veröffentlichten Erkenntnisse tragen dazu bei, die Implementierung von Nanogelen der nächsten Generation voranzutreiben, weitere Informationen über die Modalitäten der Wirkungen von auf Stimuli reagierenden Nanogelen zu offenbaren und zu deren Übertragung in klinische Therapien beitragen. Es gibt keine Grenzen für die Implementierung neuer Nanopartikel, die moderate Wechselwirkungen zwischen Polymeren und Wirkstoffen für eine nachhaltige Freisetzung von Arzneimitteln nutzen, solange die Wechselwirkungen zwischen Polymer und Protein identifiziert werden und Kompatibilität mit dem beabsichtigten therapeutischen Zweck zeigen.

Um die Umsetzung der Kernergebnisse dieser Arbeit weiter voranzutreiben, wird derzeit intensiv an der Synthese von biokompatiblen weichen Nanogelen gearbeitet, die unter physiologischen Bedingungen einem kontrollierten Abbau unterlaufen können, um eine

wirksame Ausscheidung aus dem Körper zu erreichen, nachdem sie ihren therapeutischen Zweck erfüllt haben. Um dies zu erreichen, werden üblicherweise Disulfidbindungen oder proteolytisch spaltbare Bindungen in die Nanogelstruktur eingebracht, die zum Abbau der Nanogele zu kleineren Polymerketten/-partikeln führen, die letztendlich von den Nieren ausgeschieden werden können. In diesem Sinne ist ein großer synthetischer Aufwand erforderlich, um eine Akkumulation von Nanopartikeln im Körper zu verhindern, was zu langfristigen Toxizitätsproblemen führen kann.

Die in dieser Arbeit veröffentlichten Erkenntnisse über die Proteinkorona decken nicht die Interaktion zwischen einer selbstorganisierten Korona und der Freisetzungskinetik geladener Biomoleküle aus den Nanogelen ab. In gewisser Weise kann das Vorhandensein einer Proteinkorona einer zu schnellen Freisetzung der geladenen Therapeutika entgegenwirken und dadurch die Leistungsfähigkeit der Nanogele in bestimmten Fällen aufgrund sterischer Hinderung von Nanogelen durch die Proteinschichten verbessern. Nichtdestotrotz kann eine kontinuierliche Freisetzungskinetik *in vitro* in Abwesenheit von Proteinen eine zu langsame Freisetzung in Gegenwart einer Proteinkorona bedeuten. Es empfiehlt sich daher, Wirkstofffreisetzungsstudien in Gegenwart einer Proteinkorona durchzuführen, da sie die physiologischen Bedingungen, unter denen Nanogele wirken sollen, genauer darstellen.[124, 125, 171]

Ein Beispiel für eine vorher zusammengesetzte Proteinkorona mit therapeutischer Wirksamkeit, die in **Abschnitt 3.3** vorgestellt wurde, eröffnet eine Reihe neuer unbeantworteter Fragen bezüglich der intrinsischen therapeutischen Potenz von Proteinkoronen, die sich spontan um Nanogele bilden und deren Potenzial als eigenständige Wirkstoffe. Eine Proteinkorona-abhängige Aggregation von dPG-pNIPAM oberhalb der VPTT wie in **Abschnitt 3.1** beobachtet, kann eine Modellfallstudie sein, um lokalisierte Toxizität bei temperaturinduzierter Aggregation durch thermoresponsive Nanogele zu erzeugen.

Die systematischen Untersuchungen über die Charakterisierung von Proteinkoronen können in zukünftigen Studien auf SIPN- oder Copolymer-Nanogele ausgeweitet werden. Da das Vorhandensein eines SIPNs eine erhöhte Steifigkeit von Nanogelen bewirkt, kann dies die Proteinkorona-Zusammensetzung bei der Inkubation der Nanogele in Blutplasma und/oder Serum unvorhersehbar beeinflussen. Die Anwesenheit eines hydrophoben oder geladenen SIPN-Polymers kann zu einer Zunahme der Proteinadsorption und zu einer Änderung der Zusammensetzung der Korona führen und sollte daher als direkte Folgeuntersuchung aus dieser Arbeit betrachtet werden.

Die sinnvolle Wahl der Polymerstruktur, Nanogel-Architektur und Wechselwirkungen mit Umweltbedingungen sind die Hauptanforderungen für die erfolgreiche Entwicklung von makromolekularen Therapeutika. Das Zuschneiden dieser Eigenschaften hilft synergistisch,

die Proteinkorona-Struktur zu definieren, die bei Kontakt mit einer biologischen Flüssigkeit zu erwarten ist und übersetzt die chemische Struktur des Nanopartikels in sein Verhalten *in vivo*. Die in dieser Arbeit verwendeten Synthesestrategien können mit den Ergebnissen der Untersuchungen der Proteinkorona weiter optimiert werden, um die Struktur des Nanogels und die therapeutische Wirkung weiter zu verbessern.

7. References

1. P. M. Kosaka, V. Pini, J. J. Ruz, R. A. da Silva, M. U. González, D. Ramos, M. Calleja and J. Tamayo, *Nat Nano*, 2014, **9**, 1047-1053.
2. T. Dvir, B. P. Timko, D. S. Kohane and R. Langer, *Nat Nano*, 2011, **6**, 13-22.
3. Y. Gao, J. Lim, S.-H. Teoh and C. Xu, *Chemical Society Reviews*, 2015, **44**, 6306-6329.
4. M. Ferrari, *Nat Rev Cancer*, 2005, **5**, 161-171.
5. D. Peer, J. M. Karp, S. Hong, O. C. Farokhzad, R. Margalit and R. Langer, *Nat Nanotechnol*, 2007, **2**, 751-760.
6. D. E. Lee, H. Koo, I. C. Sun, J. H. Ryu, K. Kim and I. C. Kwon, *Chem Soc Rev*, 2012, **41**, 2656-2672.
7. T. Lammers, S. Aime, W. E. Hennink, G. Storm and F. Kiessling, *Accounts of Chemical Research*, 2011, **44**, 1029-1038.
8. S. Reichert, M. Calderon, K. Licha and R. Haag, in *Multifunctional Nanoparticles for Medical Applications: Imaging, Targeting and Drug Delivery*, Springer, New York / Berlin, 2012, pp. 315-344.
9. S. S. Kelkar and T. M. Reineke, *Bioconjug Chem*, 2011, **22**, 1879-1903.
10. P. Cai, W. R. Leow, X. Wang, Y. L. Wu and X. Chen, *Adv Mater*, 2017, **29**.
11. J. Shi, P. W. Kantoff, R. Wooster and O. C. Farokhzad, *Nat Rev Cancer*, 2017, **17**, 20-37.
12. P. Serra and P. Santamaria, *Clinical Immunology*, 2015, **160**, 3-13.
13. J. Catalan-Figueroa, S. Palma-Florez, G. Alvarez, H. F. Fritz, M. O. Jara and J. O. Morales, *Nanomedicine (London, England)*, 2016, **11**, 171-187.
14. K. M. El-Say and H. S. El-Sawy, *International Journal of Pharmaceutics*, 2017, **528**, 675-691.
15. V. P. Torchilin, *Pharm Res*, 2007, **24**, 1-16.
16. R. R. Castillo, M. Colilla and M. Vallet-Regi, *Expert opinion on drug delivery*, 2017, **14**, 229-243.
17. M. Colombo, S. Carregal-Romero, M. F. Casula, L. Gutierrez, M. P. Morales, I. B. Bohm, J. T. Heverhagen, D. Prosperi and W. J. Parak, *Chemical Society Reviews*, 2012, **41**, 4306-4334.
18. M. Nurunnabi, Z. Khatun, G. R. Reeck, D. Y. Lee and Y.-k. Lee, *ACS Applied Materials & Interfaces*, 2014, **6**, 12413-12421.
19. J. Bergueiro and M. Calderon, *Macromol Biosci*, 2015, **15**, 183-199.
20. Y. Wenrong, T. Pall, J. J. Gooding, P. R. Simon and B. Filip, *Nanotechnology*, 2007, **18**, 412001.
21. N. P. Dasgupta, J. Sun, C. Liu, S. Brittman, S. C. Andrews, J. Lim, H. Gao, R. Yan and P. Yang, *Advanced Materials*, 2014, **26**, 2137-2184.
22. Y. Chen, C. Tan, H. Zhang and L. Wang, *Chemical Society Reviews*, 2015, **44**, 2681-2701.
23. X. Liu and S. Wang, *Chemical Society Reviews*, 2014, **43**, 2385-2401.
24. S. Das, L. Jagan, R. Isiah, B. Rajesh, S. Backianathan and J. Subhashini, *Indian Journal of Pharmacology*, 2011, **43**, 409-413.
25. H. Ringsdorf, *Journal of Polymer Science: Polymer Symposia*, 1975, **51**, 135-153.
26. J. Khandare, M. Calderon, N. M. Dagia and R. Haag, *Chem Soc Rev*, 2012, **41**, 2824-2848.
27. Y. Yi, U. Buttner and I. G. Foulds, *Lab on a Chip*, 2015, **15**, 3540-3548.
28. J. O'Brien and K. J. Shea, *Acc Chem Res*, 2016, **49**, 1200-1210.
29. K. A. Willets, A. J. Wilson, V. Sundaresan and P. B. Joshi, *Chemical Reviews*, 2017, **117**, 7538-7582.
30. J. Yang, M.-H. Yao, L. Wen, J.-T. Song, M.-Z. Zhang, Y.-D. Zhao and B. Liu, *Nanoscale*, 2014, **6**, 11282-11292.
31. L. D. Lavis, *Biochemistry*, 2017, DOI: 10.1021/acs.biochem.7b00529.

32. S. Kaur, G. Venktaraman, M. Jain, S. Senapati, P. K. Garg and S. K. Batra, *Cancer letters*, 2012, **315**, 97-111.
33. M. J. Goette, G. M. Lanza, S. D. Caruthers and S. A. Wickline, *Journal of magnetic resonance imaging : JMRI*, 2015, **42**, 488-494.
34. P. W. Miller, N. J. Long, R. Vilar and A. D. Gee, *Angew Chem Int Ed Engl*, 2008, **47**, 8998-9033.
35. D. Pal, T. De and A. Baral, *International Journal of Pharmaceutical and Chemical Sciences*, 2012, **2**, 1227-1232.
36. J. E. Lemaster and J. V. Jokerst, *Wiley Interdisciplinary Reviews: Nanomedicine and Nanobiotechnology*, 2017, **9**, e1404-n/a.
37. J. Guo, K. Rahme, Y. He, L. L. Li, J. D. Holmes and C. M. O'Driscoll, *Int J Nanomedicine*, 2017, **12**, 6131-6152.
38. E. Polo, M. Collado, B. Pelaz and P. del Pino, *ACS Nano*, 2017, **11**, 2397-2402.
39. S. Jayant, J. J. Khandare, Y. Wang, A. P. Singh, N. Vorsa and T. Minko, *Pharm Res*, 2007, **24**, 2120-2130.
40. Y. Matsumura and H. Maeda, *Cancer Research*, 1986, **46**, 6387-6392.
41. M. Hamidi, A. Azadi and P. Rafiei, *Advanced Drug Delivery Reviews*, 2008, **60**, 1638-1649.
42. S. Nayak and L. A. Lyon, *Angewandte Chemie International Edition*, 2005, **44**, 7686-7708.
43. Y. Gao, J. Xie, H. Chen, S. Gu, R. Zhao, J. Shao and L. Jia, *Biotechnology Advances*, 2014, **32**, 761-777.
44. B. Sierra-Martin and A. Fernandez-Barbero, *Soft Matter*, 2015, **11**, 8205-8216.
45. Y. Ma, Y. Ge and L. Li, *Materials Science and Engineering: C*, 2017, **71**, 1281-1292.
46. K. Knop, R. Hoogenboom, D. Fischer and U. S. Schubert, *Angewandte Chemie International Edition*, 2010, **49**, 6288-6308.
47. M. Nic, J. Jirat and B. Kosata, *Journal*, 2014.
48. W. Wu and S. Zhou, *Nanomaterials in Drug Delivery, Imaging, and Tissue Engineering*, John Wiley & Sons, Inc., 2013.
49. M. Molina, M. Asadian-Birjand, J. Balach, J. Bergueiro, E. Miceli and M. Calderón, *Chem. Soc. Rev.*, 2015, **44**, 6161-6186.
50. A. M. Smith, M. C. Mancini and S. Nie, *Nat Nano*, 2009, **4**, 710-711.
51. E. C. Dreaden, L. A. Austin, M. A. Mackey and M. A. El-Sayed, *Therapeutic delivery*, 2012, **3**, 457-478.
52. J. Thevenot, H. Oliveira, O. Sandre and S. Lecommandoux, *Chemical Society Reviews*, 2013, **42**, 7099-7116.
53. F. Meeussen, E. Nies, H. Berghmans, S. Verbrugghe, E. Goethals and F. Du Prez, *Polymer*, 2000, **41**, 8597-8602.
54. F. Meeussen, Y. Bauwens, R. Moerkerke, E. Nies and H. Berghmans, *Polymer*, 2000, **41**, 3737-3743.
55. M. A. Ward and T. K. Georgiou, *Polymers*, 2011, **3**, 1215-1242.
56. T. Cedervall, I. Lynch, M. Foy, T. Berggard, S. C. Donnelly, G. Cagney, S. Linse and K. A. Dawson, *Angew Chem Int Ed Engl*, 2007, **46**, 5754-5756.
57. M. Asadian-Birjand, J. Bergueiro, F. Rancan, J. C. Cuggino, R. C. Mutihac, K. Achazi, J. Dernedde, U. Blume-Peytayi, A. Vogt and M. Calderón, *Polym. Chem.*, 2015, **6**, 5827-5831.
58. M. Molina, M. Giulbudagian and M. Calderón, *Macromolecular Chemistry and Physics*, 2014, **215**, 2414-2419.
59. M. Giulbudagian, M. Asadian-Birjand, D. Steinhilber, K. Achazi, M. Molina and M. Calderón, *Polym. Chem.*, 2014, **5**, 6909-6913.
60. B. N. S. Thota, L. H. Urner and R. Haag, *Chemical Reviews*, 2016, **116**, 2079-2102.
61. J. I. Paez, M. Martinelli, V. Brunetti and M. C. Strumia, *Polymers*, 2012, **4**, 355-395.
62. J. M. J. Fréchet and D. A. Tomalia, *Dendrimers and other Dendritic Polymers*, Wiley, New York, 2002.
63. G. R. Newkome, C. N. Moorefield and F. Vögtle, *Dendrimers and Dendrons. Concepts, Syntheses, Applications*, Wiley-VCH, Wennheim, 2001.

64. B. Zhu, Y. Han, M. Sun and Z. Bo, *Macromolecules*, 2007, **40**, 4494-4500.
65. M. Calderon, M. A. Quadir, S. K. Sharma and R. Haag, *Adv Mater*, 2010, **22**, 190-218.
66. F. Rancan, M. Asadian-Birjand, S. Dogan, C. Graf, L. Cuellar, S. Lommatzsch, U. Blume-Peytavi, M. Calderon and A. Vogt, *J Control Release*, 2016, **228**, 159-169.
67. M. Witting, M. Molina, K. Obst, R. Plank, K. M. Eckl, H. C. Hennies, M. Calderon, W. Friess and S. Hedtrich, *Nanomedicine*, 2015, **11**, 1179-1187.
68. F. F. Sahle, M. Giulbudagian, J. Bergueiro, J. Lademann and M. Calderon, *Nanoscale*, 2017, **9**, 172-182.
69. M. Giulbudagian, F. Rancan, A. Klossek, K. Yamamoto, J. Jurisch, V. C. Neto, P. Schrade, S. Bachmann, E. Ruhl, U. Blume-Peytavi, A. Vogt and M. Calderon, *J Control Release*, 2016, **243**, 323-332.
70. A. S. De Leon, M. Molina, S. Wedepohl, A. Munoz-Bonilla, J. Rodriguez-Hernandez and M. Calderon, *Langmuir*, 2016, **32**, 1854-1862.
71. J. C. Cuggino, C. I. Alvarez I, M. C. Strumia, P. Welker, K. Licha, D. Steinhilber, R.-C. Mutihac and M. Calderón, *Soft Matter*, 2011, **7**, 11259.
72. M. Molina, S. Wedepohl and M. Calderon, *Nanoscale*, 2016, **8**, 5852-5856.
73. P. Goyal, X. Zheng and M. Weck, *Advanced Synthesis & Catalysis*, 2008, **350**, 1816-1822.
74. D. Astruc, *Nat Chem*, 2012, **4**, 255-267.
75. T. S. Carter, T. J. Mooibroek, P. F. Stewart, M. P. Crump, M. C. Galan and A. P. Davis, *Angew Chem Int Ed Engl*, 2016, **55**, 9311-9315.
76. A. Burger, R. D. Costa, V. Lobaz, W. Peukert, D. M. Guldi and A. Hirsch, *Chemistry*, 2015, **21**, 5041-5054.
77. L. Fernandez, M. Calderón, M. Martinelli, M. Strumia, H. Cerecetto, M. González, J. J. Silber and M. Santo, *Journal of Physical Organic Chemistry*, 2008, **21**, 1079-1085.
78. N. Dib, L. Fernández, L. Otero, M. Santo, M. Calderón, M. Martinelli and M. Strumia, *Journal of Inclusion Phenomena and Macrocyclic Chemistry*, 2015, **82**, 351-359.
79. I. P. Julieta, B. Veronica, A. C. Eduardo and C. S. Miriam, *Current Organic Chemistry*, 2013, **17**, 943-955.
80. A. A. Aldana, B. Barrios, M. Strumia, S. Correa and M. Martinelli, *Reactive and Functional Polymers*, 2016, **100**, 18-25.
81. R. Roychoudhury, P. A. Martinez, T. Grinnage-Pulley, R. G. Schaut, C. A. Petersen and N. L. Pohl, *Angew Chem Int Ed Engl*, 2015, **54**, 9610-9613.
82. Y.-F. Xing, Y.-H. Xu, M.-H. Shi and Y.-X. Lian, *Journal of Thoracic Disease*, 2016, **8**, E69-E74.
83. D. Bobo, K. J. Robinson, J. Islam, K. J. Thurecht and S. R. Corrie, *Pharm Res*, 2016, **33**, 2373-2387.
84. E. M. Pelegri-O'Day, E. W. Lin and H. D. Maynard, *J Am Chem Soc*, 2014, **136**, 14323-14332.
85. A. E. Nel, L. Madler, D. Velegol, T. Xia, E. M. Hoek, P. Somasundaran, F. Klaessig, V. Castranova and M. Thompson, *Nat Mater*, 2009, **8**, 543-557.
86. C. M. Goodman, C. D. McCusker, T. Yilmaz and V. M. Rotello, *Bioconjug Chem*, 2004, **15**, 897-900.
87. L. Albertazzi, L. Gherardini, M. Brondi, S. Sulis Sato, A. Bifone, T. Pizzorusso, G. M. Ratto and G. Bardi, *Molecular Pharmaceutics*, 2013, **10**, 249-260.
88. W. Wang, W. Xiong, J. Wan, X. Sun, H. Xu and X. Yang, *Nanotechnology*, 2009, **20**, 105103.
89. J. Wolfram, Y. Yang, J. Shen, A. Moten, C. Chen, H. Shen, M. Ferrari and Y. Zhao, *Colloids Surf B Biointerfaces*, 2014, **124**, 17-24.
90. O. Vilanova, J. J. Mittag, P. M. Kelly, S. Milani, K. A. Dawson, J. O. Radler and G. Franzese, *ACS Nano*, 2016, **10**, 10842-10850.
91. P. Aggarwal, J. B. Hall, C. B. McLeland, M. A. Dobrovolskaia and S. E. McNeil, *Adv Drug Deliv Rev*, 2009, **61**, 428-437.
92. M. A. Dobrovolskaia, D. R. Germolec and J. L. Weaver, *Nat Nano*, 2009, **4**, 411-414.
93. D. R. Absolom, *Methods Enzymol.*, 1986, **132**, 281-318.

94. A. Radomski, P. Jurasz, D. Alonso-Escolano, M. Drews, M. Morandi, T. Malinski and M. W. Radomski, *British Journal of Pharmacology*, 2005, **146**, 882-893.
95. L. Vroman and A. L. Adams, *J Colloid Interface Sci*, 1986, **111**, 391-402.
96. M. R. Green, G. M. Manikhas, S. Orlov, B. Afanasyev, A. M. Makhson, P. Bhar and M. J. Hawkins, *Annals of Oncology*, 2006, **17**, 1263-1268.
97. S. Ritz, S. Schottler, N. Kotman, G. Baier, A. Musyanovych, J. Kuharev, K. Landfester, H. Schild, O. Jahn, S. Tenzer and V. Mailander, *Biomacromolecules*, 2015, **16**, 1311-1321.
98. S. Schöttler, G. Becker, S. Winzen, T. Steinbach, K. Mohr, K. Landfester, V. Mailander and F. R. Wurm, *Nat Nanotechnol*, 2016, **11**, 372-377.
99. C. Gräfe, A. Weidner, M. V. Luhe, C. Bergemann, F. H. Schacher, J. H. Clement and S. Dutz, *Int J Biochem Cell Biol*, 2015, **75**, 196-202.
100. S. Palchetti, L. Digiacomo, D. Pozzi, G. Peruzzi, E. Micarelli, M. Mahmoudi and G. Caracciolo, *Nanoscale*, 2016, **8**, 12755-12763.
101. A. L. Barran-Berdon, D. Pozzi, G. Caracciolo, A. L. Capriotti, G. Caruso, C. Cavaliere, A. Riccioli, S. Palchetti and A. Lagana, *Langmuir*, 2013, **29**, 6485-6494.
102. D. Pozzi, G. Caracciolo, A. L. Capriotti, C. Cavaliere, S. Piovesana, V. Colapicchioni, S. Palchetti, A. Riccioli and A. Lagana, *Mol Biosyst*, 2014, **10**, 2815-2819.
103. M. M. Yallapu, N. Chauhan, S. F. Othman, V. Khalilzad-Sharghi, M. C. Ebeling, S. Khan, M. Jaggi and S. C. Chauhan, *Biomaterials*, 2015, **46**, 1-12.
104. V. Mirshafiee, M. Mahmoudi, K. Lou, J. Cheng and M. L. Kraft, *Chem Commun (Camb)*, 2013, **49**, 2557-2559.
105. Q. Dai, C. Walkey and W. C. Chan, *Angew Chem Int Ed Engl*, 2014, **53**, 5093-5096.
106. B. S. Varnamkhasti, H. Hosseinzadeh, M. Azhdarzadeh, S. Y. Vafaei, M. Esfandyari-Manesh, Z. H. Mirzaie, M. Amini, S. N. Ostad, F. Atyabi and R. Dinarvand, *Int J Pharm*, 2015, **494**, 430-444.
107. B. Kang, P. Okwieka, S. Schottler, S. Winzen, J. Langhanki, K. Mohr, T. Opatz, V. Mailander, K. Landfester and F. R. Wurm, *Angew Chem Int Ed Engl*, 2015, **54**, 7436-7440.
108. A. Salvati, A. S. Pitek, M. P. Monopoli, K. Prapainop, F. B. Bombelli, D. R. Hristov, P. M. Kelly, C. Aberg, E. Mahon and K. A. Dawson, *Nat Nanotechnol*, 2013, **8**, 137-143.
109. Q. Dai, Yan, Y., Ang, C.-S., Kempe, K., Kamphuis, M. M. J., Dodds, S. J., Caruso F., *ACS Nano*, 2015, **9**, 2876-2885.
110. V. D. Maximov, V. V. Reukov, J. N. Barry, C. Cochrane and A. A. Vertegel, *Nanotechnology*, 2010, **21**, 265103.
111. M. Eriksson, L. A. Carlson, T. A. Miettinen and B. Angelin, *Circulation*, 1999, **100**, 594-598.
112. Z. Zhang, Wang, C., Zha, Y., Hu, W., Gao, Z., Zang, Y., Chen, J., Zhang, J., Dong, L., *ACS Nano*, 2015, **9**, 2405-2419.
113. J. Kreuter, D. Shamenkov, V. Petrov, P. Ramge, K. Cychutek, C. Koch-Brandt and R. Alyautdin, *J Drug Target*, 2002, **10**, 317-325.
114. B. Petri, A. Bootz, A. Khalansky, T. Hekmatara, R. Muller, R. Uhl, J. Kreuter and S. Gelperina, *J Control Release*, 2007, **117**, 51-58.
115. G. Caracciolo, F. Cardarelli, D. Pozzi, F. Salomone, G. Maccari, G. Bardi, A. L. Capriotti, C. Cavaliere, M. Papi and A. Lagana, *ACS Appl Mater Interfaces*, 2013, **5**, 13171-13179.
116. V. Escamilla-Rivera, M. Uribe-Ramirez, S. Gonzalez-Pozos, O. Lozano, S. Lucas and A. De Vizcaya-Ruiz, *Toxicol Lett*, 2016, **240**, 172-184.
117. M. Garvas, A. Testen, P. Umek, A. Gloter, T. Koklic and J. Strancar, *PLoS One*, 2015, **10**, e0129577.
118. F. Wang, L. Yu, M. P. Monopoli, P. Sandin, E. Mahon, A. Salvati and K. A. Dawson, *Nanomedicine*, 2013, **9**, 1159-1168.
119. K. Saha, D. F. Moyano and V. M. Rotello, *Mater Horiz*, 2014, **2014**, 102-105.
120. C. C. Fleischer and C. K. Payne, *Acc Chem Res*, 2014, **47**, 2651-2659.
121. G. M. Mortimer, N. J. Butcher, A. W. Musumeci, Z. J. Deng, D. J. Martin and R. F. Minchin, *ACS Nano*, 2014, **8**, 3357-3366.

122. Y. Yan, K. T. Gause, M. M. J. Kamphuis, C.-S. Ang, N. M. O'Brien-Simpson, L. J. C., E. C. Reynolds, E. C. Nice and C. F., *ACS Nano*, 2013, **7**, 10960-10970.
123. S. Dominguez-Medina, L. Kisley, L. J. Tauzin, A. Hoggard, B. Shuang, D. S. I. AS, S. Chen, L. Y. Wang, P. J. Derry, A. Liopo, E. R. Zubarev, C. F. Landes and S. Link, *ACS Nano*, 2016, **10**, 2103-2112.
124. S. Nappini, S. Fogli, B. Castroflorio, M. Bonini, F. Baldelli Bombelli and P. Baglioni, *J. Mater. Chem. B*, 2015, **4**, 716-725.
125. S. Behzadi, V. Serpooshan, R. Sakhtianchi, B. Muller, K. Landfester, D. Crespy and M. Mahmoudi, *Colloids Surf B Biointerfaces*, 2014, **123**, 143-149.
126. G. Caracciolo, L. Callipo, S. C. De Sanctis, C. Cavaliere, D. Pozzi and A. Lagana, *Biochim Biophys Acta*, 2010, **1798**, 536-543.
127. A. Cifuentes-Rius, de Puig, H., Kah, J. C. Y., Borros, S., Hamad-Schifferli, K., *ACS Nano*, 2013, **7**, 10066–10074.
128. R. Cukalevski, S. A. Ferreira, C. J. Dunning, T. Berggård and T. Cedervall, *Nano Research*, 2015, **8**, 2733-2743.
129. T. L. Moore, L. Rodriguez-Lorenzo, V. Hirsch, S. Balog, D. Urban, C. Jud, B. Rothen-Rutishauser, M. Lattuada and A. Petri-Fink, *Chem Soc Rev*, 2015, **44**, 6287-6305.
130. L. K. Müller, J. Simon, S. Schöttler, K. Landfester, V. Mailänder and K. Mohr, *RSC Adv.*, 2016, **6**, 96495-96509.
131. K. Rausch, A. Reuter, K. Fischer and M. Schmidt, *Biomacromolecules*, 2010, **11**, 2836-2839.
132. E. Casals, Pfaller, T., Duschl, A., Oostingh, G. J., Puntes V., *ACS Nano*, 2010, **4**, 3623–3632.
133. M. P. Monopoli, D. Walczyk, A. Campbell, G. Elia, I. Lynch, F. B. Bombelli and K. A. Dawson, *J Am Chem Soc*, 2011, **133**, 2525-2534.
134. D. Walczyk, F. B. Bombelli, M. P. Monopoli, I. Lynch and K. A. Dawson, *Journal of the American Chemical Society*, 2010, **132**, 5761-5768.
135. T. Cedervall, I. Lynch, S. Lindman, T. Berggard, E. Thulin, H. Nilsson, K. A. Dawson and S. Linse, *Proc Natl Acad Sci U S A*, 2007, **104**, 2050-2055.
136. S. Tenzer, D. Docter, S. Rosfa, A. Wlodarski, J. Kuharev, A. Rekik, S. K. Knauer, C. Bantz, T. Nawroth, C. Bier, J. Sirirattanapan, W. Mann, L. Treuel, R. Zellner, M. Maskos, H. Schild and R. H. Stauber, *ACS Nano*, 2011, **5**, 7155-7167.
137. S. H. D. P. Lacerda, J. J. Park, C. Meuse, D. Pristinski, M. L. Becker, A. Karim and J. F. Douglas, *ACS Nano*, 2010, **4**, 365-379.
138. G. Maiorano, S. Sabella, B. Sorce, V. Brunetti, M. A. Malvindi, R. Cingolani and P. P. Pompa, *ACS Nano*, 2010, **4**, 7481-7491.
139. M. Mahmoudi, I. Lynch, M. R. Ejtehadi, M. P. Monopoli, F. B. Bombelli and S. Laurent, *Chem Rev*, 2011, **111**, 5610-5637.
140. Z. J. Deng, M. Liang, M. Monteiro, I. Toth and R. F. Minchin, *Nat Nanotechnol*, 2011, **6**, 39-44.
141. P. E. Scopelliti, A. Borgonovo, M. Indrieri, L. Giorgetti, G. Bongiorno, R. Carbone, A. Podestà and P. Milani, *PLoS ONE*, 2010, **5**, e11862.
142. N. Welsch, Y. Lu, J. Dzubiella and M. Ballauff, *Polymer*, 2013, **54**, 2835-2849.
143. H. Noh and E. A. Vogler, *Biomaterials*, 2007, **28**, 405-422.
144. S. M. Slack and T. A. Horbett, *Journal of Colloid and Interface Science*, 1989, **133**, 148-165.
145. F. Fang and I. Szleifer, *Biophysical Journal*, 2001, **80**, 2568-2589.
146. P. Gong and I. Szleifer, *Journal of Colloid and Interface Science*, 2004, **278**, 81-90.
147. N. Welsch, Dr. rer. nat., Humboldt Universität zu Berlin, 2012.
148. A. Striegel, W. W. Yau, J. J. Kirkland and D. D. Bly, *Modern Size-Exclusion Liquid Chromatography: Practice of Gel Permeation and Gel Filtration Chromatography, 2nd Edition*, Wiley, 2009.
149. C. Scherer, S. Noskov, S. Utech, C. Bantz, W. Mueller, K. Krohne and M. Maskos, *Journal of nanoscience and nanotechnology*, 2010, **10**, 6834-6839.
150. S. Winzen, S. Schoettler, G. Baier, C. Rosenauer, V. Mailaender, K. Landfester and K. Mohr, *Nanoscale*, 2015, **7**, 2992-3001.

151. K. Mohr, S. S. Muller, L. K. Muller, K. Rusitzka, S. Gietzen, H. Frey and M. Schmidt, *Langmuir*, 2014, **30**, 14954-14962.
152. E. Omanovic-Miklicanin, I. Manfield and T. Wilkins, *Journal of Thermal Analysis and Calorimetry*, 2017, **127**, 605-613.
153. J. H. Shannahan, R. Podila and J. M. Brown, *Int J Nanomedicine*, 2015, **10**, 6509-6521.
154. L. Shang and G. U. Nienhaus, *Acc Chem Res*, 2017, **50**, 387-395.
155. M. Matysiak, L. Kapka-Skrzypczak, K. Brzoska, A. C. Gutleb and M. Kruszewski, *J Proteomics*, 2016, **137**, 35-44.
156. A. L. Capriotti, G. Caracciolo, C. Cavaliere, V. Colapicchioni, S. Piovesana, D. Pozzi and A. Laganà, *Chromatographia*, 2014, **77**, 755-769.
157. D. Docter, U. Distler, W. Storck, J. Kuharev, D. Wunsch, A. Hahlbrock, S. K. Knauer, S. Tenzer and R. H. Stauber, *Nat Protoc*, 2014, **9**, 2030-2044.
158. L. E. Murr and K. M. Garza, *Atmospheric Environment*, 2009, **43**, 2683-2692.
159. N. Panyala, E. Pena-Mendze and J. Havel, *J Appl Biomed*, 2008, **6**, 117-129.
160. A. L. Di Virgilio, M. Reigosa, P. M. Arnal and M. Fernández Lorenzo de Mele, *Journal of Hazardous Materials*, 2010, **177**, 711-718.
161. J. W. Wiechers and N. Musee, *Journal of Biomedical Nanotechnology*, 2010, **6**, 408-431.
162. S. Smita, S. K. Gupta, A. Bartonova, M. Dusinska, A. C. Gutleb and Q. Rahman, *Environmental Health*, 2012, **11**, S13.
163. T. Bartlomiejczyk, A. Lankoff, M. Kruszewski and I. Szumiel, *Annals of agricultural and environmental medicine : AAEM*, 2013, **20**, 48-54.
164. E. Allémann, P. Gravel, J.-C. Leroux, L. Balant and R. Gurny, *J. Biomed. Mater. Res.*, 1996, **37**, 229-234.
165. R. Gref, Lück, M., Quellec, P., Marchand, M., Dellacherie, E., Harnisch, S., Blunk, T., Müller, R. H., *Colloids and Surfaces B: Biointerfaces*, 2000, **18**, 301-313.
166. G. Gaucher, K. Asahina, J. Wang and J.-C. Leroux, *Biomacromolecules*, 2009, **10**, 408-416.
167. K. Sempf, T. Arrey, S. Gelperina, T. Schorge, B. Meyer, M. Karas and J. Kreuter, *Eur J Pharm Biopharm*, 2013, **85**, 53-60.
168. C. Lemarchand, R. Gref, C. Passirani, E. Garcion, B. Petri, R. Muller, D. Costantini and P. Couvreur, *Biomaterials*, 2006, **27**, 108-118.
169. K. Yu, B. F. L. Lai, J. H. Foley, M. J. Krisinger, E. M. Conway and J. N. Kizhakkedathu, *ACS Nano*, 2014, **8**, 7687-7703.
170. E. Hellstrand, I. Lynch, A. Andersson, T. Drakenberg, B. Dahlback, K. A. Dawson, S. Linse and T. Cedervall, *FEBS J*, 2009, **276**, 3372-3381.
171. K. Obst, G. Yealland, B. Balzus, E. Miceli, M. Dimde, C. Weise, M. Eravci, R. Bodmeier, R. Haag, M. Calderon, N. Charbaji and S. Hedtrich, *Biomacromolecules*, 2017, **18**, 1762-1771.
172. S. A. Ferreira, C. Oslakovic, R. Cukalevski, B. Frohm, B. Dahlback, S. Linse, F. M. Gama and T. Cedervall, *Biochim Biophys Acta*, 2012, **1820**, 1043-1051.
173. D. Labarre, C. Vauthier, C. Chauvierre, B. Petri, R. Muller and M. M. Chehimi, *Biomaterials*, 2005, **26**, 5075-5084.
174. H. R. Kim, K. Andrieux, C. Delomenie, H. Chacun, M. Appel, D. Desmaele, F. Taran, D. Georgin, P. Couvreur and M. Taverna, *Electrophoresis*, 2007, **28**, 2252-2261.
175. K. Obst, G. Yealland, E. Miceli, M. Dimde, B. Balzus, C. Weise, M. Eravci, R. Bodmeier, R. Haag, M. Calderon, N. Charbaji and S. Hedtrich, HVI Symposium 2016 - Multifunctional Biomaterials for Medicine, Berlin, 2016.
176. E. Miceli, M. Kar and M. Calderón, *J. Mater. Chem. B*, 2017, **5**, 4393-4405.
177. M. A. Dobrovolskaia, B. W. Neun, S. Man, X. Ye, M. Hansen, A. K. Patri, R. M. Crist and S. E. McNeil, *Nanomedicine*, 2014, **10**, 1453-1463.
178. V. Mirshafiee, R. Kim, S. Park, M. Mahmoudi and M. L. Kraft, *Biomaterials*, 2016, **75**, 295-304.
179. Q. Peng, S. Zhang, Q. Yang, T. Zhang, X. Q. Wei, L. Jiang, C. L. Zhang, Q. M. Chen, Z. R. Zhang and Y. F. Lin, *Biomaterials*, 2013, **34**, 8521-8530.

180. G. N. Rimondino, E. Miceli, M. Molina, S. Wedepohl, S. Thierbach, E. Rühl, M. Strumia, M. Martinelli and M. Calderón, *J. Mater. Chem. B*, 2017, **5**, 866-874.
181. M. Molina, S. Wedepohl, E. Miceli and M. Calderón, *Nanomedicine*, 2016, **12**, 117-129.

8. Curriculum Vitae

For reasons of data protection, the curriculum vitae is not published in the electronic version.

9. Publications and Conference Contributions

Publications

- M. Molina, M. Asadian-Birjand, J. Balach, J. Bergueiro, E. Miceli and M. Calderón (2015). "Stimuli-responsive nanogel composites and their application in nanomedicine." Chem. Soc. Rev. 44(17): 6161-6186.

- M. Molina, S. Wedepohl, E. Miceli and M. Calderon (2017). "Overcoming drug resistance with on-demand charged thermoresponsive dendritic nanogels." Nanomedicine (Lond) 12(2): 117-129.

- G. N. Rimondino, E. Miceli, M. Molina, S. Wedepohl, S. Thierbach, E. Ruhl, M. Strumia, M. Martinelli and M. Calderon (2017). "Rational design of dendritic thermoresponsive nanogels that undergo phase transition under endolysosomal conditions." Journal of Materials Chemistry B 5(4): 866-874.

- K. Obst, G. Yealland, B. Balzus, E. Miceli, M. Dimde, C. Weise, M. Eravci, R. Bodmeier, R. Haag, M. Calderon, N. Charbaji and S. Hedtrich, “Protein Corona Formation on Colloidal Polymeric Nanoparticles and Polymeric Nanogels: Impact on Cellular Uptake, Toxicity, Immunogenicity, and Drug Release Properties.” Biomacromolecules, 2017, 18(6), 1762-1771.

- E. Miceli, M. Kar and M. Calderon (2017). "Interactions of organic nanoparticles with proteins in physiological conditions." Journal of Materials Chemistry B 5(23): 4393-4405.

- E. Miceli, B. Kuropka, C. Rosenauer, E. R. Osorio Blanco, L. Fechner, M. Kar, C. Weise, S. Morsbach, C. Freund, M. Calderón (2017). "Temperature dependency of elusive protein corona around thermoresponsive nanogels: key interactions above the lower critical solution temperature." Submitted.

- E. Miceli, S. Wedepohl, E. R. Osorio Blanco, G. N. Rimondino, M. Martinelli, M. Strumia, M. Molina, M. Kar, M. Calderón (2017). "Semi-interpenetrated, dendritic, dual-responsive nanogels with cytochrome c corona induce controlled apoptosis in HeLa cells." Submitted.

Conference contributions

- E. Miceli, M. Molina, C. Weise, M. Calderón (2014). “Competitive Protein Absorption Analysis on Thermoresponsive Polyglycerol-Based Nanogels”. Polydays. Berlin.

- E. Miceli, M. Molina, C. Weise, M. Calderón (2015). "Protein corona analysis on thermoresponsive nanogels." HVI - Consortium Meeting 2015.

- E. Miceli, M. Molina, C. Weise, M. Calderón (2015). “Competitive Protein Absorption Analysis on Thermoresponsive Polyglycerol-Based Nanogels”. ICTP-SAIFR Minischool on Biophysics of Protein Interactions. UNESP, Sao Paulo.

- E. Miceli, M. Molina, C. Weise, M. Calderón (2015). "Protein corona separation and characterization from thermoresponsive polyglycerol-based nanogels." EPF Dresden 2015.

- E. Miceli, E. R. Osorio-Blanco, L. Fechner, M. Kar and M. Calderón (2016). “Protein Adsorption on Thermoresponsive Polyglycerol-based Nanogels”. CRC 1066 Symposium. Mainz.

- E. Miceli, E. Glitscher, E. R. Osorio-Blanco, L. Fechner, J. Bergueiro, M. Kar and M. Calderón (2016). “Protein Corona Analysis on Thermoresponsive Nanogels and Au Nanoparticles”. HVI Symposium. Berlin.